Granular open filter in rubble mound sand retaining structures

Physical model tests of a negative geometrically open filter layer

D.P. van de Ven

Technische Universiteit Delft

TU Delft
Van Oord
Marine ingenuity

Granular open filter in rubble mound sand retaining structures

Physical model tests of a negative geometrically open filter layer

by

D.P. van de Ven

In partial fulfilment of the degree of Master of Science
at the Delft University of Technology,
to be defended publicly on Monday November 18, 2019 at 2:00 PM.

Student number:	4226305	
Project duration:	Februari 18, 2019 – November 18, 2019	
Thesis committee:	Dr. Ir. B. Hofland	TU Delft, supervisor
	Dr. Ir. A. Antonini	TU Delft
	Ir. G.M. Smith	TU Delft & Van Oord
	Ir. D.C.P. van Kester	Van Oord

An electronic version of this thesis is available at http://repository.tudelft.nl/.

TU Delft Van Oord

Preface

This thesis is written for the completion of the MSc program Hydraulic Engineering, at the faculty of Civil Engineering and Geosciences of the Delft University of Technology (TU Delft). In nine months, from February 18 until November 18, research was conducted in the field of an open filter under the supervision of both the TU Delft and Van Oord Dredging and Marine Contractors (Van Oord)).

The process started with uncertainties and also committee members that did not believe the feasibility of the research. To prove this feasibility, I went to the TU Delft Laboratory of Fluid mechanics, where I constructed a test setup. For more than two months, I have been testing and working in the fluid mechanics laboratory almost seven days a week. I was eager to finish the testing in the Laboratory, this even resulted in checking the setup from a hotel room in Italy during a weekend off. This testing wouldn't be possible without the help of the staff from the laboratory. I would like to thank them for their discussion and help on the physical model.

I also would like to thank Van Oord for allowing me to do my thesis within their company. The practical view from a contractor's viewpoint combined with the technical knowledge provided by the employees turned out to be a good combination for my research. I would like to thank Dennis van Kester and Greg Smith, for both helping me formulating the problem but also guiding me through the research, and also for being part of my graduation committee. Especially Dennis helped me a lot with our weekly meetings, which formed my research.

I would also like to thank the Delft University of Technology for their supervision, especially Bas Hofland and Alessandro Antonini for their guidance throughout the project. Both helped me a lot with the physical understanding of the problem. A special thanks to Bas Hofland for being the chair of my graduation committee and for helping me to create the physical model in the laboratory.

I am also thankful to all Van Oord graduates that studied together with me at the Rivium, and helped me during my project by discussing the topic over numerous coffee breaks and our weekly Friday lunches at the "Zebra". At last, a special thanks to Maxime, who was my biggest supporter over the last months and possibly read this report more often than I did myself.

D.P. van de Ven
Rotterdam, November 2019

Summary

All over the world, land reclamations are built in coastal areas. To protect the sand used for these reclamations rubble mound breakwaters could be used. The interface between the sand and the core of the rubble mound breakwater is not sand tight. For this reason, the interface between the reclamation and the breakwater core has to be protected against erosion. A method for this protection could be a geotextile, but the use of a geotextile is not preferred since these are difficult and labour intensive to install at larger depth. An alternative method is a granular filter layer, which can be either geometrically open or closed. A closed filter requires more layers, due to more strict guidelines, than an open filter. Fewer layers mean an improvement in material and construction costs, which makes an open filter preferable.

This research is about the erosion through a geometrically open but hydraulically closed filter layer with the base layer placed on top of the filter layer. The objective of this thesis is to determine whether or not it is possible to create a sand tight interface with the use of a single reversed granular geometrically open filter layer. This interface has been studied with the analysis of the loads on and resistance of the reversed filter. The pressure distribution inside the breakwater has been determined, and a physical model has been constructed. The single 'reversed' open filter layer considered in this research, together with the considered breakwater cross-section, is depicted in Figure 1.

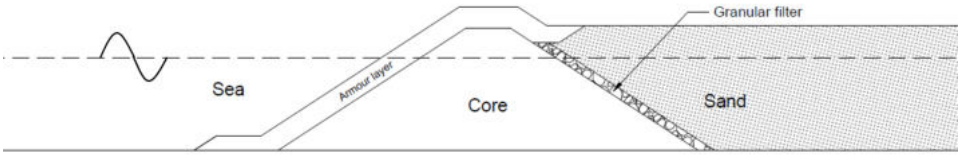

Figure 1: Example drawing of a considered rubble mound land reclamation cross-section.

The loads on the filter layers originate from the wave climate outside the breakwater. The pressure distribution inside the breakwater has been calculated using both numerical and empirical models. Both models gave an estimate for the pressures around and inside the open filter layer. The entire research was split into two directions of flow; parallel and perpendicular to the interface between the open filter layer and sand reclamation. The results of the numerical model, together with the critical gradients obtained from the physical model tests, are depicted in Figure 2. Observations from these graphs are: The parallel gradients (Figure 2a) are almost two orders of magnitude smaller than the perpendicular gradients (Figure 2b), and the parallel gradients are more depth-dependent than the perpendicular gradients.

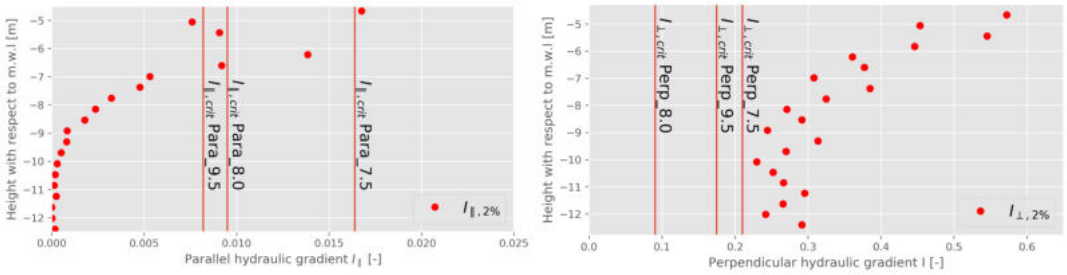

(a) Parallel gradients

(b) Perpendicular gradients

Figure 2: The 2% highest gradients plotted against the height with respect to mean water level, being a result from the numerical model for the two directions. The top of the open filter layer is located at the -5m line. The vertical lines depict the critical gradients obtained from the physical model tests.

As there was little understanding of the exact behaviour of a sand layer that is placed on top of a geometrically open filter layer, a physical model setup has been built to develop guidelines for the design of these open filters. Similar to the numerical model, the physical model was also split into two configurations, which both forced the flow in the two main directions; parallel and perpendicular. The two configurations used the same setup and are only different in the closed boundaries, see Figures 3a and 3b.

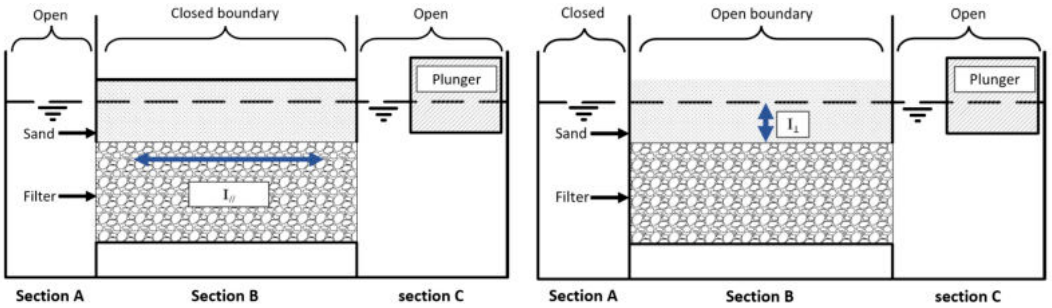

(a) Parallel setup. The gradient is determined inside the open filter layer.

(b) Perpendicular setup. The gradient is determined inside the sand layer.

Figure 3: Side views of both configurations with their open boundaries and directions of gradients.

Each model setup is tested with five sand-filter combinations. The ratio between the sand and filter grain sizes is governing for the strength of the sand-filter combination. The ratio is given by the stability number D_{15F}/D_{85B}, represent the ratio between D_{15F}, the fraction of the filter layer for which 15% of the grain sizes are smaller, and D_{85B}, the fraction of the sand for which 85% is smaller. The used ratios are: 4.0, 7.5, 8.0, 9.5 and 16.5. The critical gradient has been determined for these as the hydraulic gradient for which no erosion visible. For the upper bound (16.5) and lower bound(4.0) tests, no critical gradient was found, due to limitations of the model setup.

The final graphs, with the loads ($I_{\parallel}$ or $I_{\perp}$) plotted against the strength (D_{15F}/D_{85B}), are depicted below (Figures 4a and 4b). The graphs give the critical gradients, together with errorbars that depict the stepsize of the hydraulic gradients of the physical model. The three obtained critical gradients in each direction are also plotted against the gradients obtained from the analysis of the case study, with six lines in Figure 2. The graphs show it is possible to create a geometrically open but hydraulically closed reversed filter. With the use of these graphs, rubble mound land reclamations can be built using a granular geometrically open filter construction when the gradients are low enough, which could result in better constructability and lower costs.

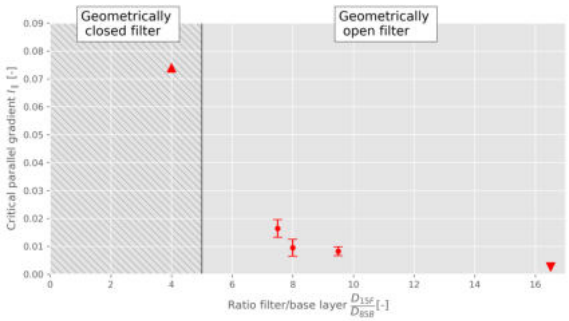

(a) Relationship between the ratio of the base layer and open filter layer and the critical gradient

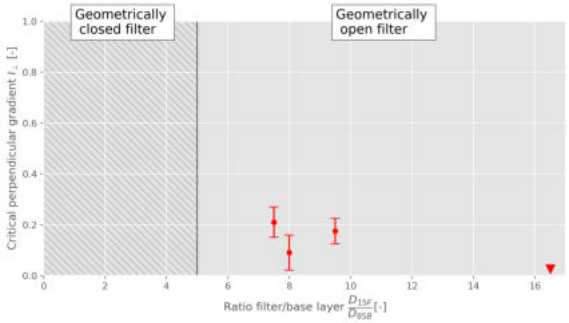

(b) Relationship between the ratio of the base layer and open filter layer and the critical gradient

Figure 4: Critical gradients of both parallel and perpendicular flow plotted against the base to filter ratio

Contents

Summary v

1 Introduction 1
- 1.1 Problem description . . . 3
- 1.2 Objective . . . 4
  - 1.2.1 Hypothesis . . . 4
- 1.3 Axis system . . . 5
- 1.4 Glossary . . . 6

2 Literature study 7
- 2.1 Hydraulic processes inside a breakwater core . . . 7
  - 2.1.1 Porous flow . . . 7
  - 2.1.2 Wave propagation through breakwater . . . 8
  - 2.1.3 Wave attenuation through breakwater . . . 9
  - 2.1.4 Hydraulic gradients and directions . . . 10
  - 2.1.5 Numerical modelling of flow through porous media . . . 11
- 2.2 Erosion of sediments . . . 11
  - 2.2.1 Sum of forces . . . 12
  - 2.2.2 Arching . . . 13
  - 2.2.3 Initial movement . . . 13
- 2.3 Flow through granular filters . . . 14
  - 2.3.1 Geometrically open filters . . . 14
  - 2.3.2 Critical gradient . . . 14
  - 2.3.3 Previous research of erosion through breakwaters . . . 15
  - 2.3.4 Geotextiles . . . 18
- 2.4 Conclusion Literature . . . 19

3 Determination of the hydraulic gradients 21
- 3.1 Hydraulic gradients calculated with empirical model . . . 21
- 3.2 Hydraulic gradients from numerical model . . . 22
  - 3.2.1 Comparison numerical model with physical tests and empirical model . . . 23
  - 3.2.2 Hydraulic gradients from the numerical model . . . 25
- 3.3 Direction of flow . . . 30
- 3.4 Conclusion hydraulic gradients . . . 32

4 Model setup 33
- 4.1 Test setup . . . 33
  - 4.1.1 Goal of the tests . . . 34
  - 4.1.2 Processes of importance . . . 34
  - 4.1.3 Parameters of importance . . . 35
- 4.2 Forcing of hydraulic gradients . . . 35
- 4.3 Grain sizes . . . 36
- 4.4 Measurements . . . 37
  - 4.4.1 Writing of measurements . . . 37
  - 4.4.2 Calibration . . . 37
  - 4.4.3 Pressure sensors . . . 38
  - 4.4.4 Laser . . . 39
  - 4.4.5 Water level gauges . . . 39
  - 4.4.6 Filtering signals . . . 40

4.5 Erosion measurements . . . 41
4.6 Model effects . . . 42
4.6.1 Wall effects . . . 42
4.6.2 Piping through sand layer . . . 42
4.6.3 Sorting of material . . . 42
4.6.4 Flow bypassing through boxes . . . 43
4.6.5 Vibrations in the setup . . . 43
4.6.6 Inflow and outflow effects . . . 43
4.7 Geometry . . . 43
4.7.1 Parallel setup . . . 44
4.7.2 Perpendicular setup . . . 45
4.8 Test sequence . . . 45
4.8.1 Building the setup . . . 45
4.8.2 Preparation of equipment and setup . . . 46
4.9 Test schedules . . . 46
4.9.1 Reference tests . . . 46
4.9.2 Final test sequence . . . 47
4.9.3 Special test cases . . . 47
4.10 Analysis . . . 48
4.10.1 Detrending results . . . 48
4.10.2 Splitting the signal . . . 48
4.10.3 Calculating hydraulic gradients . . . 49
4.10.4 Finding critical gradient . . . 49

5 Results **51**
5.1 Hydraulic gradients over multiple tests . . . 51
5.1.1 Velocity to parallel hydraulic gradients compared . . . 51
5.1.2 Ratio between plunger velocity and hydraulic gradient over one test . . . 52
5.1.3 Difference in hydraulic gradient for other granular filter layers . . . 53
5.1.4 Consistency of gradient signal . . . 54
5.1.5 Phase between forcing and pressure sensors for parallel flow . . . 54
5.1.6 Hydraulic gradients created by plunger . . . 56
5.2 Erosion during reference tests . . . 59
5.2.1 Spreading of granular filter layer . . . 60
5.2.2 Allocation of sand in sand trap . . . 60
5.2.3 Critical gradient reference tests . . . 60
5.3 Results final model tests . . . 61
5.3.1 Sensor malfunction . . . 61
5.3.2 Visual observations . . . 62
5.3.3 Relations granular filter-base ratio to critical gradient . . . 63
5.3.4 Special test cases . . . 65
5.4 Critical gradients compared to case study . . . 66
5.5 Conclusions results . . . 67

6 Discussion, conclusions and recommendations **69**
6.1 Discussion . . . 69
6.1.1 Measurement inaccuracies . . . 69
6.1.2 Comparison to existing guidelines and research . . . 71
6.1.3 Hydraulic gradients in reality . . . 72
6.1.4 Uncertainties in application . . . 73
6.1.5 Preliminary guideline for design . . . 74
6.2 Conclusion . . . 75
6.2.1 Hydraulic gradients from numerical and empirical models . . . 75
6.2.2 Magnitude of critical hydraulic gradients from physical model . . . 75
6.2.3 Special test cases . . . 76
6.2.4 Comparison critical gradient with case study . . . 76
6.2.5 Main conclusion . . . 77

6.3 Recommendations . . . 78
6.3.1 Increasing the accuracy . . . 78
6.3.2 Quantification of results . . . 78
6.3.3 Broadening the knowledge . . . 79

Bibliography **81**

List of Figures **83**

List of Tables **87**

A Literature study **89**
A.1 Previous filter research . . . 89
A.1.1 Closed filters . . . 91
A.1.2 Open filters . . . 91
A.1.3 Conclusion resistance . . . 93
A.2 Vanneste 2012 . . . 93
A.3 Physical moddeling . . . 94

B Hydraulic pressures **95**
B.1 Calculated gradients . . . 95
B.1.1 Model setup measurements . . . 95
B.1.2 Comparison between OpenFOAM® model and empirical calculations for the lengthward gradient . . . 97
B.2 Direction of flow in breakwater . . . 98

C Model setup **99**
C.1 Preliminary model test . . . 99
C.1.1 Preliminary test results . . . 99
C.2 Model evolution . . . 100
C.2.1 Model setup 1 . . . 100
C.2.2 Model setup 2 . . . 100
C.2.3 Model setup 3 . . . 101
C.2.4 Model setup 4 . . . 102
C.2.5 Model setup 5 . . . 103
C.2.6 Final model setup . . . 104
C.3 Additional measurement devices . . . 105
C.4 Sieving of sediments . . . 105
C.5 Calibration . . . 105
C.6 Plunger movement . . . 107
C.7 Parameters of importance . . . 107
C.8 Setup at TU Delft laboratory of fluid mechanics . . . 109

D Results model tests **111**
D.1 Consistency of gradient during one test . . . 111
D.2 Phase lag sensors . . . 111
D.2.1 Ref_8.0_4 . . . 112
D.2.2 Ref_8.0_6 . . . 115
D.3 Sensors malfunction . . . 118
D.4 Standard deviation tests . . . 118
D.5 Reference tests . . . 119
D.6 Parallel tests . . . 120
D.6.1 Para_4.0 . . . 120
D.6.2 Para_7.5 . . . 121
D.6.3 Para_8.0 . . . 121
D.6.4 Para_9.5 . . . 121
D.6.5 Para_16.5 . . . 122
D.6.6 Para_8.0_super . . . 122
D.6.7 Para_8.0_long . . . 122

D.7 Perpendicular tests 123
D.7.1 Perp_4.0 123
D.7.2 Perp_7.5 123
D.7.3 Perp_8.0 124
D.7.4 Perp_9.5 125
D.7.5 Perp_16.5 125

1

Introduction

With a continuously growing population, land is becoming scarce all over the world. Over half of the world's population lives in urban areas, located in coastal regions. Cities are growing and therefore need more space, which could be found on the waterfront in the form of land reclamations (for example Figure 1.1a). Not only cities grow into the seas, port areas protrude seawards (Figure 1.1b), airports can be constructed in seas (Figure 1.1c), and the latest developments in offshore wind does create a demand for a centralized hub, which can also be built in the form of an artificial island (Figure 1.1d).

(a) Palm Jumeirah (Source: Van Oord)

(b) Maasvlakte II (Source: Van Oord)

(c) Macau international airport (Source: Van Oord)

(d) Doggersbank concept (Source: Tennet)

Figure 1.1: Examples of land reclamations

These reclamations are constructed with dredged sand, as this is a cheap building material and available worldwide. The seaward sides of the land reclamation could be protected against hydraulic loads, to prevent erosion. For this research, the focus is on a hard revetment in the form of a rubble mound breakwater. The revetment structure is considered in this study is not closed for erosion through the interface between breakwater core and sand. A cross section is depicted in Figure 1.2. Possible measures are depicted in Figure 1.4. The characteristics of the methods and the construction of these are explained below.

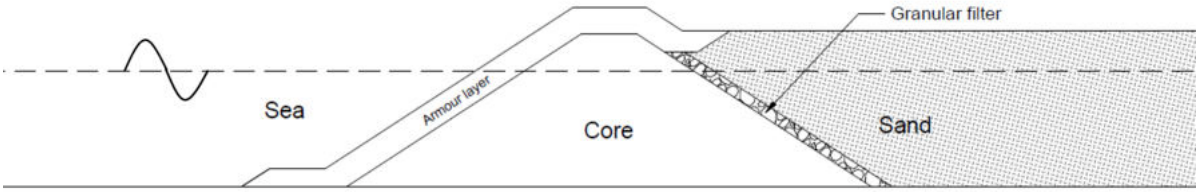

Figure 1.2: Example drawing of a considered breakwater/reclamation cross section.

Geotextile
A geotextile can be used to create a sand tight interface. A geotextile is a permeable fabric so it won't build up hydraulic pressure, but is closed for sand transport. This textile is placed in between the breakwater core and the sand fill. The geotextile is placed after the core is built by rolling out the sheets and sinking them through placing sand or rocks on top (see Figure 1.3a). Preferably geotextiles are placed above the water line or slightly below as the placement of the geotextile is limited by the maximum reach of the crane.

Granular filter
The interface between the breakwater core and the sand reclamation can also be closed for sediment transport by the placement of a granular filter. A granular filter consists of one or more rock layers as a transition between the large rocks of the breakwater and the sand to prevent erosion. A granular filter layer is placed by dumping stones against the core with a side stone dumping vessel (Figure 1.3b), or if more accuracy is required a similar crane can be used as the crane used for rolling out the geotextiles (Figure 1.3a).

A granular filter can be either geometrically open and geometrically closed. A geometrically closed filter will have the same effect as a geotextile as the sand cannot physically move through the filter layer since the sand grains are too large to fit through the pores of the filter layer. The placement of a geometrically closed filter is however difficult and expensive as it will consist of multiple layers. Each layer should have a minimum thickness to ensure the filter is geometrically closed, which means that the thickness, of the entire filter, increases a lot if more layers are used. This increase in thickness will lead to a higher price because of material and placement costs.

A more economical solution could be a geometrical open filter, which is geometrically open but hydraulically closed. This open filter is a granular filter in which the grains are physically able to move through the pores of the filter, but the hydraulic loading is lower than the critical loading. For such a granular geometrically open and hydraulically closed filter, fewer layers are needed to provide sufficient stability against erosion. This could result in a lower production cost.

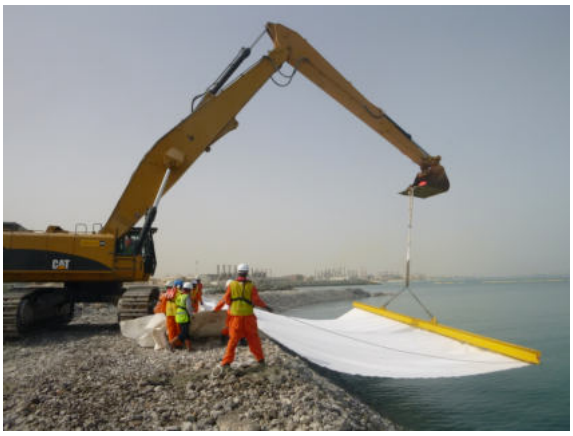

(a) Installation of a geotextile with a crane
(Source: Van Oord)

(b) Installation of a stone layer with a side stone dumping vessel
(Source: Van Oord)

Figure 1.3: Installation techniques

1.1. Problem description

As stated above a single geometrically open filter layer can have a large reduction in both cost and ease of construction use of land reclamations. For this reason, it would be beneficial to develop a method which could be used to construct these geometrically open filters.

”When the base layer is on top of the filter layer and the flow is downward, the finer grains will easily fall through the filter layer and it is therefore recommended to follow the rules for geometrically closed filters” This is the second sentence of the paragraph on open filters for perpendicular flow in the book Introduction to bed, bank and shore protection (Schiereck and Verhagen, 2012). It states that it is not recommended to follow the open filter rules for a flow through a base and filter layer in which the base layer is the upper layer. Despite this recommendation, a reversed open filter can have a positive influence on both the constructibility and the price of rubble mound strengthened land reclamations.

The current open filter design guidelines are based on scale tests that have been performed with a filter layer on top of a base layer and/or tests with numerical models. In the filter described in this thesis, the orientation of these layers is changed, meaning base layer on top and filter layer below. This type of filter is from here on referred to as a reversed filter, because the filter and base layers are reversed with respect to the conventional filter layout.

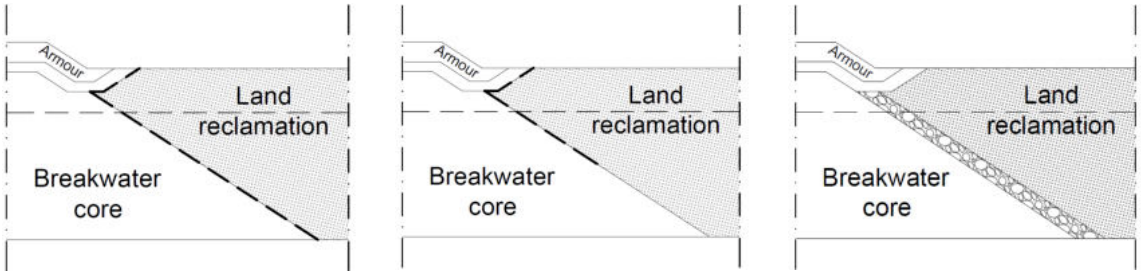

(a) Geotextile along entire interface (b) Partial geotextile (c) Granular filter

Figure 1.4: Examples of boundaries between breakwater cores and land reclamations. The thick dotted line between the reclamation and the core depicts the geotextile. The cross section displayed here is a small section from the entire cross section as shown in Figure 1.2

Previous research on geometrically open filter was focussed on filters that were subject to steady flow, amongst others;(de Graauw et al., 1983),(Klein Breteler, 1989),(Bakker et al., 1995) or to wave attack, amongst others; (Uelman, 2006),(Ockeloen, 2007),(Wolters et al., 2012). These situations are very different from the open filter considered in this thesis. Not only because of the orientation that is discussed above but as the filter is placed between two large permeable layers, the sand and the breakwater core, the hydrodynamical loads are different than what is studied before. For this reason and the recommendation from Schiereck and Verhagen (2012), it is hard to find a reliable method for the design of this type of filter.

In a previous research (Tutein Nolthenius, 2018), the shortening of geotextile (Figure 1.4b) was studied with a scale model test. The study focused on a breakwater land reclamation without a filter layer without the protection on the interface the sand infiltrated the core material and created a boundary inside the core material. In the scale model test, the critical gradient for the erosion of the core sediment mixture has been determined. Tutein Nolthenius (2018) also found that a filter ratio of $\frac{D_{15F}}{D_{85B}} \approx 8$ was capable of stopping the erosion of the base layer, but the research of this ratio was beyond the scope of the thesis.

1.2. Objective

The objective of this thesis is to describe the movement of sediments through an open filter layer with the following research question:

"How is it possible to create a boundary between a breakwater core and a land reclamation through which the sand does not excessively migrate with the use of a granular geometrically open filter layer?"

This will be studied with the following subquestions:

- Is the critical hydraulic gradient over the filter layer that is responsible for the largest erosion a perpendicular or parallel gradient or is it a combination of these two?
- Is the current design formula in the form of Wolters et al. (2012) sufficient to describe the erosion through the filter layer?
- To what extent is an open filter capable of preventing erosion of the base layer when this base layer is on top of the open filter layer?
- Does the load on top of the base layer influence the erosion through the open filter layer as proposed by de Graauw et al. (1983)?

Because there is little known about the processes present in this type of structures a physical model test is designed to create an understanding of the behaviour of the sediments at the considered interface, but also to verify if the current design models are sufficient to ensure the stability of these filters. A numerical model is used to create an understanding of the pressure gradients at the considered interface.

The main steps followed in the approach are:

- Determining the gradients using an OpenFOAM® model;
- Calculating the gradients using design guidelines;
- Constructing a model;
- Testing with the model.

1.2.1. Hypothesis

The hypothesis for the main objective is: The granular geometrically open filter with a sand layer on top of the filter layer will have a fragile equilibrium. Meaning that it is possible to create a granular geometrically open filter with a sand layer on top of this filter layer, which is hydraulically closed for limited gradients.

1.3. Axis system

In this research three gradients are distinguished:

- Lengthward gradient;
- Perpendicular gradient;
- Parallel gradient.

For this research only a two dimensional flow is considered, in reality a fourth gradient could be present which is the longshore gradient. The direction of this gradient would be perpendicular to the cross section as is depicted in Figure 1.5.

In Figure 1.5 the three gradients are depicted with their respective positive direction. The gradients are a result of the incoming wave pattern schematized with the significant wave height H_s and the peak period T_p. In Figure 1.6 a small cut out of the filter is depicted with the parallel and perpendicular gradient directions.

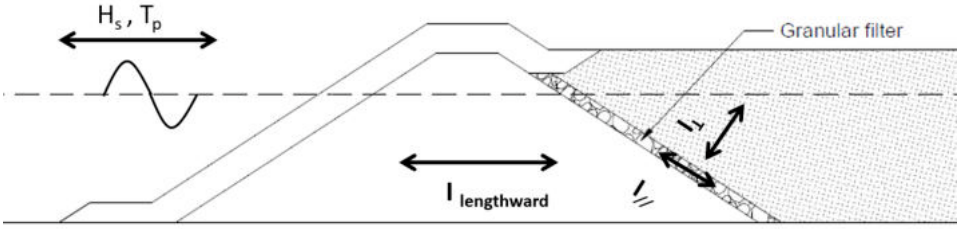

Figure 1.5: The directions of the three gradients

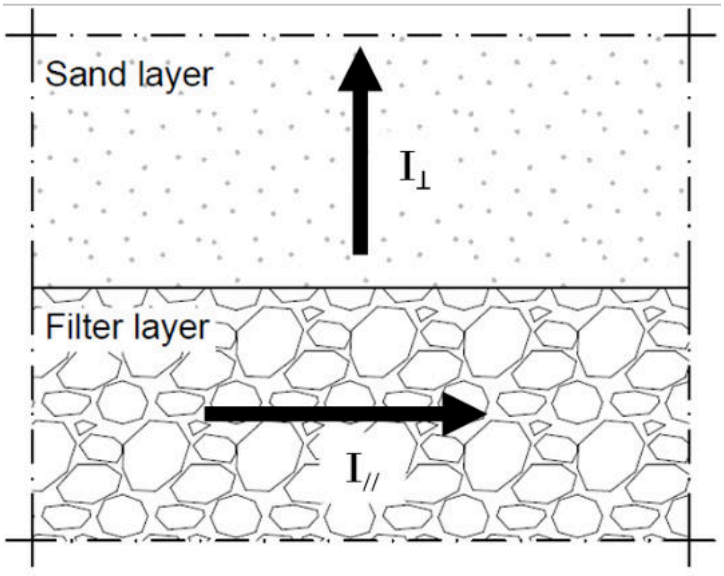

Figure 1.6: The directions of the two gradients in the filter-base layer region plus the position where they are determined

1.4. Glossary

Granular filter	Granular material used to create an interface through which no erosion can take place.
Base layer	One of two layers that are used for the quantification of a granular filter. The base layer is the layer with the smallest grain sizes.
Filter layer	One of two layers that are used for the quantification of a granular filter. The filter layer is the layer with the largest grain sizes.
Geometrically closed filter	Granular filter which is closed for sediment transport of the base layer.
Geometrically open filter	Granular filter in which the base layer can physically move through the filter layer.
Empirical model	Model based on empirical observations.
Numerical model	Mathematical model that simulates the physical behavior over a finite number of time steps.
Physical model	Simplified representation of reality to simulate physical processes.
Hydraulic gradient	Hydraulic head difference between two points divided by the distance between these points.
Critical hydraulic gradient	Hydraulic gradient for which there is just no erosion

2

Literature study

To form an image of similar and previous research, a literature study is performed. As this report is about the erosion through a geometrically open filter layer which is located landward of a breakwater, this literature study is split into two parts; the loads and the erosion induced by these loads.

In the first part, the loads on the structure are described. The load consists of flow through the breakwater. In this part, the flow is analysed, and it is concluded if the available research is sufficient to calculate the hydraulic loads on the rear face of the breakwater.

The second part is about the resistance against erosion. Therefore it analyses previous research that is performed on the erosion of sediments, and more specifically on the erosion through granular filter layers.

2.1. Hydraulic processes inside a breakwater core

Because of the variation in water levels in coastal regions, the core of breakwaters, and the sand used as land reclamation are subject to a porous flow. This flow results from a water level difference between the outside (sea) and the inside(land) of the structure. This difference can have various reasons, all with different flow characteristics. The two main water level differences occur because of wave action against the breakwater and tidal influence on the breakwater. The wave impact is a short time scale flow, with a period of a few seconds. Tidal influence has a period of multiple hours.

Both of these load are described separately. The research is started with the flow induced by the tidal motion. This flow through the structure is changed approximately every 6 or 12 hours, depending on the local climate.

2.1.1. Porous flow

Porous flow is the movement of a fluid from point A to B through a porous medium. The porous media induces friction on the water, which results in a pressure difference that is expressed as the dimensionless hydraulic gradient denoted with a small or capital i.

As all flow can be described with the Navier-Stokes equation, this is a good starting point. If water is considered incompressible and density differences can be neglected, the Navier-Stokes equation can be rewritten in the form of the Darcy equation(Equation 2.1). The first requirement is always valid as water is considered incompressible if the velocities are small, which is always the case inside a breakwater. The second requirement is not always valid; the water inside the land reclamation can be salt/brackish/freshwater while the seawater is saltwater, which gives a difference in density. However,

as the considered distances are small, the water is assumed to be homogeneous.

$$Q = kA\frac{(h_1 - h_2)}{L} \tag{2.1}$$

With: Q: Flow $[m^3/s]$, k: Hydraulic conductivity [m/s], A: flow area $[m^2]$, h_1 and h_2: Hydraulic heads of considered points [m], L: Length between considered points [m] (Schiereck and Verhagen, 2012)

This equation describes the relationship between a head difference and a flow. This implies that there will always be a flow through a porous medium when there is a head difference. Although this equation can be used for the long time scale flow which is induced by for instance a well or even tidal flow. It cannot be used for short time scale oscillatory flow such as wave penetration into a structure.

For these flows, the Forchheimer equation can be used (Forcheimer (1901) from (Schiereck and Verhagen, 2012)). The equation is depending on a linear (viscous shear stress) and a quadratic term (turbulent shear stresses) and is written as:

$$I = \underbrace{au}_{Viscous\ shear\ stress} + \underbrace{b|u|u}_{Turbulent\ shear\ stress} \tag{2.2}$$

With: I: Hydraulic gradient [-], u: Bulk velocity[m/s], a: Laminar coefficient [s/m], b: Turbulent coefficient $[s^2/m^2]$

If there is no influence of turbulence, it can be seen that Equation 2.2 reduces to Equation 2.1 with a = 1/k.

To be able to use this formula for non-stationary flow, another coefficient is added. This is called the extended Forchheimer equation (Polubarinova Kochina (1962) from (Schiereck and Verhagen, 2012)). In this equation, a third term is added. This term is time-dependent. The equation is:

$$I = au + b|u|u + c\frac{\partial u}{\partial t} \tag{2.3}$$

With: c: Time-dependent turbulent coefficient $[s^2/m]$

Coefficients ”a”, ”b” and ”c” are subject to previous research, both have been determined empirically by multiple researchers amongst others; (Kozeny (1927), Carman (1937), Ergun (1952), Engelund (1953), Koenders (1985), Den Adel (1987), Smith (1990) and van Gent (1993) from (Muttray and Oumeraci, 2005)). These empirical relations all consist of a relation between the porosity-gravitational acceleration and a relevant diameter. For the ”a” coefficients also the kinematic viscosity is taken into account. An overview of the formulae for the coefficients a,b and c can be found in Muttray and Oumeraci (2005)

2.1.2. Wave propagation through breakwater

The formulas discussed in the paragraph above can be used for flow through porous media which are fully submerged and rectangular shaped. This means that the formulae can compute the flow inside the breakwater and inside the sand layer. However, the distribution of pressures from the open water surface to the inside of the breakwater cannot be calculated with these methods.

Most of these researches (Burcharth et al., 1999),(Muttray and Oumeraci, 2005),(Vanneste and Troch, 2012) are focussed on the wave attenuation in a breakwater with an open rear side, for example the breakwater in Figure 2.1a. Meaning that the excess pressures inside of the breakwater form a new transmitted wave on the landward side of the breakwater. However Polidoro et al. (2015) did some tests with a breakwater with a closed rear side. The breakwater considered in this thesis also has a closed rear side, see Figure 2.1b, which makes the latter research representative.

For the research that is done in this thesis, it is essential that the pressures that work on the rear

face of the breakwater can be described. Most of all, it is important to get a clear picture of the directions of flow in this rear end. Also of high importance is the magnitude of the hydraulic gradients, before a design can be made.

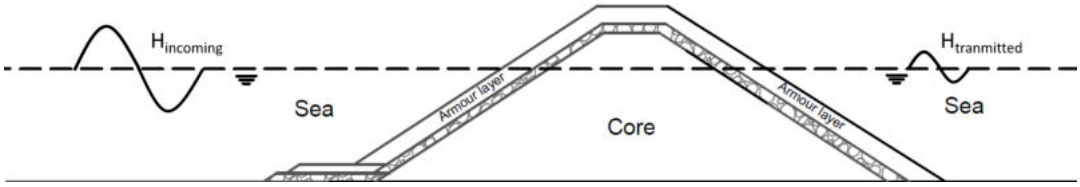

(a) Conventional breakwater design with water on both sides as is researched by amongst others: Burcharth et al. (1999),Muttray and Oumeraci (2005) and Vanneste and Troch (2012), with incoming wave $H_{incoming}$ and transmitted wave $H_{transmitted}$

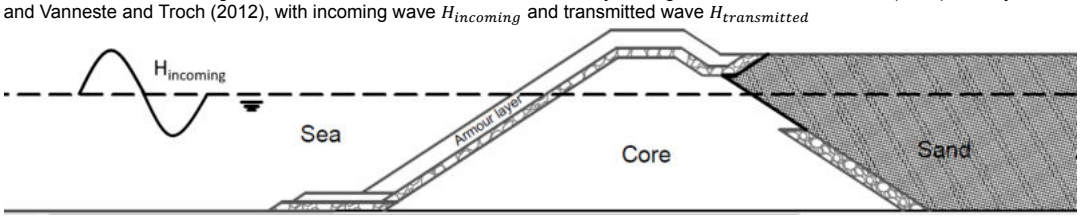

(b) Breakwater layout with land reclamation as considered in this thesis as well as in the research by Polidoro et al. (2015)

Figure 2.1: Example drawings of two different breakwater layout types which are studied for wave attenuation, with incoming wave $H_{incoming}$

2.1.3. Wave attenuation through breakwater

For the attenuation of wave energy inside a breakwater, multiple empirically derived methods are available. Most of these methods use a similar description as the Forcheimer equation does (Equation 2.3).

The most accurate method for the wave attenuation inside a permeable breakwater is the Vanneste and Troch (2012) method, of which an expanded description can be found in Appendix A.2. Vanneste and Troch (2012) designed a method for which the wave attenuation was split into two zones, with the separation line at the point of the highest run-up during wave impact, as can be seen in Figure 2.2. The breakwater that is considered in the research is a breakwater with an open rear side, see Figure 2.1a for the Vanneste and Troch (2012) breakwater and Figure 2.1b for a breakwater configuration as used in this thesis. A breakwater with an open rear side will have a lengthward gradient that is zero at the rear side.

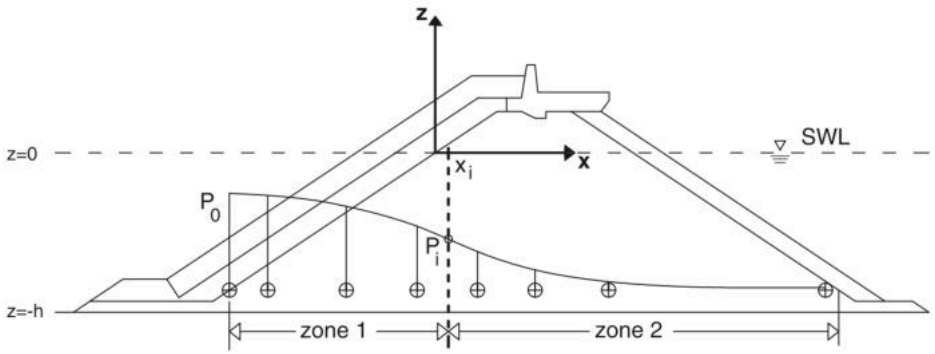

Figure 2.2: Definitions of zone 1 and 2 as proposed by Vanneste and Troch (2012), the transition location x_i is defined as the point of the maximum run-up on the breakwater core slope.

The model by Vanneste and Troch (2012) calculates the pressures inside the breakwater by subtracting the pressure at a location inside the breakwater, from the pressure at transition location x_i, see Figure 2.2. The pressure at a location inside the breakwater is calculated with the gradients at that location. Since the gradients are zero at the rear side of the breakwater as considered by Vanneste and Troch (2012), the pressures are also zero at the rear side. The calculation of hydraulic gradients in a breakwater with a closed rear side with the empirical model by Vanneste and Troch (2012) is therefore

not suited to calculate the pressure in the lower rear side of the breakwater. As a breakwater with a closed rear side can have a pressure difference over this rear side. The Polidoro et al. (2015) case can be used to compare the results with the calculation methods.

In Figure 2.3 the setup that was used by Polidoro et al. (2015) is depicted. In this research, the pressure distribution inside the breakwater for the abbreviation of geotextile was researched.

To check the Vanneste and Troch (2012) method, a similar calculation as done by Tutein Nolthenius (2018) has been performed to check whether this method can be used to give insight in the pressure gradient distribution, for breakwaters with a closed rear side. This calculation can be found in Section 3.1. Because the exact measurements of the Polidoro et al. (2015) experiment were not available, all distances are estimated to create a rough idea for the applicability of the Vanneste and Troch (2012) model.

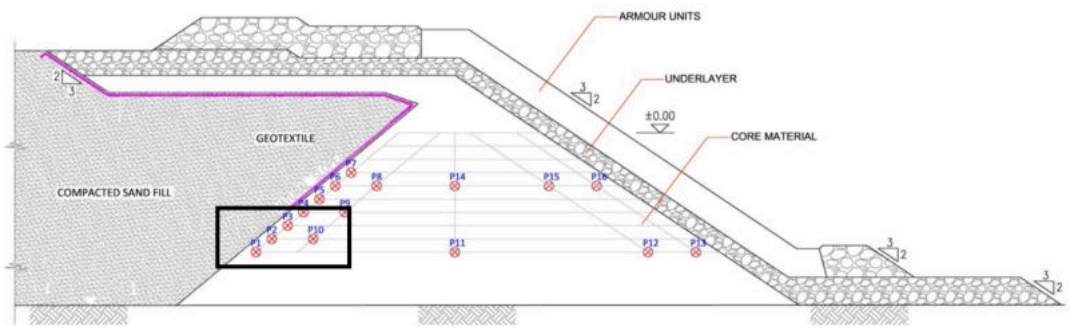

Figure 2.3: Example breakwater as used by Polidoro et al. (2015), in the black box the sensors used to calculate the gradients along the rear face are depicted.

The wave attenuation can also be determined with a transmitted wave through the breakwater. In the case of a transmitted wave through the breakwater, see Figure 2.1a, the breakwater is open at the rear side, but the pressure at this rear side is not zero. In a closed rear breakwater the transmitted wave will be reflected as the sand layer can be assumed to be impermeable for the short time scales that the waves have. The total pressure amplitude at the rear side will be double the transmitted wave height, as it is the sum of the incoming wave height and the reflected wave. The transmitted wave height can be calculated with a transmission coefficient, which is for small waves and relatively large freeboards: (Ahrens (1987), from (CIRIA, CUR, 2007))

$$C_t = 1.0 / \left(1.0 + \frac{H_s}{L_p} * \frac{A_t}{D_{n50}^2}^{0.592} \right) \tag{2.4}$$

With: A_t : Total cross-sectional area [m^2]

2.1.4. Hydraulic gradients and directions

Polidoro et al. (2015) only measured lengthward hydraulic gradients. In the tests, the rear side of the breakwater, which is sand in the actual design, was modelled with impermeable plywood. It expected in this research that this would be correct to model the sand layer that was behind this breakwater. In reality, there will be a permeable layer behind the breakwater, which will contribute to the attenuation of pressures. The output from the tests is given as the hydraulic gradients. The hydraulic lengthward gradients give the gradient attenuation through the breakwater core. This attenuation is the difference between the two graphs below (Figure 2.4.

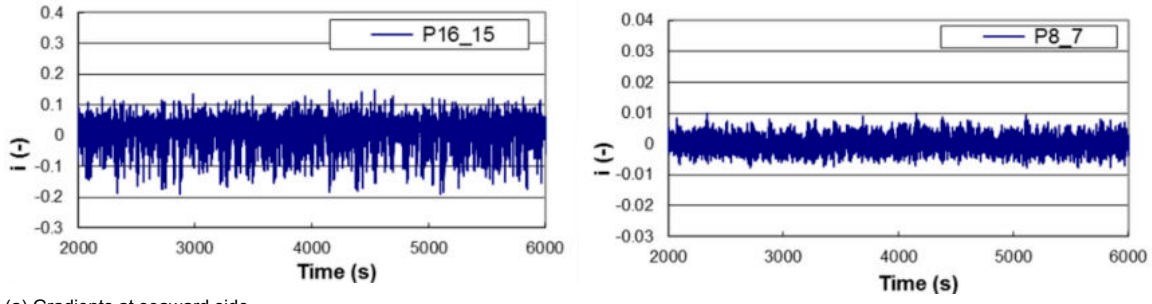

(a) Gradients at seaward side

(b) Gradients at landward side

Figure 2.4: Lengthward gradients as found by Polidoro et al. (2015). The locations of the sensors 6, 7, 15 and 16 can be found in Figure 2.3.

Another outcome of the experiment was the difference between negative and positive gradients during overload conditions. The direction of the gradients that were used is similar to the direction used in this research, which is depicted in Figure 1.5. The gradients that were measured over the rear interface during the base case test are depicted in Figure 2.5a. It can be seen from these that the gradient is relatively stable between +0.01 and -0.01, which means that there is a symmetrical result. In case of the overload conditions, the gradients are a lot larger, as expected with larger hydraulic loads. However, the gradients, in this case, fluctuate between +0.02 and -0.05. This means that there is a large outgoing gradient which is pointed from the rear end of the breakwater into the core.

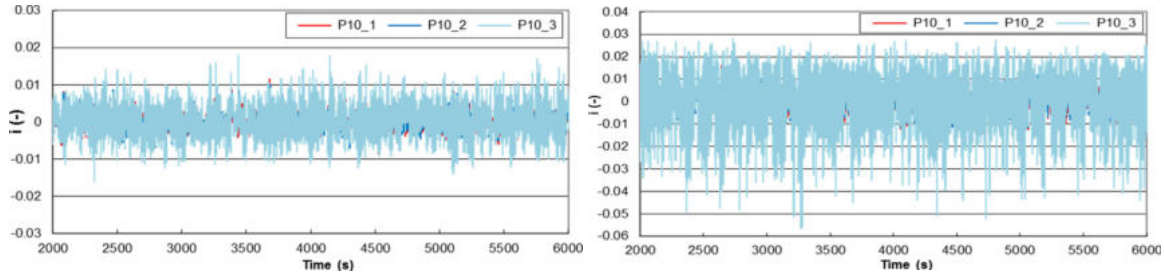

(a) Case 3, which is the base case.

(b) Case 9, which is the case with overload conditions.

Figure 2.5: Lengthward gradients as found by Polidoro et al. (2015). The locations of the sensors 1,2,3 and 10 can be found in Figure 2.3, within the black box. The exact composition of the case studies by Polidoro et al. (2015) can be found in Appendix B.1.1

The depth dependency was also determined in this research. For both tests that are described above the gradients are determined along the rear face of the physical modelled breakwater, which was an impermeable piece of plywood. The depth is plotted as the distance to the CD level. The mean water level was +2.25m to the CD level. The results are plotted below in Figure 2.6

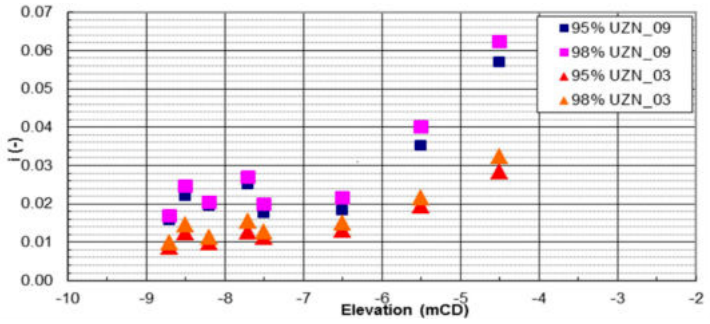

Figure 2.6: Depth dependency of the lengthward gradients as determined by Polidoro et al. (2015). The gradients are determined with two tests, UZN_09 with H_s= 5.80m and T_p = 10.5s and UZN_03 with H_s= 3.00m and T_p = 9.2s

It can be seen that in the physical model the range of parallel gradients along the rear side of the

breakwater was around 0.01-0.03, which can be used as a first estimation for the parallel gradients if the designed breakwater has a similar layout with a similar wave forcing.

2.1.5. Numerical modelling of flow through porous media

Besides the empirical and physical modelling, the flow and gradients inside a breakwater can be calculated with the use of numerical models (Jacobsen et al., 2015). Numerical models are a relatively new method for the computation of porous flow. The numerical models rely on scale model tests to be calibrated (Wolters et al., 2014). These numerical models solve simplified Navier-Stokes equation in discrete volumes which make up a grid. For the OpenFOAM model, the flow through porous media is analysed with the Forcheimer equation, which is explained in Paragraph 2.1.1. The parameters that are used in this equation are from van Gent (1995).

2.2. Erosion of sediments

The main goal of this thesis is to describe the movement of particles inside the open filter layer between the breakwater and the sand reclamation. To prevent the particles from eroding through the open filter layer, the resistance against this erosion has to be known. This resistance is investigated in this paragraph.

2.2.1. Sum of forces

Any movement is a result of an imbalance in forces. That is one of the fundamental physic law, formulated by Newton in the 17th century. For a particle inside of a sediment layer, this is no different. To see what the main cause is for the erosion it is first needed to see where the forcing is originated. An overview of all forces acting on a grain, either due to water or induced by the grain itself, inside a granular layer is given in Figure 2.7. The forces acted by the other grains on this grain are not taken into consideration in this paragraph but will be further elaborated in Paragraph 2.2.2.

Figure 2.7: Forces on a grain, with: 1. Drag force, 2. Lift force, 3. Gravitational force, 4. Shear force, 5. Normal force.

The particle will move when the sum of these forces is greater than zero. Although this is not expected as the grains in the middle of the layer are interlocked and will act as a single layer, the force will be balanced by the normal forces (number 5 in Figure 2.7). If multiple grains in a layer do not interlock, due to a large difference in grain size, erosion can occur, and therefore a critical velocity can be obtained. This will be the case at the boundary between the open filter and the sand, which will be elaborated in Paragraph 2.3

2.2.2. Arching

If the particles do not interlock, there is another mechanism that can take place at the boundary between the sand and the open filter layer. This mechanism is described as arching (Schiereck and Verhagen, 2012). Arching is the interlocking of particles to form a bridge over a gap through which the individual particles can protrude. This arching is illustrated in Figure 2.8. This arching is considered to be the main mechanism that influences the stability of the reversed open filter.

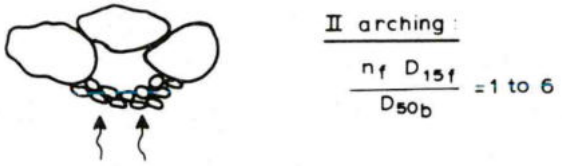

Figure 2.8: Soil arching as illustrated by de Graauw et al. (1983)

This arching should not be confused with the blocking of granular filter pores as depicted with b in Figure 2.9, which is sometimes referred to as arching. This type of arching is mostly responsible for the erosion resistance in geometrically closed filters, which are discussed in Paragraph 2.3.

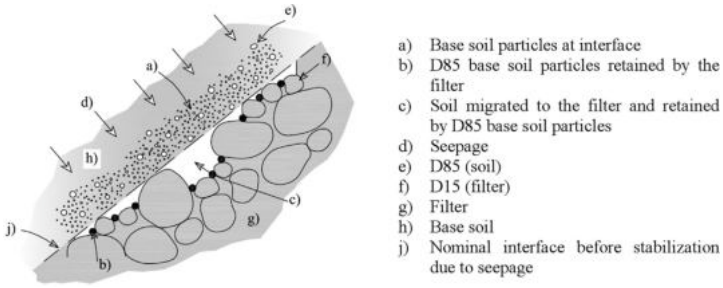

Figure 2.9: Arching by blocking the voids with the largest grains from the base layer, as it is proposed by Cedergren (1977). This type of arching is only possible with geometrically closed filters(See paragraph 2.3)

The third type of arching is described in the research by Chew et al. (2003), which states that soil can form an arch over a gap in a geotextile from 10 to 60mm, which is a larger scale than the other arching types. The arches considered in this research are strengthened by a load that is placed on top of the sand. This arching only takes place under certain circumstances, and it can help with increasing the erosion resistance, it is, however, beyond the scope of this thesis.

2.2.3. Initial movement

The stability of grains that are subject to flow is extensively studied. In this specific case, there is no load from above and also arching is not considered. This research focusses entirely on particles that are free to move and subject to a flow.

Granular particles have a certain critical velocity in which the uplifting forces on a grain are larger than the forces keeping it at its location (Paragraph 2.2.1). For the first estimation of movement, the formula created by Izbash (1930), from (Schiereck and Verhagen, 2012) can be used. This formula links the velocity to the grain size of the base material.

$$\Delta d = 0.7 \frac{u_c^2}{2 * g} \tag{2.5}$$

The critical velocity is researched by Shields (1932), from (Schiereck and Verhagen, 2012). If this critical velocity is reached or even exceeded the base material will be in motion. A diagram was produced that links stream velocity to the grain size. (Schiereck and Verhagen, 2012). This diagram can be used to determine the critical velocity for movement. For turbulent flow, the critical velocity can be determined with:

$$u_* = \frac{0.55 * \nu}{d} \tag{2.6}$$

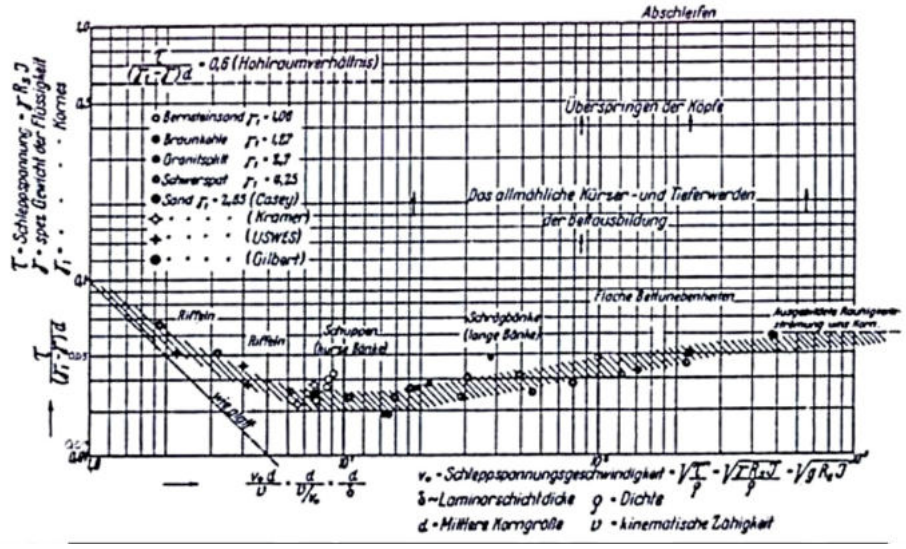

Figure 2.10: Original Shield diagram

2.3. Flow through granular filters

The resistance against erosion through a granular filter layer will be discussed in this part as the main topic of this research is the geometrically open filter layer which prevents sand from eroding through the core of a breakwater.

Granular filter layers have been the topic of research, starting with Terzaghi (1932), from (Schiereck and Verhagen, 2012) in the early 20th century. Terzaghi formed three closed filter rules that describe ratios between the base material and the granular filter material. These rules are:

$$\frac{d_{15F}}{d_{85B}} < 5 \qquad (2.7a) \qquad \frac{d_{60}}{d_{10}} < 10 \qquad (2.7b) \qquad \frac{d_{15F}}{d_{15B}} < 5 \qquad (2.7c)$$

Geometrically closed filter rules with rules for: Stability (2.7a), Internal Stability (2.7b) and Permeability (2.7c)

The theory of this set of rules is, that if these rules were followed, the sediments of the base layer could not physically move through the layer (2.7a), Both layers don't erode from within (2.7b) and the total set of layers is permeable to prevent pressure build-up (2.7c). Due to the fact that erosion through these granular filters is physically not possible, these are referred to as geometrically closed filters, also called closed filters in this thesis. However, in some cases, these rules are not strict enough, and erosion is occurring through a geometrically closed filter (Schürenkamp et al., 2015). The stability ratio is also used for a geometrically open filter to determine the resistance against erosion.

2.3.1. Geometrically open filters

In certain cases the construction of geometrically closed filters is impractical. In such cases, geometrically open filters can be used. These open filters are not only designed with the use of the material grading, but also the loads on these granular filters has to be taken into account. In this thesis the main focus is on granular geometrically open filters, whether or not the gradients through the considered open filter are sufficiently low that excessive loss of fill material does not occur.

2.3.2. Critical gradient

The critical gradient is determined in the literature as the gradient at which there is a continuous erosion of the base layer (de Graauw et al., 1983). If the occurring gradient is smaller than the critical gradient,

there will be no erosion. It is possible to have some movement in the layers as the velocity can be larger than the critical Shields velocity (Paragraph 2.2.3), but the sediment will return to its initial state when the gradient is lower, due to gravitational pull.

This cannot be the case with a base layer on top of an open filter layer. If there is downward movement through the open filter layer, the sediment cannot return, as the gravitational force pulls it down through the open filter layer instead of returning it back to its original position. This means that the critical gradient has to be determined as the gradient for which there is just no erosion.

2.3.3. Previous research of erosion through breakwaters

The erosion of sediments through a breakwater core was investigated by Tutein Nolthenius (2018). In that study, the proposition that a geotextile at the rear of a breakwater could be abbreviated (Polidoro et al., 2015) was investigated with the use of a scale model. This research proposed that the sand would erode into the breakwater core, but create a stable interface inside this core. The research focussed on the interface of the infill in the breakwater core, which is depicted in Figure 2.11 with the assumed triangle of sand inside the breakwater core. The research focussed purely on parallel flow. In the research, it was found that an infill of sand in the breakwater core is stable from a parallel gradient of 0.046. This infill of sand into the breakwater had a stability ratio ($\frac{D_{15F}}{D_{85B}}$) of 63.2.

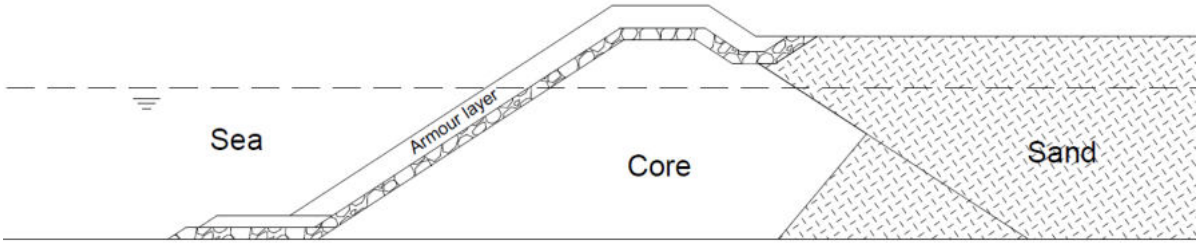

Figure 2.11: Breakwater configuration with geotextile shortening as studied by Tutein Nolthenius (2018), together with the sand infill inside the breakwater core.

Parallel or perpendicular gradients

To determine the resistance against the erosion of the open filter layer, not only the gradient but also the direction of the flow is of importance. The flow through the granular filter/sand layer can be divided into a perpendicular, parallel or a combination of both. In previous research, the flow was either perpendicular or parallel(See Paragraph 2.3), which is only valid if one of the two can be neglected.

Because the difference in permeability between the sand layer and the core material is very large, the velocity of the perpendicular flow is assumed to be small. If Equation 2.1 is used. It can be seen that with a large seepage length and a very low permeability, the pressures have to be very large to obtain a flow through the media. The perpendicular gradients, however, are large as the pressure attenuates a lot a quicker in the impermeable sand layer.

The pressure gradients that were used in the Polidoro et al. (2015) case cannot be used to give a decisive conclusion to the distribution of pressure gradients, because no sensors were located inside the modelled sand fill (see Figure 2.3), and the rear side was modelled as an impermeable layer. To estimate the pressures that work in this region, an OpenFOAM model is used. The results of the study can be found in Chapter 3

The critical gradients are determined inside the normative layer, which can be either the base or filter layer depending on the flow pattern (Figure 2.12).

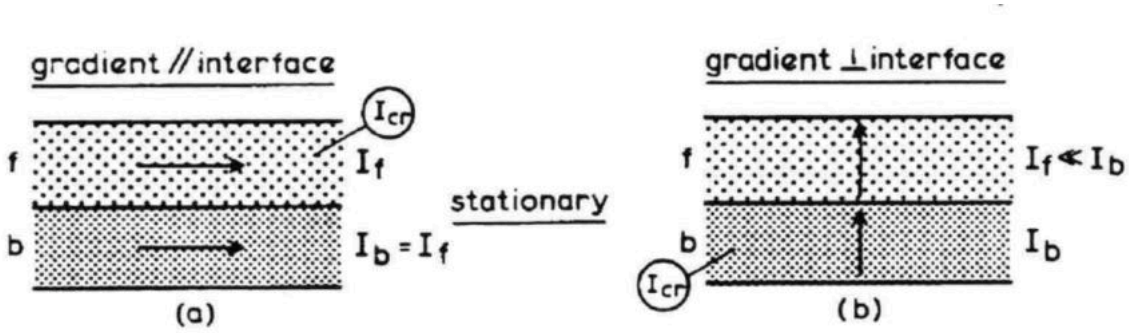

Figure 2.12: Locations were the gradients are defined, which are; in the parallel case(2.12a) the granular filter layer, and for the perpendicular situation (2.12b) in the base layer. (Schiereck and Verhagen, 2012)

Parallel gradients through the open filter layer

As most early research is performed for bed protection in river banks, parallel flow is mostly investigated. This research was initiated by de Graauw et al. (1983) with scale model tests for different flow patterns. For parallel flow de Graauw et al. (1983) did two tests. One with steady flow and one with cyclic flow. For both flow types de Graauw found an empirical relationship, this relationship was depending on the critical Shields velocity, for steady flow. The relation that de Graauw et al. (1983) found is Equation 2.8:

$$I_C = \left(\frac{0.06}{n_F^3 d_{15F}^{4/3}} + \frac{n_F^{5/3} d_{15F}^{1/3}}{1000 d_{50B}^{5/3}} \right) u_{*c}^2 \tag{2.8}$$

With: I_c: Critical gradient [-], n_F: Porosity granular filter layer [-], u_{*c}: Critical Shields velocity [m/s]

In this equation the two terms correspond to the laminar and the turbulent flow, similar to the Forcheimer terms in Equation 2.2. Four lines calculated with this formula are plotted in Figure 2.13. Besides this lines the datapoints that were measured are depicted. It can be seen that the tested critical gradients range from 0.03 until 1.2 [m/m].

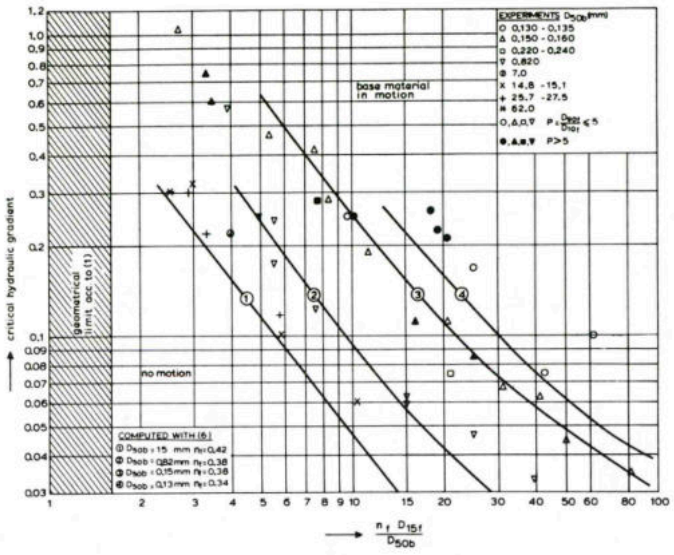

Figure 2.13: Critical parallel gradients as determined by de Graauw et al. (1983)

From Figure 2.13 it is clear that the critical gradient does not only depend on the ratio between the grain size of the granular filter and base layer, but also on the absolute size of both layers. It can be seen that with an equal filter/base ratio, the critical gradient decreases with increasing base layer grain

size.

Klein Breteler (1989) did some tests and developed a different formula which links the critical velocity to a critical gradient. A summary of this research can be found in Appendix A.1.2. Klein Breteler (1989) found that with an increasing slope, the erosion was lower.

A more recent design guideline for open filters is Wolters et al. (2012). This research created a formula which also takes into account the filter layer thickness, as this gives an estimate of the damping over the filter layer. The equation found by Wolters et al. (2012) is given below. A more extensive summary of this research can be found in Appendix A.1.2.

$$\frac{d_F}{D_{15F}} = 2ln\left(\alpha_k \frac{D_{50F}}{D_{50B}} \frac{1-\gamma V_{GF}}{1-\gamma V_{GB}} \frac{\Psi_{cF}}{\Psi_{cB}} \frac{\Delta_F}{\Delta_B}\right) \tag{2.9}$$

With: α_k coefficient related to turbulence intensity: α_k= 0.05 for low turbulence and α_k 0.5 for high turbulence. γ parameter determining allowable transport of bed material advised value: 0.625. V_G variation coefficient for non-uniformity of material, determined as: $1 - \frac{D_{15}}{D_{50}}$.

The formula created by Wolters et al. (2012) is not suitable for the base on top of an open filter combination. The process that is described in Paragraph 2.3.2 is dependent on the thickness of the open filter layer for a 'normal' filter configuration. For the considered open filter configuration this thickness is not of importance as the sediment will not return to its original position as long as it stays inside of the granular filter layer.

Perpendicular flow over the open filter layer

The perpendicular flow through both filter and base layer has been researched by de Graauw et al. (1983). The research pointed out that the gradient for a vertical perpendicular flow through both layers was equal to 1, as gravity pulled the particles into the base layer. For higher gradients, the resistance against erosion mostly depended on the formation of arches (Paragraph 2.2.2). These arches formed on the interface between the filter and base layer and were dependent on the stability criterion as proposed by Terzaghi Equation 2.7a). The formation of arches is depicted in Figure 2.8.

It was found by de Graauw et al. (1983) that the arches were broken under the influence of cyclic flow. This meant that with cyclic flow perpendicular to the interface, the gradients were much lower than with steady flow. The critical gradients as found by de Graauw et al. (1983) are depicted in Figure 2.14. For the granular open filter considered in this thesis, the lower limit should be lower than depicted in Figure 2.14, as the gravity works preferably for erosion instead of against the erosion.

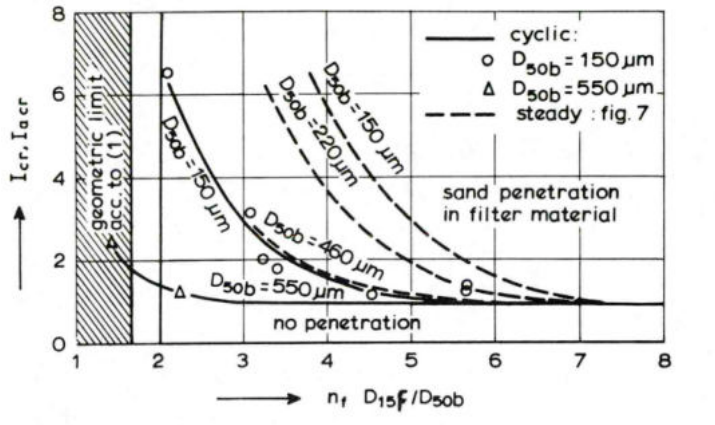

Figure 2.14: Critical perpendicular gradients as determined by de Graauw et al. (1983)

Schürenkamp et al. (2015) researched the perpendicular flow in more detail. They found that if there is a large cyclic flow, the formulae proposed by Terzaghi were not even sufficient. That means that with large cyclic perpendicular flows, the use of a geometrically open filter has to be designed very carefully.

Superimposed load on the layers

Since the open filter layer that is considered in this research is only constructed in the lower part of the breakwater, there is much soil that is placed on top of this filter layer. These soil particles all exert pressure on top of the filter layer by means of their weight. This pressure can be seen as a superimposed load.

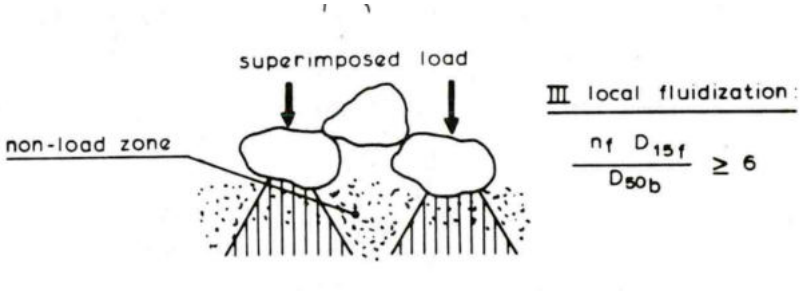

Figure 2.15: Superimposed load on the filter layer as depicted by de Graauw et al. (1983).

De Graauw et al. (1983) investigated the influence of this superimposed load on the critical hydraulic gradient for granular filters. The effect was only believed to have an influence for the perpendicular gradients, not for the parallel gradients. For this reason, all hydraulic gradients discussed in this paragraph are perpendicular gradients. The effect is visualised in Figure 2.15. It was found that if arching occurred, meaning that: $\frac{n_f D_{15f}}{D_{50b}} = 1 - 6$, the critical perpendicular gradient increases as can be seen in Figure 2.16 for soil A. What can be seen further is that if the granular filter to base grain size ratio is larger, $\frac{n_f D_{15f}}{D_{50b}} \geq 6$, the critical perpendicular gradient is less influenced by this load, as can be seen for granular filter B in Figure 2.16.

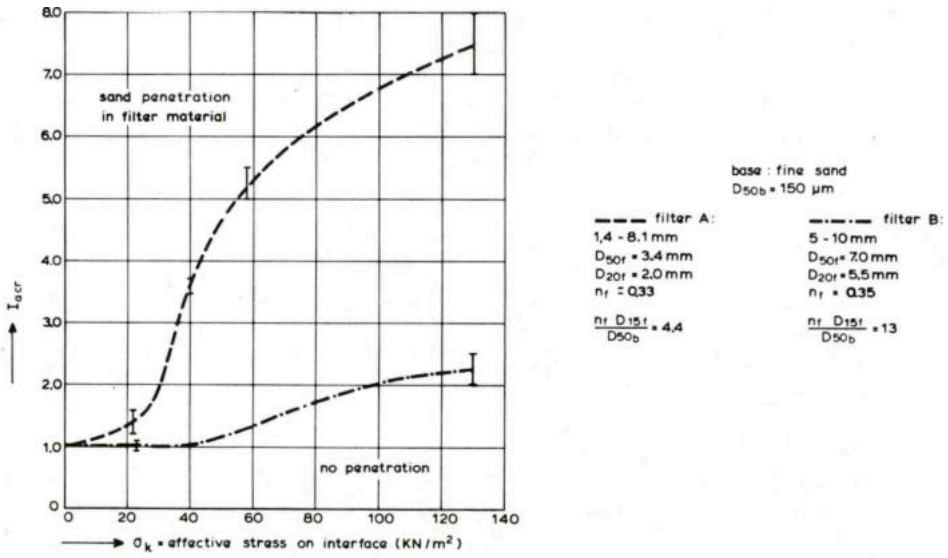

Figure 2.16: The effect of superimposed load on the critical perpendicular gradient of the base layer as found by de Graauw et al. (1983) In granular filter A the arching effect occurs (Figure 2.8 II), and in granular filter B local fluidisation occurs (Figure 2.8 III)

It is expected that the superimposed load only adds strength for a perpendicular flow pattern, as that is when the arches are most adding to the erosional resistance of the base layer.

2.3.4. Geotextiles

One or multiple granular filter layers can also be replaced with geotextiles in a design. The geotextile can prevent a layer from eroding, while keeping the interface permeable. Geotextiles have similar criteria for permeability and stability as Terzaghi has formulated for geometrically closed filters(Equations 2.7) (Schiereck and Verhagen, 2012). Because the research in this thesis is focussed on replacing a geotextile with a granular filter layer, no research is conducted for the applicability of a geotextile.

2.4. Conclusion Literature

The research that is for wave attenuation through permeable breakwaters is focussed on the attenuation through breakwaters with an open rear end. This means that the gradients at the rear side are zero in most research. The gradients from the research by Polidoro et al. (2015) can be used to get an estimate for the lengthward gradient, but for the occurring perpendicular and parallel gradients, no research was found. Although a lot is known about the flow inside of breakwaters, the literature cannot give an answer to whether the flow is perpendicular or parallel. This means that this has to be investigated before conclusions can be drawn. The Vanneste and Troch (2012) method seems promising to calculate the pressure attenuation inside a breakwater, but as the geometry of the breakwater is different, the results will differ as well.

There is little known about a sand layer which is placed on top of a geometrically open filter. The stability rules as proposed by Terzaghi (1932), from (Schiereck and Verhagen, 2012) should give an estimate for when a filter is geometrically open or closed, but this has to be checked for the reversed filter-sand layout, as research by Schürenkamp et al. (2015) showed that even geometrically closed filters could be hydraulically open. Furthermore, the use of a superimposed load could lead to an increase in critical gradient., but also that is not certain. This superimposed load is believed to be only of influence for perpendicular gradients as the arching effect has a smaller influence on parallel flow.

The mechanism considered to be governing for the resistance against erosion is the arching mechanism as proposed by de Graauw et al. (1983). This mechanism is according to that research only responsible for the perpendicular stability in a conventional filter. For the reversed filter the arching is believed to be governing for both the parallel and perpendicular resistance.

3

Determination of the hydraulic gradients

In Chapter 2, it was concluded that the knowledge about the flow regimes inside a breakwater is not sufficient to estimate the magnitude and directions of flow or hydraulic gradients purely based on the literature. For this reason, an estimate of the pressures is created using both empirical- and numerical models. As stated in the previous chapter, the erosion of a sand body through an open filter layer is dependent on a critical hydraulic gradient. This hydraulic gradient is the difference in pressure along a certain length. It can be approximated with:

$$I = \frac{\partial p}{\partial x} \approx \frac{\Delta p}{\Delta x} \tag{3.1}$$

With: p: Pressure head [m] and x: distance [m]

These pressures are difficult to obtain as there is little known about the pressure distribution in the rear side of breakwaters (Paragraph 2.1). To approximate these hydraulic gradients, both an empirical model as well as a numerical model, are used. Both models use the same breakwater characteristics.

3.1. Hydraulic gradients calculated with empirical model

Vanneste and Troch (2012) showed that the wave attenuation in a breakwater with an open rear side could be estimated with an empirical model (Paragraph 2.1.3). To check whether this can also be used to calculate the attenuation in a land reclamation breakwater, the method is compared to the research by Polidoro et al. (2015).

All calculations below are done with estimated measurements from drawings, graphs and photos and are only used for rough estimates. The results of two physical scale model tests performed by Polidoro et al. (2015), which can be found in Figure 2.5, are compared to calculations made with the Vanneste and Troch (2012) formulas. The sizes of the breakwater, together with the locations of the pressure sensors, are estimated with the physical model sketch (Figure 2.3).

All the hydraulic gradients from the empirical model and the Polidoro et al. (2015) research are lengthward hydraulic gradients. For that reason, all gradients that are discussed in this paragraph are lengthward hydraulic gradients. The description of the two individual tests together with an estimation of the breakwater sizes and the final calculations can be found in Appendix B.1. In the table below, only the results are depicted.

Elevation w.r.t. still waterline	Test 3 (H_m0 = 3.00m, T_p = 9.2s)		Test 9 (H_m0 = 5.80m, T_p = 10.5s)	
	$\frac{I_{Polidoro}}{I_{Vanneste,1}}$	$\frac{I_{Polidoro}}{I_{Vanneste,2}}$	$\frac{I_{Polidoro}}{I_{Vanneste,1}}$	$\frac{I_{Polidoro}}{I_{Vanneste,2}}$
$[m]$	$[-]$	$[-]$	$[-]$	$[-]$
-8.75	1.5	15	2.1	2.0
-8.25	11	5.5	3.3	3.5
-7.75	8.0	16	2.5	6.8

Table 3.1: Overview of the comparison between the Polidoro et al. (2015) test results and the Vanneste and Troch (2012) empirical calculation, for each test performed by Polidoro et al. (2015), two estimated distances are used, which can be found in Appendix B.1.2. The outcomes give the ratios between the calculated lengthward gradients and the measured gradients with the physical model.

The comparison is done for the two physical scale model tests performed by Polidoro et al. (2015) of which the results can be found in Figures 2.5a and 2.5b. The wave parameters can be found in Table 3.1. Both tests have a upper and a lower bound, which are calculated with two different estimations of the length scales.

The difference between the calculations and the results by Polidoro et al. (2015) can be found in Table 3.1. For both cases the results of the calculation differ a lot from the model tests. This was expected, not only because of previously mentioned reasons, also the differences in breakwater design play a significant role (Closed and open rear side, see Paragraph 2.1.2). The Vanneste and Troch (2012) model underestimates the hydraulic gradients for every case as is expected.

3.2. Hydraulic gradients from numerical model

Because there is no information about the range of hydraulic gradients in both parallel and perpendicular direction on the rear side of a breakwater, an OpenFOAM model is used to come up with the hydraulic gradients that are found inside a real-life structure. The used numerical model was produced at Van Oord. Although this model is not yet scientifically verified, the results can give an estimation of the occurring pressure distribution over the granular open filter layer. The main goals of this model are:

- Understanding the relation between the two directions of hydraulic gradients($I_\perp$ and $I_\parallel$).
- Finding the order of magnitude of the occurring hydraulic gradients to be used in a physical scale model.

The model has the same properties like that are mentioned in Paragraph 2.1.5, which means that it uses the Forcheimer equation with the resistance coefficients as described by van Gent (1995). The turbulence model that is used is a Reynolds average turbulence model, the $k-\omega$ model.

Figure 3.1: Virtual wave flume and breakwater as modelled in OpenFOAM. The dotted box depict the area of interest where the open filter is located.

The breakwater is modelled inside a virtual wave flume. This wave flume is depicted in Figure 3.1. The area of interest is depicted with the dotted box. In this area of interest, three different layers are present; the rubble mound, the sand fill and the granular open filter in between those layers. The layout of the model is similar to the breakwater that can be seen in Figure 1.2. These three layers are modelled with the following properties:

Layer	Porosity [-]	D_{50} [m]
Core	0.40	0.22
Granular filter	0.40	$01.45 * 10^{-}4$
Sand fill	0.36	$10^{-}4$

Table 3.2: Layer input coefficients for the used OpenFOAM model

The modelled wave climate in the OpenFOAM model is an irregular JONSWAP spectrum with a H_s of 3.5m and a T_p of 11s. The water depth h is 12.4m. The duration of a single simulation is 250s. The water level at the incoming boundary is plotted and can be seen in Figure 3.2. What can be seen is that the highest wave enters the boundary at t =188s

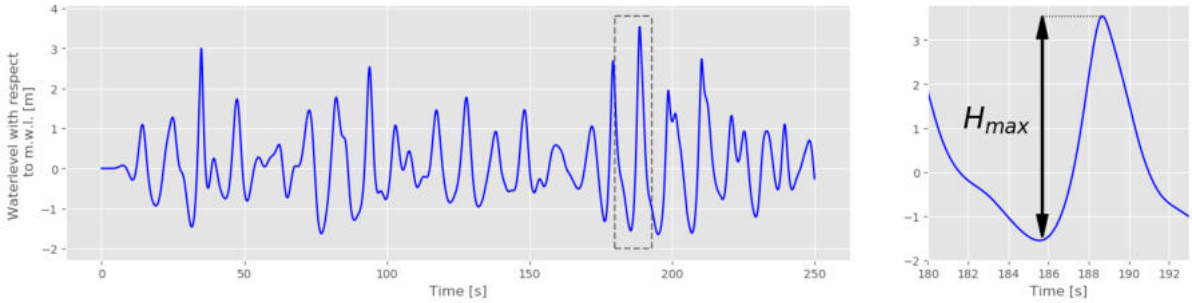

(a) (b)

Figure 3.2: Water level during the simulation, the dashed line indicates the highest wave of the simulation, which is shown in the cut-out on the right figure

The highest wave from this spectrum is the wave at T = 186[s] depicted in Figure 3.2b. Since the highest waves are responsible for the highest gradients, this wave will produce the largest gradients. The maximum wave height of the spectrum is H_{max} = 5.1m.

3.2.1. Comparison numerical model with physical tests and empirical model

To see whether the calculations with the empirical model by Vanneste and Troch (2012) can be used for this situation, a calculation is performed with the empiricalVanneste and Troch (2012) model with the same input parameters as the numerical OpenFOAM model. The calculations were done on the measurements points depicted in Figure 3.3, these points are placed on the depths for which the Vanneste and Troch (2012) was validated.

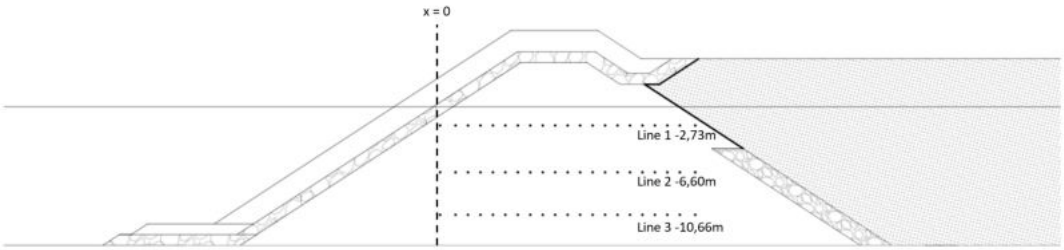

Figure 3.3: Measurement points used to evaluate the OpenFOAM model that was used. The three dotted lines depict the locations of the numerical pressure transducers on the z/h lines of -0.86,-0.53 and -0.22, which coincide with the locations for which the empirical model of (Vanneste and Troch, 2012) was calibrated. The image is not on scale.

As the empirical models that could be used for the calculations of the wave attenuation through the breakwater are all created for a breakwater with an open rear side, the gradient at this rear side is determined to be zero at this rear side interface. In this paragraph, the pressures along the rear interface are therefore considered to be a better estimate of the process at this rear side. In Figure B.4

the pressure distribution along the three lines as depicted in Figure 3.3 are depicted. In the figure, the maximum hydraulic pressures in the breakwater, during the 250-second simulation, are depicted.

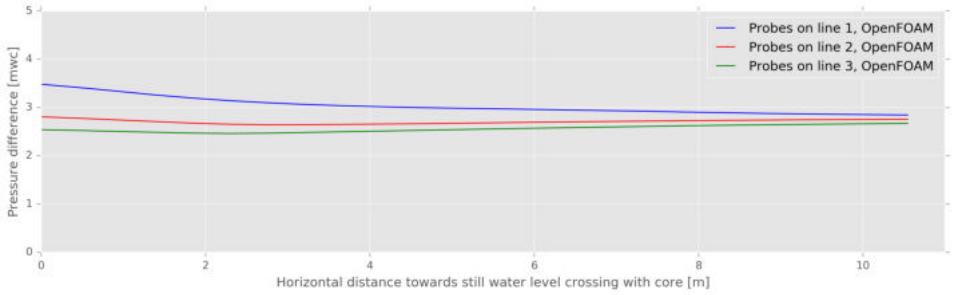

Figure 3.4: Maximum pressures, from OpenFOAM, at the three lines inside the breakwater core as depicted in Figure 3.3. In that figure also the zero point of the x-axis is depicted

It can be seen that the pressures decrease in the first part of the breakwater, but do not decline further in the breakwater. The pressures at the same points are also calculated with the empirical model by Vanneste and Troch (2012). The pressure head calculated with this method is depicted in Figure 3.5. Because the empirical model is created for a breakwater with an open rear end, it is believed that the gradients differ a lot. The gradient is zero at the rear side of the breakwater. The hydraulic pressure attenuation inside the breakwater is believed to be more comparable than the gradient. The pressure on the rear side of the considered closed rear side will be double the pressure on the rear side of a breakwater with an open rear side. This will be due to a reflected wave.

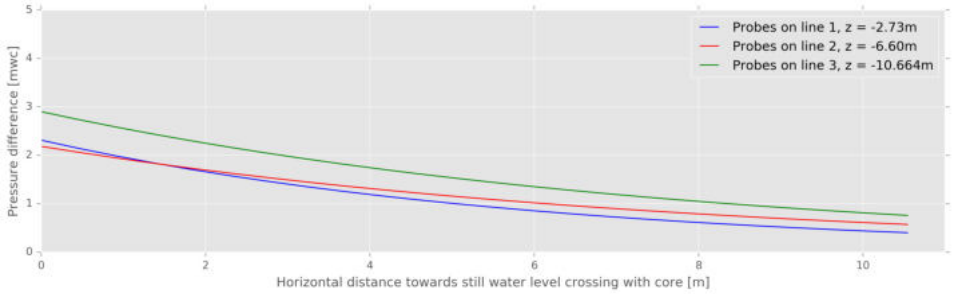

Figure 3.5: Maximum pressures, calculated with the empirical model by Vanneste and Troch (2012), at the three lines inside the breakwater core as depicted in Figure 3.3. In that figure also the zero point of the x-axis is depicted

With the comparison of these two figures, it was concluded that the model by Vanneste and Troch (2012) suitable to calculate the pressure attenuation.

A calculation performed with the transmitted wave height as discussed in Paragraph 2.1.3 gave the following transmission coefficient; C_t= 0.55 [-], which will result in a wave of 2.8m. This transmitted wave can also be seen as the pressure difference at the rear side of the breakwater. If this wave height is compared with Figure B.4, it can be seen that the pressure difference calculated with the transmitted wave is similar to the pressure difference calculated with the OpenFOAM model.

Besides the comparison of the hydraulic pressures with empirical models, the hydraulic gradients from the numerical model have been compared to the results from the physical model tests performed by Polidoro et al. (2015). The maximum lengthward hydraulic gradients as calculated with the OpenFOAM model are depicted in Figure 3.6. The results from the physical model tests were available at the seaward and landward side (see Figure 2.4 in Chapter 2). The attenuation of those hydraulic gradients is similar to the lower two lines, line two and three, from OpenFOAM.

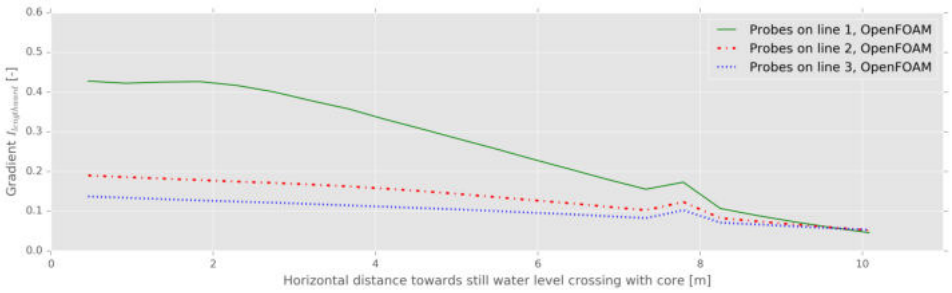

Figure 3.6: Maximum lengthward gradients, as determined with OpenFOAM, at the three lines inside the breakwater core as depicted in Figure 3.3. In that figure also the zero point of the x-axis is depicted

The pressures of both the numerical model, depicted in Figure B.4, and empirical model are compared, but give a different number which is due to the calculation of the model by Vanneste and Troch (2012), with the use of the lengthward gradients in the breakwater. It was seen in the research by Polidoro et al. (2015) that the model, as proposed by Burcharth et al. (1995) from (Polidoro et al., 2015), was a better estimation of the wave attenuation. As all calculations in this paragraph are only compared with the results from a single run with a numerical model and the empirical models were validated for a different layout, the results have considerable uncertainty.

3.2.2. Hydraulic gradients from the numerical model

After these runs, the OpenFOAM model was used to extract the range of hydraulic gradients that are present inside the breakwater, the direction of these hydraulic gradients and the velocity field inside the breakwater. This would show the appearing behaviour of flows inside of the breakwater. This can be used to design a more precise setup for testing but most importantly see to what extent the results from the physical model tests can be translated to reality. Since the hydraulic input into the model was an irregular wave field, the resulting hydraulic gradients are also irregular. For this reason, first, the hydraulic gradients are plotted against the time for the different sensor pairs both in perpendicular gradients and also for parallel gradients, after which the 2% highest gradients are plotted for both directions. This 2% gradient is determined as 2% the highest gradients during the entire interval, which is the

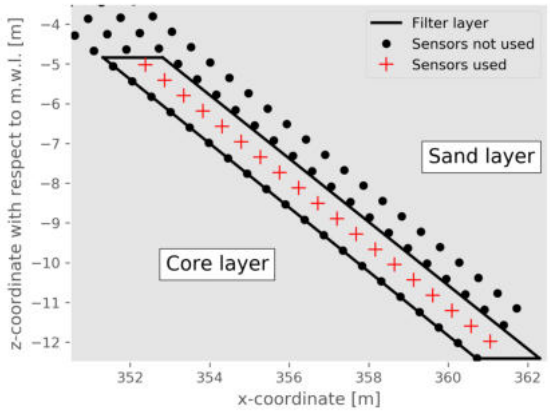

(a) Location of the sensors in the granular filter layer. For the calculation of the parallel hydraulic gradient, $I_{\parallel}$

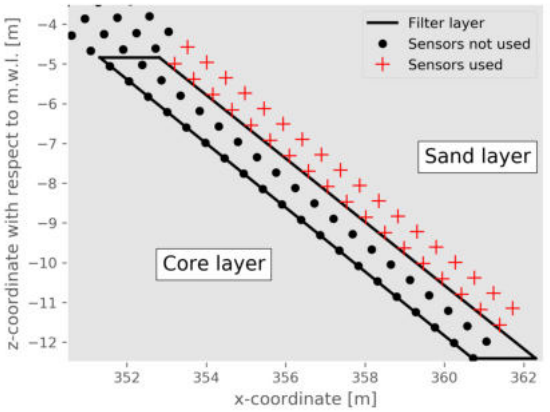

(b) Location of the sensors in the sand layer. For the calculation of the perpendicular hydraulic gradient, $I_{\perp}$

Figure 3.7: Locations of the numerical sensors that are used to extract the hydraulic gradients from the OpenFOAM model. In both figures, the plusses represent the sensors that are actually used for the calculations.

Both hydraulic gradients are determined on the location where the hydraulic gradient is governing for erosion. For the parallel hydraulic gradients, this is inside of the granular filter layer, the perpendicular hydraulic gradient is determined inside of the sand layer (See Paragraph 2.3.3). The hydraulic gradients are determined by the difference in pressure divided by the absolute distance between the two virtual

probes. The positive direction of these hydraulic gradients is depicted in Chapter 1. The location of the sensors with respect to the granular filter layer can be seen in Figure 3.7.

Parallel hydraulic gradients
The parallel hydraulic gradients are calculated inside the granular filter layer. This calculation was performed for every pair of sensors over the entire granular filter layer. The results are plotted for three sensor pairs over the filter layer and depicted in Figure 3.8a,b and c. The depth dependency of the hydraulic gradient can be seen from these figures. The uppermost sensors pairs have a maximum parallel gradient of around 0.015 while in the lowest part almost no parallel gradient is present.

Another thing that can be seen is the number of waves that reach the filter layer. Only 22 peaks can be distinguished in Figure 3.8a while the original signal contains 27 peaks. Due to the porous flow inside the breakwater, the waves are attenuated by friction. This loss of energy makes the signal from the hydraulic gradients much smoother than the original wave signal outside the breakwater. The gradient signal for most waves is similar in Figure 3.8a, which is around 0.005. At T>200s the gradient is much larger, resulting from the consecutive large waves.

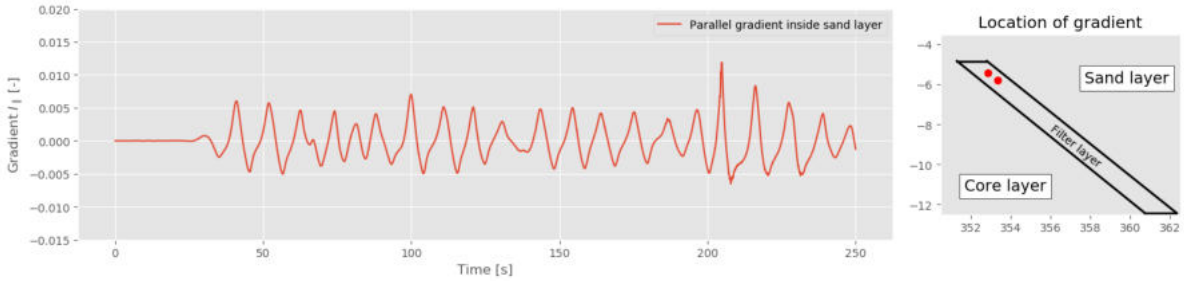

(a) Parallel hydraulic gradient in the granular filter layer over the highest part of the granular filter.

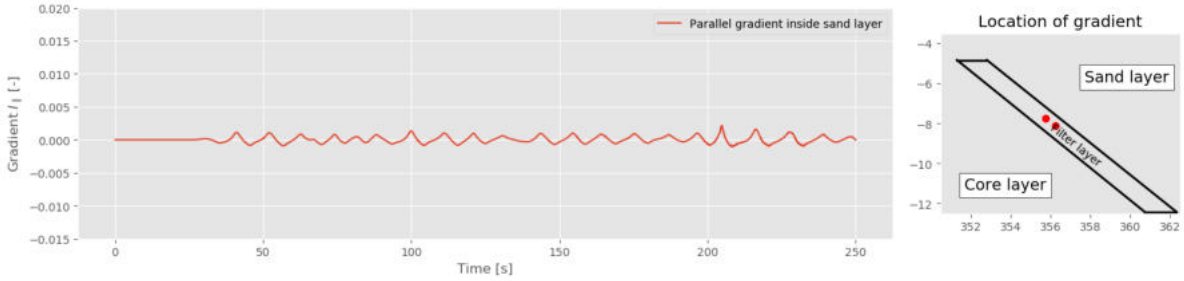

(b) Parallel hydraulic gradient in the granular filter layer over the middle part of the granular filter.

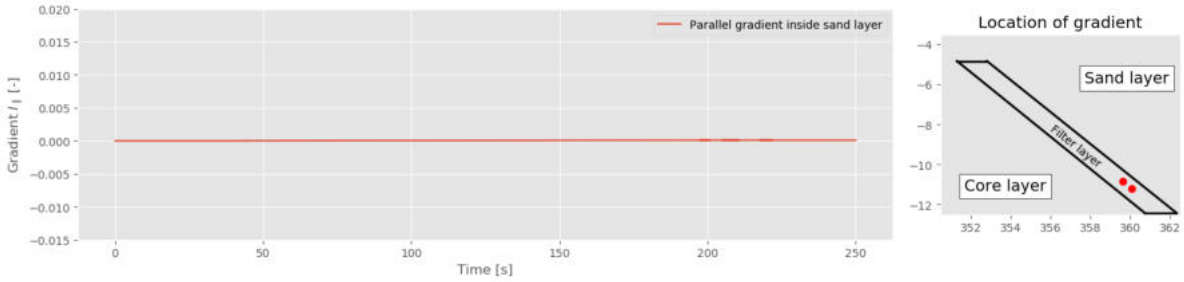

(c) Parallel hydraulic gradient in the granular filter layer over the lower part of the granular filter.

Figure 3.8: Parallel gradients over the granular filter layer for three different sensor pairs. The right graphs show the two sensors between which the hydraulic gradients are determined. These sensors are all within the filter layer.

The depth dependency over the granular filter layer can be seen better in Figure 3.9, where the absolute 2% largest parallel hydraulic gradients are plotted. It can be seen that higher in the granular filter the hydraulic gradients are much larger.

The outliers in the graph are possible due to the geometry of the OpenFOAM model. The outliers

are all located at the top of the granular filter layer, where the water flows in from the core into the top of the granular filter layer. These points are not used for the estimation of the occurring hydraulic gradient. The hydraulic gradient that is used as estimation is ranging from almost zero in the lower part of the granular filter layer up to almost 0.015 in the upper parts of the granular filter.

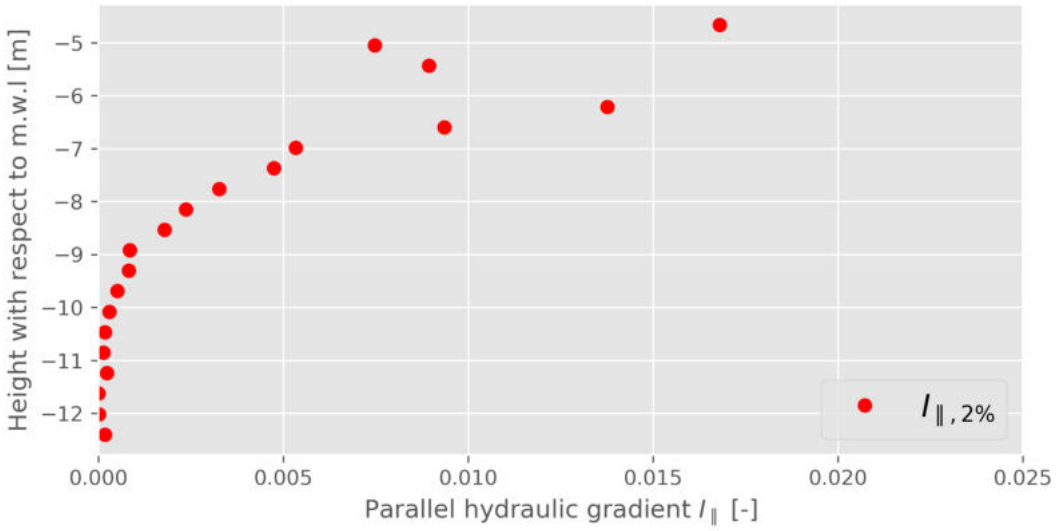

Figure 3.9: The 2% highest hydraulic parallel gradients through the granular filter layer.The granular filter is located at the -5m level. as modelled in OpenFOAM with respect to the mean water level

The hydraulic parallel gradients should not be influenced by the granular filter layer. This is checked with an additional run, where the properties of the granular filter layer were changed to be the same as the properties of the core, meaning that in that simulation no granular filter layer was present. The results of this simulation were exactly the same as the results depicted in Figure 3.9. This indicated that the filter layer did not influence the parallel hydraulic gradients.

Perpendicular hydraulic gradients

The perpendicular hydraulic gradients were calculated in the same way as the parallel hydraulic gradients, with the difference in pressure over two virtual pressure gauges divided by the distance between these sensors. The virtual pressure gauges used to calculate the perpendicular hydraulic gradients are all located in the sand layer.

The perpendicular hydraulic gradients are depicted in the same way as the parallel hydraulic gradients. First, the behaviour over the depth is plotted with three gradients and secondly the gradients are plotted quantitatively over the depth. The perpendicular hydraulic gradients do not change in shape of signal over the depth, which can be seen from the figures below.

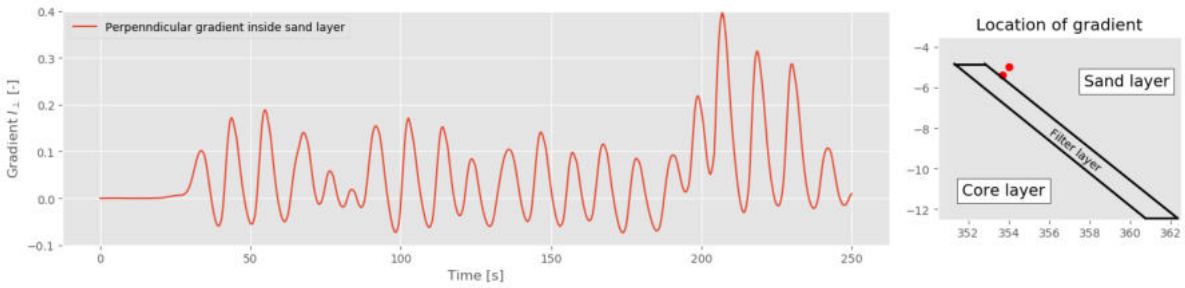

(a) Perpendicular gradient in the granular filter layer over the highest part of this granular filter.

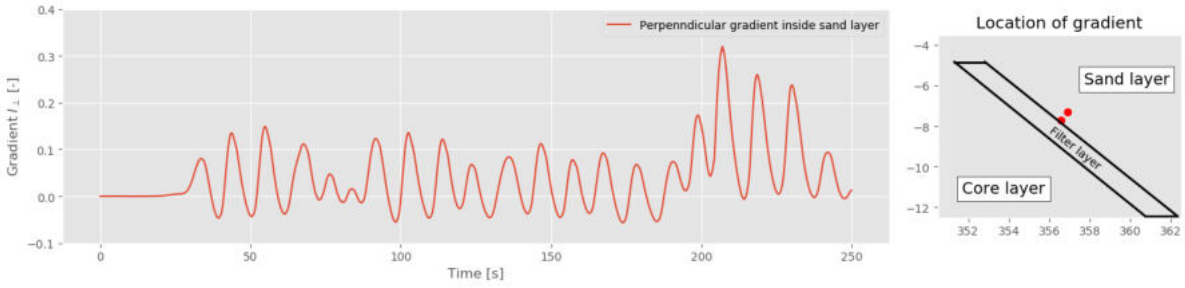

(b) Perpendicular gradient in the granular filter layer over the middle part of this granular filter.

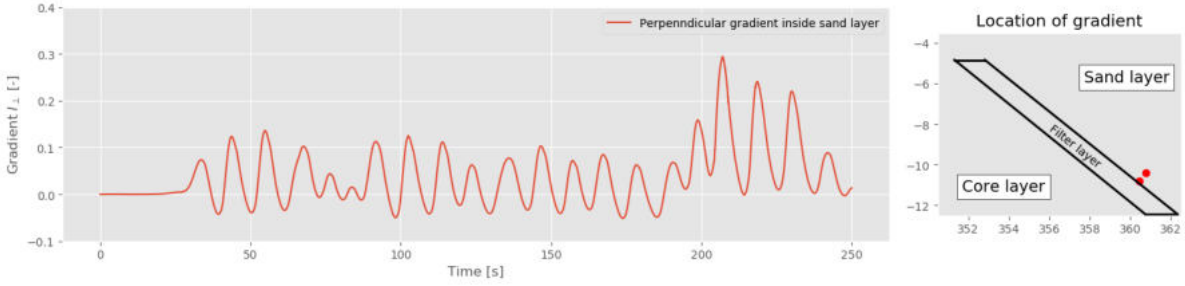

(c) Perpendicular gradient in the granular filter layer over the lower part of this granular filter.

Figure 3.10: Perpendicular gradients over the granular filter layer for three different sensor pairs. The right graphs show the two sensors over which the hydraulic gradients are determined. The locations of these sensors are all within the sand layer.

The excess pore pressure inside the breakwater core and granular filter material can be assumed to be similar over the interface, as these layers have a high permeability compared to the sand layer. The perpendicular hydraulic gradients, however, decrease with an increase in depth, which can be seen in either Figure 3.10 and Figure 3.11. This decrease in hydraulic gradient can be explained with the larger distance to the phreatic water level lower inside the filter layer.

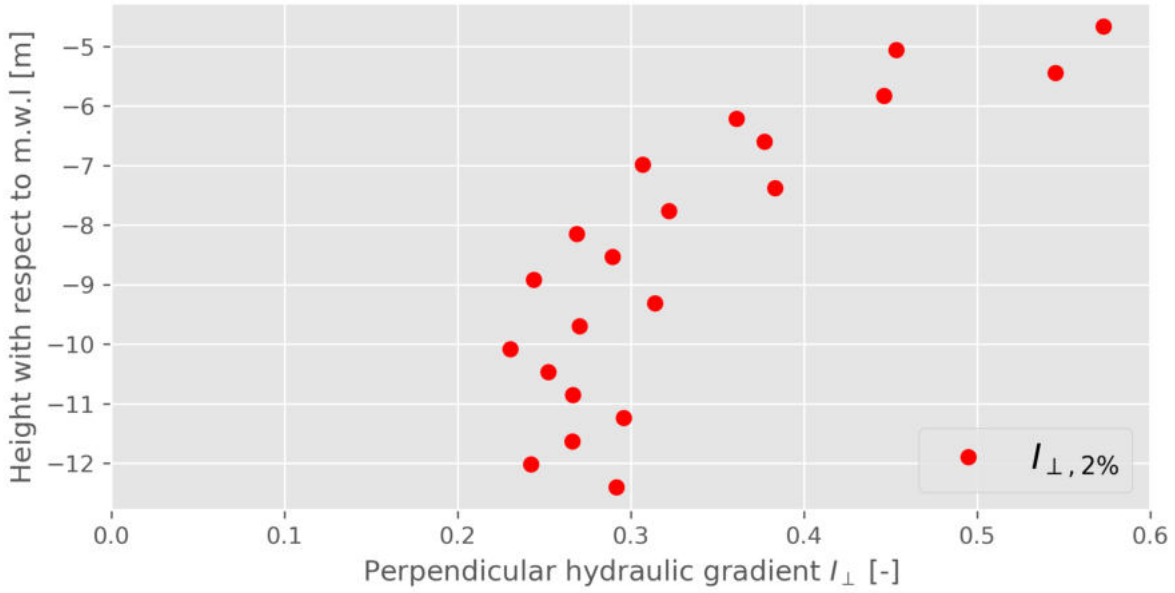

Figure 3.11: The 2% highest hydraulic perpendicular gradients in the granular filter layer. The top of the granular filter layer is located at the -5m level.

The hydraulic gradients that are calculated for the hydraulic perpendicular gradient are depicted in Figure 3.11. The hydraulic perpendicular gradients range from 0.2 to 0.5-0.6. The pressure over the sand layer can be described as a Darcy flow (see Paragraph 2.1.1). This means that the pressure should decrease linearly over the sand layer until the pheatric level. This indicates that the perpendicular hydraulic gradients would be equal to the excess pore water pressure in the granular filter layer divided by the distance to the pheatric level inside the sand layer.

The perpendicular hydraulic gradient in the middle of the filter layer is calculated with both the smallest distance between the point of interest and the pheatric surface and the perpendicular distance from the filter layer to this pheatric surface. These gradients are plotted together with the gradient calculated with OpenFOAM, that is also depicted in Figure 3.10b, in Figure 3.12. What can be seen is that the perpendicular hydraulic gradient calculated with OpenFOAM lies in-between the two calculated hydraulic gradients, with the shortest length being the largest gradient and the perpendicular the smallest gradient. This means that the actual distance is somewhere in-between.

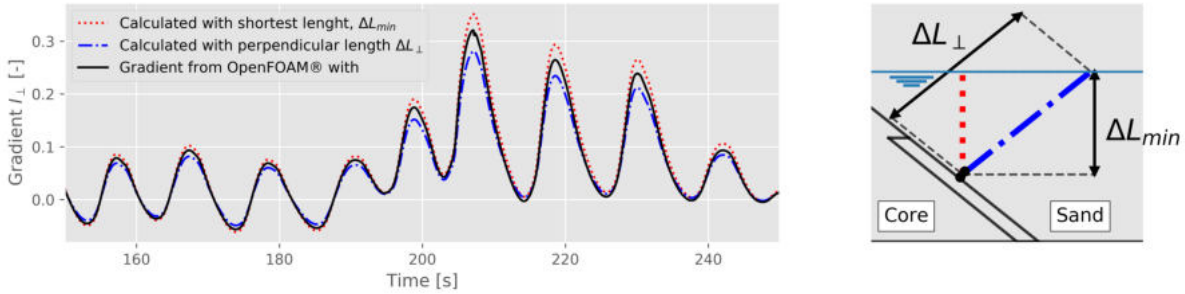

Figure 3.12: Perpendicular hydraulic gradient calculated in the middle of the filter layer. With the hydraulic gradient from OpenFOAM, the gradient calculated with the shortest length possible and the hydraulic gradient calculated with the length perpendicular to the filter layer.

3.3. Direction of flow

The directions of flow inside the granular filter was another point of interest. OpenFOAM gives the flow velocities as an output. The flow inside the breakwater and land reclamation are checked for directions. In this paragraph, three situations are depicted. At first, the situation during runup, meaning a high water level inside the breakwater. The second situation is during rundown with a low water level inside the breakwater. The third situation is during runup with a low water level inside the breakwater.

In Figure 3.13 the water level inside the breakwater is depicted on the left (Figure 3.13a) and the directions of flow at the same time on the lower rear of the breakwater on the right (Figure 3.13b). What can be seen is that the flow comes in from the top of the breakwater and it follows the sand-core interface down until it reaches the granular filter layer, from where it curves down to the bottom of the breakwater core (which is modelled as a closed boundary).

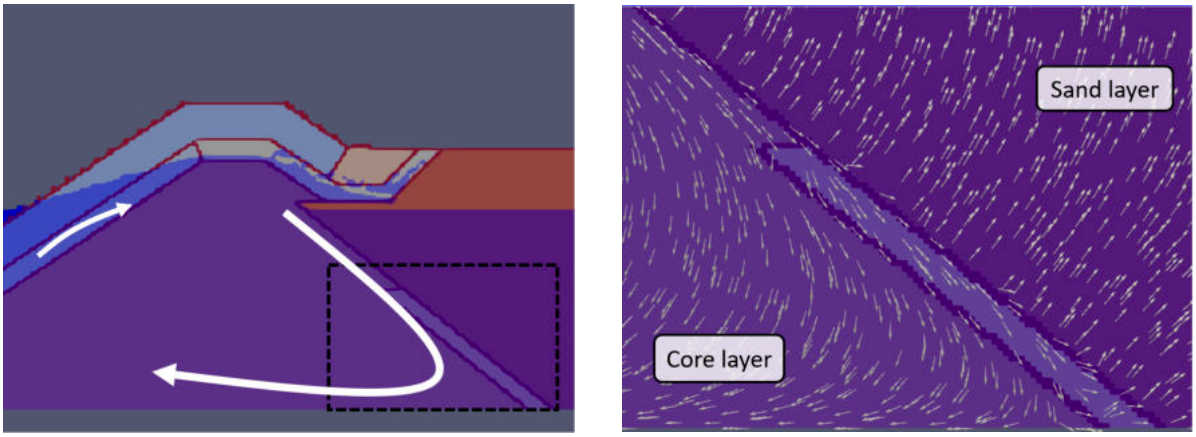

(a) Waterlevel inside breakwater

(b) Direction of flow through the granular filter.

Figure 3.13: Output of the OpenFOAM model during the inflow of a wave into the breakwater. The inflow is during the largest wave, at T =209 s. The arrows in Figure b are all equal in size and are only meant for directions and no magnitude. In Figure b the granular filter layer is depicted in between the sand layer on the upper right side and the core layer on the lower left side.

In Figure 3.14, the low water level inside the breakwater is depicted (Figure 3.14a) and the directions of flow that are induced by this water level (Figure 3.14b). What can be seen is that the direction of flow is mirrored with respect to the high water level.

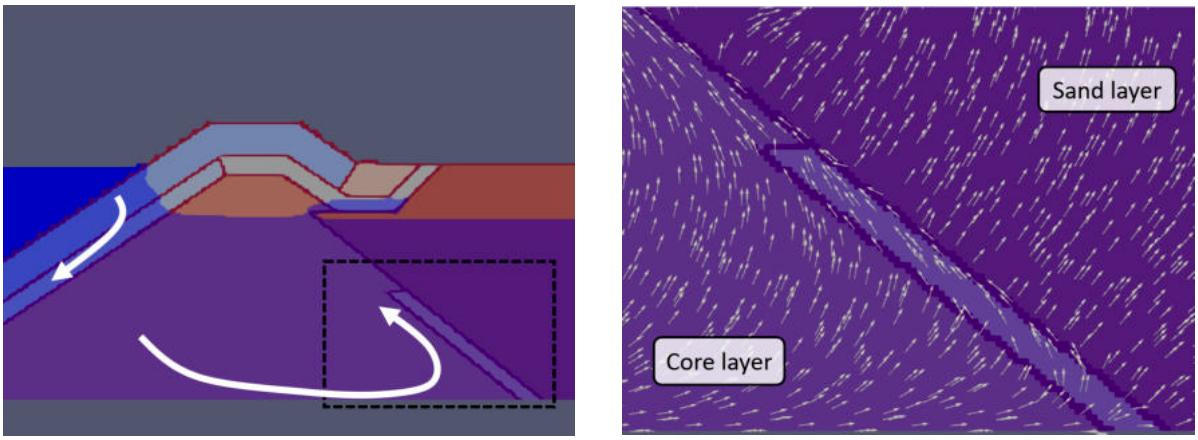

(a) Waterlevel inside breakwater

(b) Direction of flow through granular filter.

Figure 3.14: Output of the OpenFOAM model during the outflow after a wave has hit the breakwater. The outflow is at T =216 s. The arrows in Figure b are all equal in size and are only meant for directions and not for magnitude. In Figure b the granular filter layer is depicted in between the sand layer on the upper right side and the core layer on the lower left side.

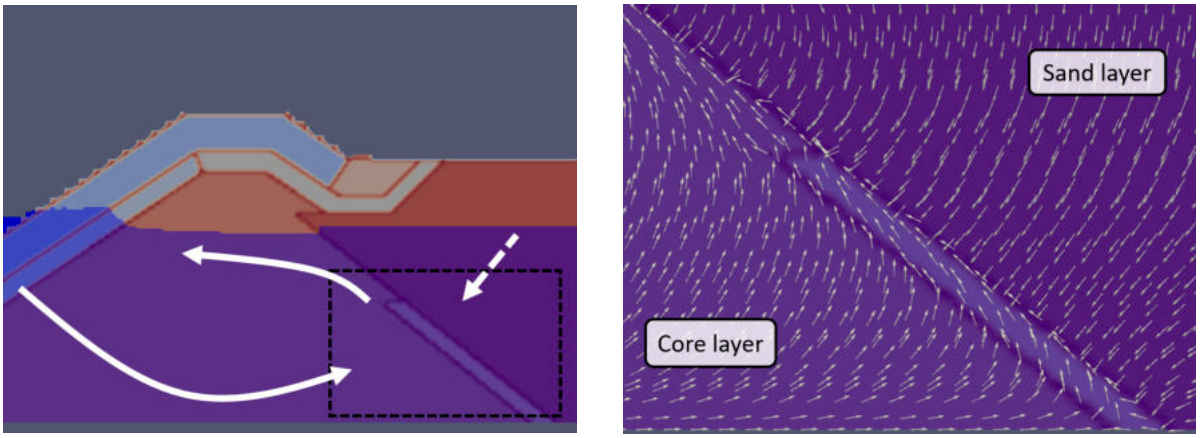

(a) Waterlevel inside breakwater

(b) Direction of flow through the granular filter.

Figure 3.15: Output of the OpenFOAM model during a low water level in the breakwater core. The outflow is at T =60 s. The arrows in Figure b are all equal in size and are only meant for directions and not for magnitude. In Figure b the granular filter layer is depicted in between the sand layer on the upper right side and the core layer on the lower left side.

In the situation depicted in Figure 3.15, the flow inside the breakwater is similar to the situation depicted in Figure 3.14. The difference is that the water level inside the sand layer is higher than the water level in the breakwater. This induces the flow outwards of the sand layer into the breakwater core.

For the other two situations, it can be seen that the flow into the sand layer is always inwards from the granular filter layer. In both situations, this is because the water level inside the breakwater is higher than the water level inside the sand layer. Due to the low permeability of the sand layer, the water level change inside this sand layer is slow. This means that the water level inside the sand layer needs more than a wave period to adjust to the water level in the breakwater.

3.4. Conclusion hydraulic gradients

The hydraulic gradients are important for a thorough understanding of the system as these gradients are responsible for the loads that work on the filter. The hydraulic gradients are determined for both directions ($I_{\parallel}$and $I_{\perp}$). In this paragraph, a conclusion is made about the magnitude, the depth dependency and the influence of irregular waves on the gradients.

- Magnitude of hydraulic gradients
  - Parallel hydraulic gradient
    The magnitude of the parallel gradient inside the granular filter layer was between 0.001 and 0.02 [-]
  - Perpendicular hydraulic gradient
    The perpendicular hydraulic gradients ranged from 0.2-0.6 [-] inside the sand layer.
  - Ratio of hydraulic gradients
    The ratio between the perpendicular and parallel hydraulic gradients is that the occurring perpendicular hydraulic gradient is more than an order of magnitude(20-50) larger than the parallel hydraulic gradients. This was expected as de Graauw et al. (1983) reported the same ratio for the critical hydraulic gradients.
- Depth dependency
  - Parallel hydraulic gradient
    The parallel hydraulic gradients were largely influenced by the depth. The gradients in the top of the filter layer were around 0.02 [-] and decreased exponentially towards zero in the lower parts of the filter layer.
  - Perpendicular hydraulic gradient
    The perpendicular hydraulic gradients were less influenced by the depth. Since these gradients are mostly influenced by the distance towards the phreatic surface. This distance is increased with increasing depth, but the decrease does not go to zero. The gradients start at 0.6 in the top of the filter layer and are 0.2 in the lower parts of the filter layer
- Behaviour irregular waves
  The highest waves contribute the most to the gradients. This was expected as the attenuation of higher waves needs a larger infiltration length (Vanneste and Troch, 2012). Both gradients are mostly influenced by consecutive high waves.

4

Model setup

As concluded in Chapter 2 little is known about the process of erosion through a granular geometrically open filter layer which is placed below a sand layer. For this reason, the design of these layers is uncertain even when the closed filter rules are used.

The feasibility of a physical model setup was tested by performing a preliminary test that is described in Appendix C.1. The preliminary test consisted of a tube with a sand layer on top of a granular open filter layer which was filled with water. There was no flow through the tube, and all loads were induced by shaking. This preliminary test showed that there is an apparent equilibrium possible on the sand-filter interface after 10 to 20 minutes without loading. This preliminary test, together with the uncertainties about the granular open filter below a sand layer design, have justified the use of a physical model.

The physical model setup described in this chapter was an evolution of five design iterations, where each iteration was an evolution of the previous setup. The iterations can be found in Appendix C.2. In this chapter, the final test setup is described together with the test sequence. The final model had two different configurations to force the flow into the two directions of gradients that were of interest. The two directions were respectively parallel and perpendicular, similar to the hydraulic gradients determined in Chapter 3. The two hydraulic gradient directions will be described independently.

4.1. Test setup

The model setup which was designed makes use of the same container used by Tutein Nolthenius (2018). The dimensions of the test setup are depicted, together with three sections in which the container was divided into, in Figure 4.1. Section A was where the left water level was measured. In section B, the granular filter and sand layer were placed. The plunger was located in section C. This plunger forces the flow through the setup and will be described in Paragraph 4.2

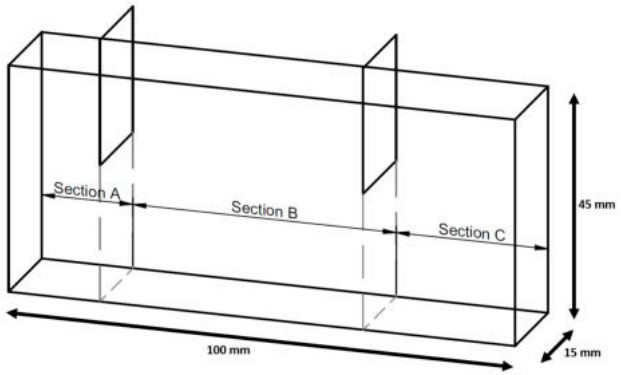

Figure 4.1: Schematic overview of the three sections in which the container was divided, the sizes of the container were: 1x0.15x0.45m and the widths of the three sections were from A to C: 0.18,0.52 and 0.3m

The three sections were separated with a wire mesh in the lower part and a plywood screen in the upper part. The mesh was used to keep the granular material inside section B while allowing the water to flow through. The plywood separation acted as a closed boundary between the sections.

As described above, two configurations have been designed inside the container. The first model setup was the parallel setup. In this setup, the top boundary of section B was closed airtight with a rubber seal, while section A and C were open. This forced the flow through the granular filter layer from section C to A and back; the direction of the parallel hydraulic gradient is depicted in Figure 4.2a.

In the perpendicular setup section A was closed with a plywood screen, while section B and C were open. This forced the flow from section C through both the sand and granular filter layer to the top of section B. This flow created the perpendicular hydraulic gradient as depicted in Figure 4.2b.

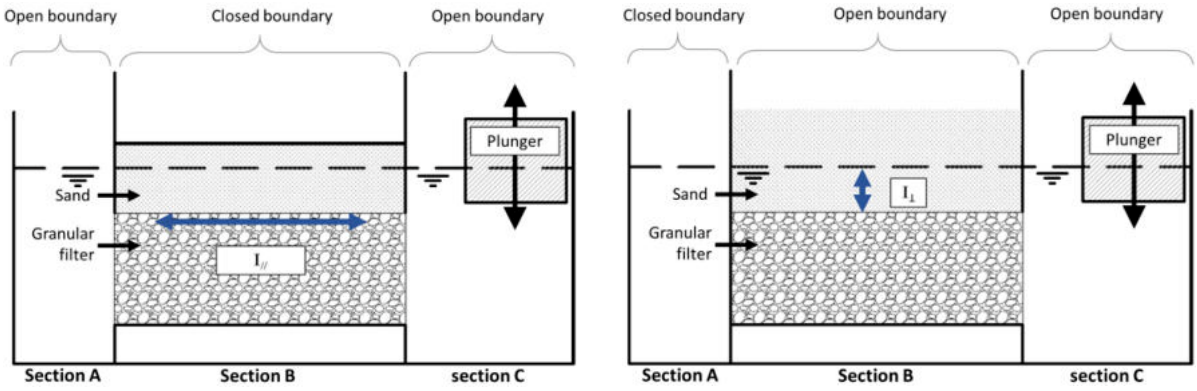

(a) Parallel setup

(b) Perpendicular setup

Figure 4.2: Both configurations with their open and closed boundaries. Also the directions of the relevant hydraulic gradients are depicted. These figures only show the directions. The dimensions and locations of the sensors can be found in Figures 4.17 and 4.17

4.1.1. Goal of the tests

The physical model has been used to create an understanding of the relation between the forcing and the resistance against erosion, of the granular filter-sand combination. To create an understanding of this relationship, in every test, a critical hydraulic gradient has been determined. The two different flow directions were tested to find the individual critical hydraulic gradients. The order of magnitudes of the hydraulic gradients was for both configurations equal to the hydraulic gradients that were determined in Chapter 3. After the tests, the goal was to link the critical hydraulic gradient to the stability ratio as is given by Equation 2.7a.

4.1.2. Processes of importance

The physical model has been created to be the best representation of reality for the important processes. These processes had to be simulated without any errors for the best effect. The reversed filter layer was most influenced by the following processes:

- **Arching**
  The stability of the sand layer on top of the filter layer was considered to be influenced by the arching mechanism (de Graauw et al., 1983). This arching was dependent on the grain size ratios of the filter and base layer. The arching was considered to be independent of the inclination of the filter layer. The arching might have been influenced by the Superimposed load.

- **Hydraulic forcing**
  The hydraulic forcing on the container was responsible for the load on the reversed filter. The hydraulic forcing could have broken the arches and conveyed the sand through the filter layer. The hydraulic forcing was determined by the hydraulic gradient.

4.1.3. Parameters of importance

In this paragraph, the parameters which were of the highest importance are explained. All other parameters that have affected the setup are described in Appendix C.7. The parameters that played an important role in the relationship between forcing and resistance were altered to be able to see the influence of these parameters on the relation. These parameters were:

1. Hydraulic gradient ($I_{\parallel}$ and $I_{\perp}$)
2. Stability ratio of granular filter-base combination ($\frac{D_{15F}}{D_{85B}}$)
3. Superimposed load

The first two parameters were altered during the tests to find a relation between these. Both parameters were dimensionless. The third parameter has been used in a single test to measure the influence of this parameter. The dimension of the third parameter was kilogram.

4.2. Forcing of hydraulic gradients

The first parameter that was altered was the hydraulic gradient. This hydraulic gradient originated from a pressure difference over the container. The pressure difference was forced to the setup by a plunger. The plunger consisted of a wooden block with dimensions: 0.22x0.14x0.16m, the block moved in a vertical oscillating motion. An example of the plunger motion can be seen in Figure 4.3. The motion of the plunger influenced the water level in section C, which induced a pressure gradient over the setup for which an example can be seen in Figure 4.4b.

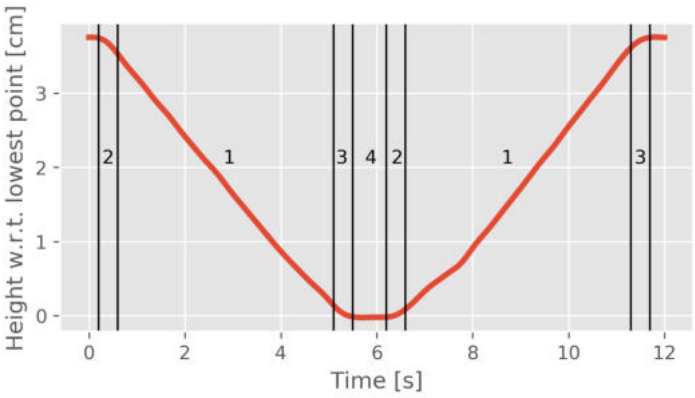

Figure 4.3: Plunger movement with the sections where the four parameters described below are leading

The plunger was moved by a stepper motor. This stepper motor was controlled with a computer running the program Step-Servo Quick Tuner. For the physical model as used in this research, four parameters have been changed to create the desired velocity signal. These four parameters, with the number corresponding to the numbers in Figure 4.3, were:

1. Velocity [rps]
   The velocity was the most important parameter. This velocity was responsible for the final hydraulic gradient that was exerted on the granular filter layer.
2. Acceleration [rps/s]
   The acceleration was used to reach the target velocity from where there was no movement. A higher acceleration reached the velocity faster while a lower acceleration created a smoother transition.
3. Deceleration [rps/s]
   The deceleration was used to stop the plunger movement. Similar to the acceleration was a higher deceleration responsible for a faster stopping time, while a low deceleration made sure the stopping was less abrupt.

4. Waiting time [s]
   The waiting time was added to the signal by stopping the plunger movement over some time. The waiting time was used to decrease the inertial effects of the water by waiting until a still water level was almost reached.

The velocity was increased during the tests to increase the hydraulic gradient. The other three parameters were altered together with the velocity to create the desired signal.

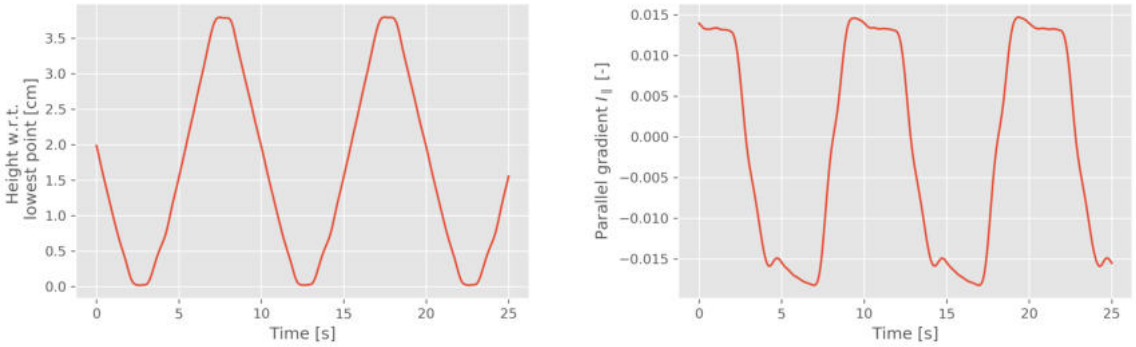

(a) Signal of the laser which displays the movement of the plunger

(b) Hydraulic gradients as calculated from the pressure sensors

Figure 4.4: Example signal

For the tests, it was important that the hydraulic gradients had the same signal, which is from here on referred to as the block signal depicted in Figure 4.4b. This block signal has been forced to have a constant hydraulic gradient, which was positive during half a wavelength and negative during the other half wavelength. To produce that hydraulic gradient, the plunger had to travel with a constant velocity. The acceleration and deceleration of the plunger were large enough to reach the target velocity quickly but had to be small enough to allow for a smooth transition between negative and positive movement, otherwise, a peak was formed. In Figure 4.4a the desired velocity signal of the plunger is given, which lead to the parallel hydraulic gradients as can be seen in Figure 4.4b.

4.3. Grain sizes

The ratio between the grain sizes of both the base and granular filter layer was the second parameter that has been changed during the tests. The ratio between grain sizes was expected to be governing for the resistance against erosion. The ratio has been altered over tests to measure the importance of this parameter. In Figure 4.5 the grading curves of both the sand and granular filter material are displayed. The sands and filter material which were used, were available in the Delft Laboratory of Fluid Mechanics, both materials were available but the filter material was sieved manually. See Appendix C.4 for more.

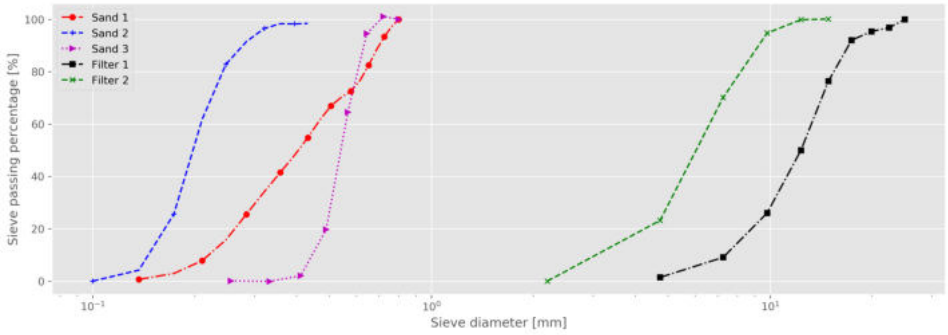

Figure 4.5: All grain sizes as used in this research

The grain sizes that were used can be characterized with cumulative grading sizes, which are referred to with a capital D with in the subscript the cumulative fraction. Besides this fraction the subscript

can include the layer of which the fraction was determined. For this research these subscripts are either: F = Granular filter layer and B = Base layer also referred as sand layer.

For the stability of the granular filter/base combination the ratio between base and granular filter layer as described by Terzaghi has been used: $(\frac{D_{15F}}{D_{85B}})$. The D_{50} is a good classification of granular material if a single classification of the layer is needed, while the $\frac{D_{60}}{D_{10}}$ gives an idea of the grading width. The parameters of all granular material that has been used during the physical model tests, can be found in Table 4.1.

		Sand 1	**Sand 2**	**Sand 3**	**Granular filter 1**	**Granular filter 2**
D_{15}	[mm]	0.243	0.158	0.48	5.6	2.6
D_{50}	[mm]	0.4	0.195	0.54	8.8	3.8
D_{85}	[mm]	0.68	0.26	0.62	10.6	6
$\frac{D_{60}}{D_{10}}$	[-]	2.1	1.4	1.2	2.0	1.7

Table 4.1: Overview of the different gradings.

4.4. Measurements

To extract results from the physical model setup, measurement devices have been used. These measurement devices have been divided into two groups, of which the first group gave a quantitative output, while the second group has been used for qualitative analysis.

The location of the sensors inside the setup that make up the first group, which are the pressure sensors, water level gauges and the laser, are depicted in Figures 4.16 and 4.17. All signals that came from the first group of measurement devices were read and stored by a computer, more on this in Paragraph 4.4.1.

The second measurement group consisted of two video cameras, and visual observations, the footage that was created by the video cameras has been stored on the same computer as the results from the first group of measurement devices.

4.4.1. Writing of measurements

The sensors that are described in the paragraphs below give an analogue signal as output. To be able to use this signal for measurement purposes, all sensors were attached to a Data Acquisition (DAQ) module. This DAQ module converted the analogue signals to digital signals that were read by a computer. The signals have been analysed with the program DASYlab . In this program, it was possible to calibrate and filter the results before saving the results into data files.

The plunger was controlled with the same computer, with a program called Step-Servo Quick tuner. Also, one webcam was controlled with the same computer with the program Skystudio. The computer which controlled the sensors, webcam and plunger could be accessed remotely with the use of Chrome remote desktop. This remote access enabled the author to interpret the results during tests and to alter the test sequence without the necessity to be present at the laboratory at all times.

4.4.2. Calibration

The sensors that were linked to the computer with the DAQ module have been calibrated. This calibration was done by a regression analysis of the voltage versus the measured quantity, which was the distance for the plunger and water level for all other sensors. This calibration has been done by noting the voltage of a sensor and writing down the measured quantity at the same time. This measured quantity was the distance for the laser and the water level for all other sensors.

The laser was only calibrated once before the first test as this laser was attached to the plunger and did not move during the testing. Because the setup was disassembled after each test, the other sensors

had to be calibrated before each test, more on this in Paragraph 4.8.1.

Calibration prior to test
Before each test, the sensors were calibrated, except the laser. This calibration was done during the filling of the container with water. The output in Volt of every sensor was noted for every cm of water level that has been added to the container. These points were used to create a regression line. The regression lines of the two tests can be found in Appendix C.5. The two tests were used to see the spreading between these tests. It was seen that the mean difference between tests of the pressure sensors was large. However, the slopes of the regression lines were similar, meaning that the behaviour of a sensor to a change of water level was constant, but that the placement was different over the tests.

In test calibration
Besides the calibration before the entire test, all sensors could be calibrated before and after each three hour section of the test. The calibration in between tests was only based on two levels, which meant that the calibration was less reliable than the calibration before the test has been started, but can nevertheless recalibrate the signal coming from a sensor.

The steps worked as follows, and as can be seen in Figure 4.6. First, the plunger has been raised until the maximum displacement was reached. This position was kept for 240 seconds. In the next step, the plunger has been lowered to the zero position, which was also kept for 240 seconds. The 240 seconds ensured that the water level was levelled over the entire container. In Figure 4.6 only the middle of the intermediate calibration cycle is depicted.

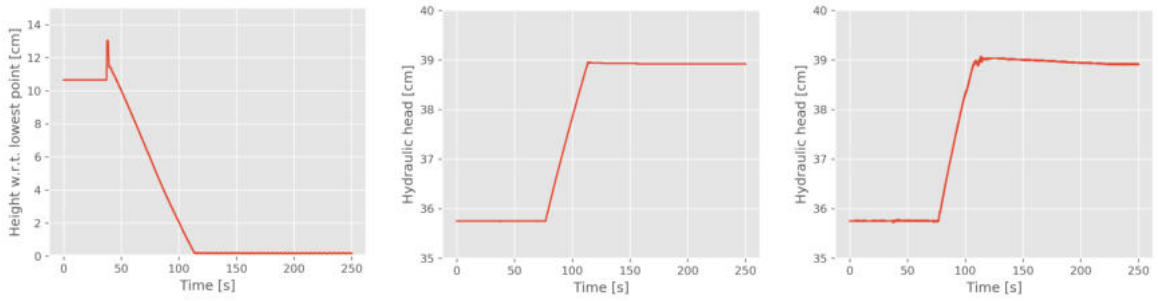

(a) Laser (b) Pressure sensor (c) Water level right

Figure 4.6: Signals during intermediate calibration steps.

Because at both points the water level was constant over the entire container, these steps could be used, during the analysis, to check whether the sensors gave an accurate result during testing, and also to see if any of the sensors had moved vertically.

4.4.3. Pressure sensors
The pressure sensors were used to calculate the hydraulic gradients. The pressure sensors measured the difference in pressure between the two adjacent pressure chambers. A pair of sensors is depicted in Figure 4.7a. One side of the sensor was connected with a tube to the free surface, the other was connected to the water at the location of placement. This means that a sensors measured the pressure differences between the atmospheric pressure and the local water pressure.

The pressure sensors could measure a maximum pressure difference of 0.5 psi, which was slightly more than 35 centimeters watercolumn. The used sensors were all connected to amplifiers, which increase the signal. The voltages given by the sensor have been changed to centimeters watercolumn in Dasylab (see Paragraph 4.4.1). Prior to each test the pressure sensors have been injected with water to prevent entrapped air from influencing the signal. This injection has been done by forcing water inside the sensors, with a small pipette. After the sensors were injected they stayed submerged during the rest of the test.

(a) Pressure sensors (b) Laser

Figure 4.7

4.4.4. Laser

The laser that was placed above the plunger has been used to measure the deviation of the plunger, the laser is depicted in Figure 4.7b. The laser light emitted by the laser pointed on top of the plunger and measured the distance between the point and the sensor. For this reason, if the entire plunger would be submerged, the results could not be trusted, as the water diffracts the beam from the laser. During testing this did not occur.

4.4.5. Water level gauges

The two water level gauges have been used to measure the water levels on both sides of the granular filter layer. The difference between these water levels could be seen as the hydraulic gradient over the entire granular filter layer. The water level gauges consisted of two metal pipes that measured the electric current between these pipes. If the water level was at a certain level it conducted the electricity between these pipes. This gave a signal in voltage, which was also changed to centimeters watercolumn in Dasylab.

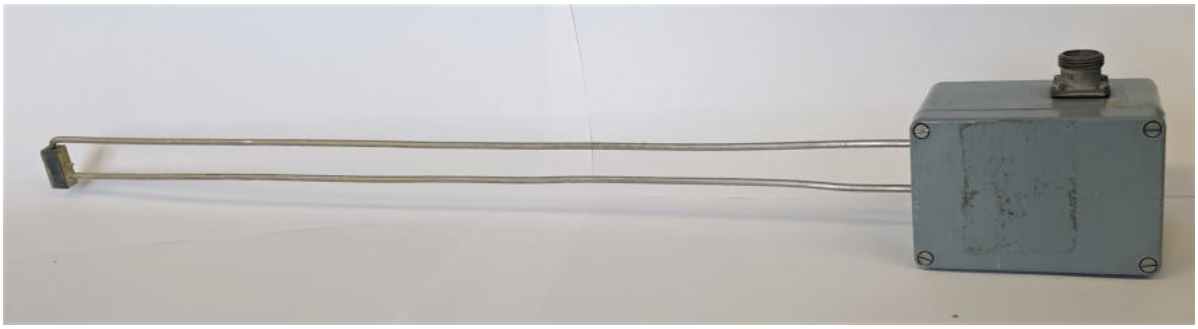

Figure 4.8: Water level gauge

4.4.6. Filtering signals

Filtering of the signal has been done for the pressure sensors. The plunger induced vibrations to the model setup. These vibrations were not measured by the water level gauges, but only by the pressure sensors. For a clear analysis of the signals it was necessary to filter the signal, this increased the visibility of the signal. See the comparison between a filtered signal(Figure 4.9b) and the unfiltered signal(Figure 4.9a).

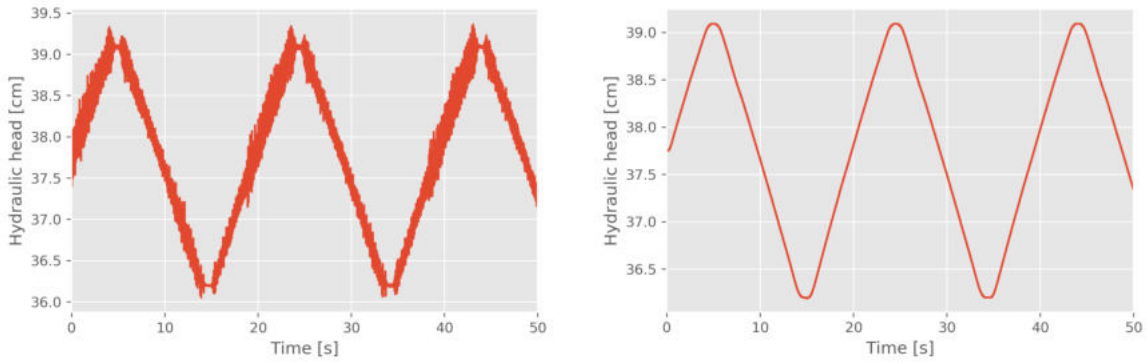

(a) Pressure signal without low pass filter

(b) Pressure signal with 1 Hz low pass filter

Figure 4.9

The filtering has been done with frequency analysis. A FFT spectrum was made for every sensor. This spectrum showed a lot of short timescale (f > 1Hz) oscillations. These oscillations were much larger in the pressure signals and almost invisible in the water level signal, as can be seen in Figure 4.10a withand Figure 4.10b. Besides that the oscillations were much faster than the oscillations that have been induced by the plunger. For this reason all oscillations higher than 1Hz were filtered with a low-pass filter in Dasylab. The FFT spectra of the other sensors can be found in Appendix C.5.

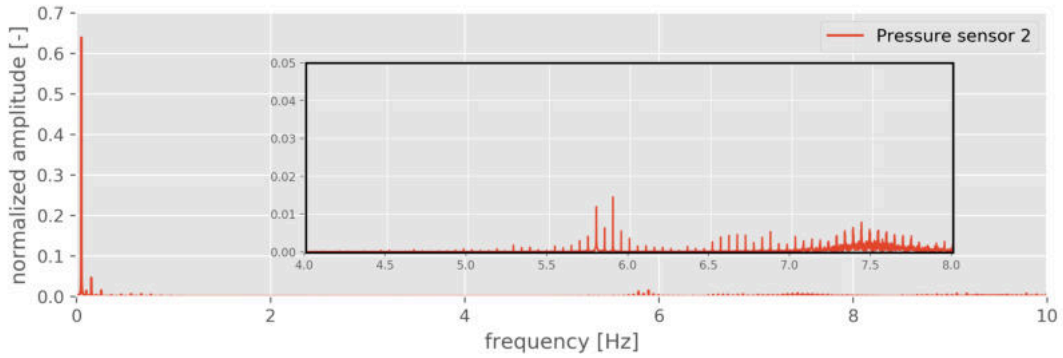

(a) Second pressure sensor

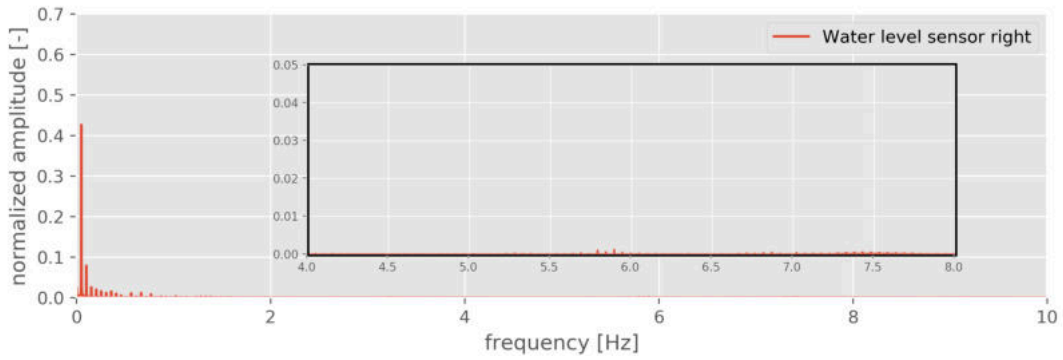

(b) Right water level sensor

Figure 4.10: Fast Fourier Transform (FFT), the black framework in the middle of each figure is a zoom between 4.0 and 8.0 Hz

4.5. Erosion measurements

To be able to find the critical hydraulic gradient, not only the occurring gradient during tests was necessary, but also the erosion through the granular filter layer had been determined. The erosion has been determined visually inside the sand trap. This sand trap was located at the bottom of the container in section B of the model setup, beneath the granular filter layer. On top of the sand trap, a wire mesh was placed to prevent the granular filter material from entering the sand trap. The sand was able to enter the sand trap through this mesh.

On the walls and bottom of the sand trap squares of 1x1cm were drawn. With these squares, a flow of sediment has been quantified. However, the research in this thesis was primarily focussed on finding the critical hydraulic gradient when there was no flow of sand. For this reason, the squares were only used as reference points in the time lapses.

Video camera

To analyse the long term effects of the erosion through the granular filter layer two webcams have been placed on either side of the container. These webcams were pointed towards the sand trap on the lower part of the container. The sandtrap was illuminated by two lights above the webcams. The lights were pointed downwards to prevent reflections on the plexiglass at the sandtrap. The table where the container was placed on has been covered in black fabric, to prevent additional reflections.

Two webcams were able to see the erosion from two sides of the container. This two sided coverage prevented blocking of the video footage by boxes inside the sandtrap in the case these boxes were partially filled. Another benefit of the double webcam computer setup was resilience of the measurements. Multiple times during experiments, the computers stalled or the webcams stopped working. The double webcam-computer setup has provided a more resilient setup.

For the tests, a time-lapse mode has been used. This time-lapse made a picture every 30s. With a frame rate of 24 frames per second and a test of 48 hours, this resulted in a four-minute-long movie. The first tests also the initial infill has been filmed. As this was a faster process, a timelapse with a photo every second has been used. For the long test that took over a week to run a photo has been made every 10 minutes.

Figure 4.11: Webcam

Visual observation

Besides the time lapses that were created, also visual observations were performed. Some processes were not possible to film with the cameras. These processes are described as visual observations and give a rough idea of the occurring processes. The results of these observations can be found in Paragraph 5.3.2

4.6. Model effects

A physical model always is a representation of reality. To prevent the model from behaving differently from the reality measures have been taken to mitigate the effects that influenced the behaviour of the scale model.

4.6.1. Wall effects

The transport of sediments through the granular filter layer was highly dependent on the porosity of the granular filter layer, with a larger porosity the transport would increase. The porosity inside a stone layer depended on the compaction of that layer. At the sides of the container, the porosity was large as the walls are straight and the stones could not interlock there.

Because the physical model setup was just a 0.15m wide container, the wall effects played a significant role in transport through the granular filter layer. This transport has been mitigated by the use of plastic bubble wrap on the side walls. This bubble wrap acted as a deformable boundary between the stones and the walls. The bubble wrap has been renewed every test to ensure that the wall effect was minimised.

(a) Without bubble wrap (b) With bubble wrap

Figure 4.12: Initial infill of two similar tests with and without bubble wrap between the granular filter layer and the walls.

4.6.2. Piping through sand layer

Water that was forced to flow through a substance would always try to find the path of least resistance. As the permeability of the granular filter layer was an order of magnitude larger than the permeability of the sand on top, this path of least resistance would be through the granular filter layer.

In the model after a long test with erosion, the amount of sand on top of the granular filter layer could decrease, which lowered the resistance of the water to flow through the sand. This flow could cause piping around the incoming boundary. As this piping progressed and eventually eroded the entire sand layer at the boundary, the water would bypass the granular filter and flow over the sand layer.

To prevent this, measures have been taken. For the parallel flow setup, the top of the sand layer has been closed off with a rubber seal to prevent air from escaping through this layer. This seal also ensured that the flow was fully parallel. The perpendicular flow setup was different, as in that case there should have been a flow through the sand layer. In the perpendicular configuration, there was sufficient sand on top to prevent a blow-out.

Piping has been prevented by the use of a geotextile at the in and outflow. With a geotextile, the water was able to flow through the textile, but the sand could not erode. The geotextile was connected to the mesh division screen (Figure 4.14).

4.6.3. Sorting of material

Previous research pointed out that the wide gradings placed in the container were not homogeneously distributed over the granular filter layer (Tutein Nolthenius, 2018). As the grain distribution was the

most crucial parameter for the resistance of the granular filter layer, it was essential to get a feeling for the influence of this sorting. The influence of this sorting has been quantified during the model tests.

4.6.4. Flow bypassing through boxes

Another place for the flow to bypass the granular filter was through the boxes that capture the sand if it eroded through the granular filter layer. The boxes had a width of 65mm that ensured that there was no flow in these boxes. This flow bypassing is tested with injecting dye into the boxes and checking visual if there was any flow.

4.6.5. Vibrations in the setup

In the prototype situation, the breakwater had a wave impact on the seaward side. This wave impact would be smoothed while it prograded through the core. In the model setup, the motor exerted the pressure difference on the water. The motor was vibrating during the movements which could be seen in the pressure signals. These vibrations were filtered as can be read in Paragraph 4.4.6.

4.6.6. Inflow and outflow effects

When there is an inflow or outflow from open water into a porous medium, there are always inflow and outflow effects. These effects were also present in the model setup but not in reality. For this reason, no measurements have been performed in the two most outer boxes (1 and 6). It was believed that the outflow and inflow effects were minimised as the conveyance width of the granular filter layer was the same size as the wire mesh so that no flow diversion or conversion would have taken place.

4.7. Geometry

The basic model setup consisted of a container made from plexiglas and plywood. For detailed dimensions see the drawings with measurements for both models in Appendix C.2.6(Figure C.11 and C.12). Both models used the same plunger (Figure 4.13). The arrow in the figure indicates the movement of the plunger .

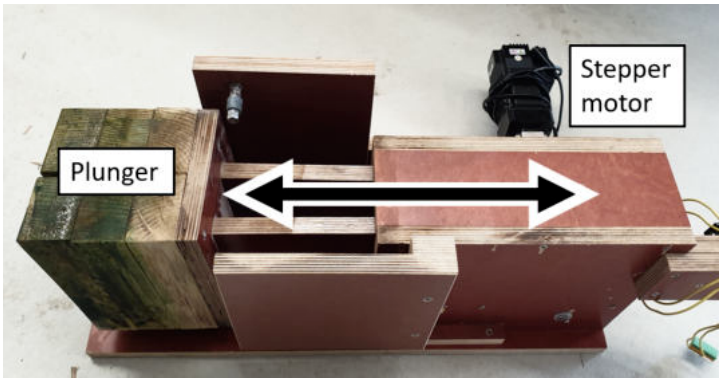

Figure 4.13: Plunger with motor, the arrow depicts the movement axis of the plunger.

Both models also have used the same wire mesh with plywood screen and geotextile as depicted in Figure 4.14. The parallel configuration used two mesh division screens, while the perpendicular only used one screen, since the other side was closed with a different screen.

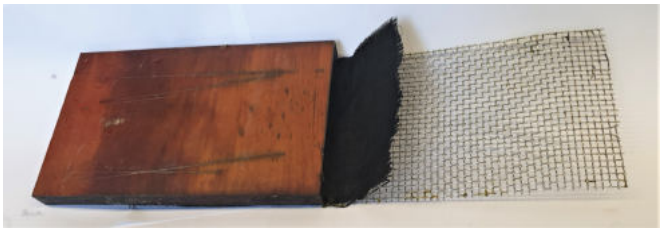

Figure 4.14: Division screen with wire mesh, plywood screen and geotextile

The plywood with rubber seals, depicted in Figure 4.15, has been used for both configurations. During parallel testing the seal was used to close off the top of the sand layer in section B. During perpendicular testing the seal was placed in between section A and B instead of the mesh, to close of section A.

Figure 4.15: Plywood that was used as a vertical divider during perpendicular flow and a closing lid during parallel flow

4.7.1. Parallel setup

The parallel setup consisted of a granular filter with a thickness of 200mm, and a sand layer of 100mm thick. The sand layer has been closed at the top with the rubber-plywood seal. This ensured that the flow was strictly parallel, and there was no flow through the sand layer.

The pressure sensors have been placed inside the granular filter layer. The sensors were placed above the separators of the sand traps. It was believed that there had been no influence on the flow caused by the sandtrap. However, the placement of these sensors ensured that the conveying thickness at the location of the sensors was equal for all three sensors. In Figure 4.16 the measurement devices for the parallel setup are portrayed. For the parallel setup, all devices described in Section 4.4 have been used.

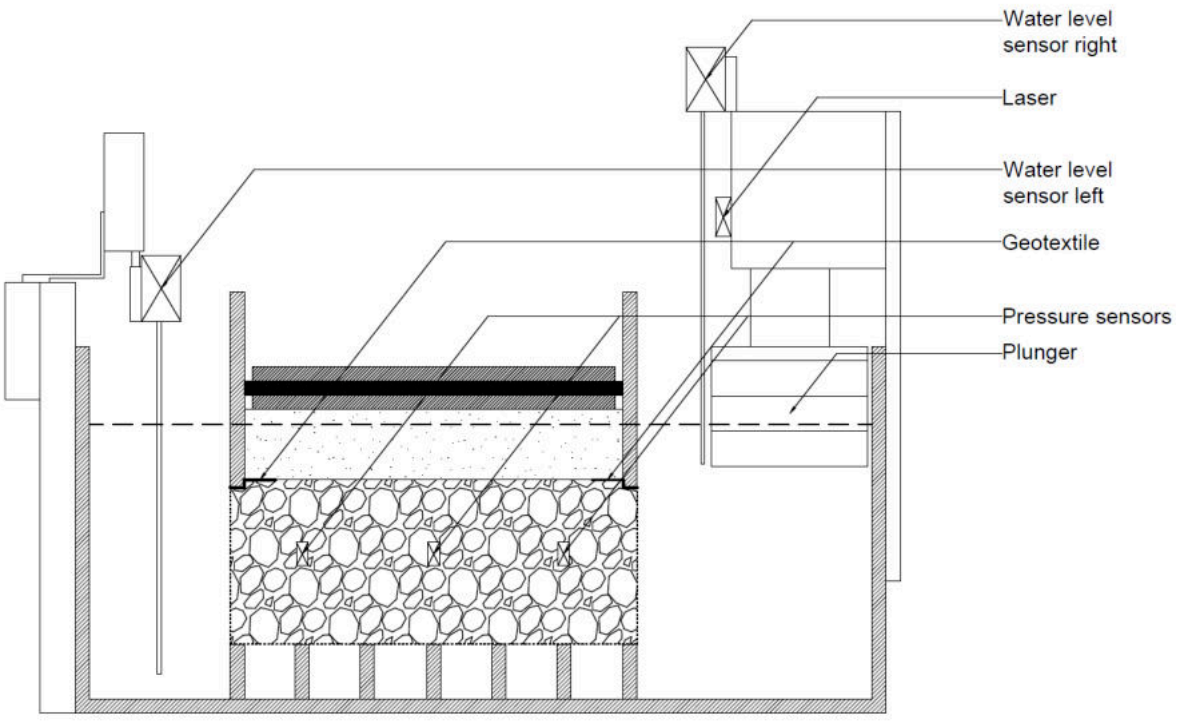

Figure 4.16: Drawing of the measurement devices in the parallel setup all sizes are in mm

4.7.2. Perpendicular setup

The perpendicular setup did not use the entire width of the container. For the perpendicular test, the width of the granular filter layer was the same as the width for the parallel tests. The left side of the container has been closed off with a piece of plywood with sealing tape to prevent leaking.

The layout of the pressure sensors was different from the placement for the perpendicular setup. Two of the three sensors were placed in the sand layer, and one sensor was placed in the granular filter layer. The hydraulic gradient has been determined in the sand layer as that is the governing layer (Schiereck and Verhagen, 2012). Besides the pressures inside the granular filter layer, the water level and the deviation of the laser have been measured.

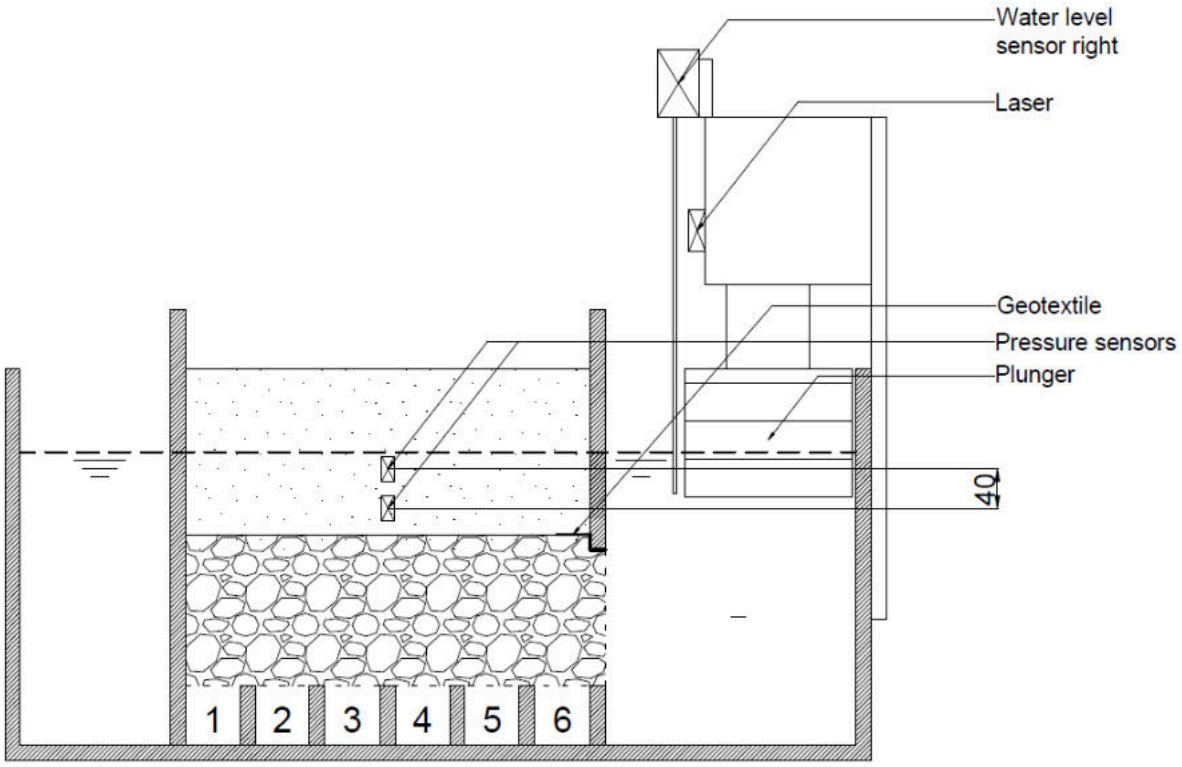

Figure 4.17: Drawing of the measurement devices in the perpendicular setup. All sizes are in mm

4.8. Test sequence

Accurate measurements required a repeatable test sequence. In the paragraphs below each step which has been taken is described. The steps were equal for each test.

4.8.1. Building the setup

Before every test, the entire setup had to be cleaned. After this cleaning, the granular filter material has been washed to remove the remaining sand. The bubble wrap had to be renewed since it broke during testing and cleaning. After the cleaning of both the setup and the granular filter material, the granular filter and sensors were installed. After the entire granular filter layer had been installed, the water level was increased to the top of the granular filter layer. Next, the sand was installed, in the dry. Depending on the test, the top of the sand is closed (Parallel), or left open (Perpendicular). Afterwards, the water level has been slowly increased until it reached 35cm.

4.8.2. Preparation of equipment and setup

After each test has been prepared, the measurements and time-lapse recordings were started. These ran during the entire test, which took more than 48 hours. Before the first measurement, the plunger was run at low velocity for some time (1-2 hours). This preliminary loading was performed because the reference tests had shown that the model strength against erosion increases overtime right after placement. After the initial erosion, the motor has been programmed to run each velocity for approximately three hours. For an extensive description of the velocity and acceleration profiles see Paragraph 4.2.

4.9. Test schedules

Three types of tests have been conducted, which are all discussed below. First, the reference tests were conducted, these tests have been used to see the behaviour of the test setup over multiple tests. These consistency tests are described in Paragraph 4.9.1. After the setup had proved to be consistent, the final tests were performed. These tests consisted of the variations in grain size ratio between the granular filter layer and the sand layer. These tests are described in Paragraph 4.9.2. After all, tests had been conducted three tests cases were ran to investigate additional behaviour of the granular filter and sand layer. These tests are described in Paragraph 4.9.3.

All tests have been given a code name to be able to distinguish the tests. The tests code names consisted of the direction of flow in the first part with 'Para' for the parallel configuration and 'Perp' for the perpendicular configuration. The second part of the code names gave the ratio between the gradings of both the granular filter material and the sand material given by the stability ratio: D_{15F}/D_{85B}. For the special test cases, the names have been extended with 'super' for the tests with superimposed load and 'long' for the test with an increased duration.

4.9.1. Reference tests

A serie of reference tests has been performed. The primary reason was to check the physical model setup for consistency. Since it was the first time that the setup has been used, the outcome was difficult to predict, and it was not clear if the results would be trustworthy. Also the spreading of stones and the reliability of the pressure sensor was important to test with the same setup, since this has been the largest issue in previous research(Tutein Nolthenius, 2018). An unforeseen benefit of the reference tests was that the author already had some experience with building the setup, which provided a more consistent building over the tests.

The reference tests consisted of six separate tests. The first two tests were used to come up with a method to accurately describe the sediment transport through the granular filter layer. These test were subject to a wide range of forcings, including high gradients and hitting the container with an hammer. This made understanding the process faster, but did not deliver reliable measurements. For this reason the first test that is considered in this paragraph is the third reference test. The reference tests all had the same structure. First the model was built according the building steps, which can be found in Paragraph 4.8.1. Afterwards the model has been subject to hydraulic gradients induced by the plunger by means of increasing the velocity and acceleration of the motor. These velocities and acceleration can be found in Table 5.1. The duration of each individual forced gradient was 15 minutes.

Test code	$\frac{D_{15F}}{D_{85B}}$	**Range of tested gradients**	**Step size**
Ref_8.0_1 Ref_8.0_2 Ref_8.0_3 Ref_8.0_4 Ref_8.0_5 Ref_8.0_6	8.0	0.0025 - 0.05	0.003

Table 4.2: Code names for the reference tests that are executed prior to the final test sequence

4.9.2. Final test sequence

The final test sequence consisted of ten tests with 5 different granular filter - sand combinations. These five combinations were all tested both for parallel and perpendicular gradients. All code names are given in the table below, together with the range of hydraulic gradients. Test 'Para_8.0' was not conducted during the final test sequence as it was extensively tested with the Reference tests. The duration of these individual forcing was three hours

Test code	$\frac{D_{15F}}{D_{85B}}$	Range of tested gradients			Step size
Para_4.0	4.0	0.05	-	0.1	0.002
Perp_4.0		0.5	-	1	0.02
Para_7.5	7.5	0.005	-	0.05	0.002
Perp_7.5		0.1	-	0.5	0.02
Para_8.0*	8.0	0.0025	-	0.05	0.003
Perp_8.0		0.05	-	0.5	0.01
Para_9.5	9.5	0.0025	-	0.05	0.001
Perp_9.5		0.05	-	0.5	0.01
Para_16.5	16.5	0.0025	-	0.005	0.001
Perp_16.5		0.025	-	0.1	0.01

Table 4.3: The entire test sequence as was executed with the model setup. The hydraulic gradients give a range of tested gradients, the actual range was within these boundaries. The step size gives an approximate step size.
* For the results of the Para_8.0 test the mean of the reference tests has been used.

4.9.3. Special test cases

Besides the effect of the ratio between the ratio of the grain sizes of both layers; also, the superimposed could have an influence on the stability of the layers. The influence of this superimposed load has been tested with the tests described below. The superimposed load test was performed for both parallel and perpendicular gradients. These tests were done with the same stability ratio as the reference tests. The load that was placed on top of the sand layer consisted of bars made of lead with a total weight of 135 kg, which resulted in a superimposed pressure of 17.7 kN/m^2, which is similar to the effective stress of around two meters of submerged sand.

Another test that has been performed was the long term test. This test has been conducted with the critical gradient obtained from the reference tests. The test was run for one week to see the long term influence of a critical gradient.

Test code	$\frac{D_{15F}}{D_{85B}}$	Range of tested gradients			Step size
Para_8.0_super	8.0	-*	-	-*	-*
Perp_8.0_super		0.025	-	0.5	0.01
Para_8.0_long	8.0	0.01			-**

Table 4.4: Special test cases
*Hydraulic gradient not know, forcing was similar to reference tests.
**Only a single gradient was tested

4.10. Analysis

After each test the measurements were analysed with the use of Jupyter notebook, a web based Python environment . The results were downloaded into the program and checked for accuracy. Due to the long duration of the tests, the setup has been affected by temperature changes, evaporation and leakage. The first influences the pressure that was recorded by the pressure sensors. This pressure difference was however relatively small($\approx 1\%$), as the difference between the cold and warm water was not more than 30°C. The latter two couldhave a larger effect on the test sequence.

4.10.1. Detrending results

As said above the measurements from the sensors have been affected by numerous events. These events had an impact on the usability of the measurements which had to be removed. To remove the effects, all measurements have been de-trended before further analysis.

The next step was to check whether the signals of the different sensors corresponded to each other. To analyse these, the signals where the water level was steady were used, which was during the intermediate calibration steps, see Figure 4.18. This meant that the sensors had the correct calibration even when a sensor changed position during tests.

4.10.2. Splitting the signal

Because the tests have been run in batches that used the same measurement file, the files that contained all measurement data were multiple days long. Besides that, the tests were not performed continuously as sometimes the author was not able to restart a new test sequence when the old sequence was ready. To have a clear overview and to delete the sections of data were no test was performed, all test have been analysed manually for the transition points. At these transition points, the test results were saved into smaller partitions which all contained the calibration steps both on the begin and at the end of the sequence.

The transition points were noted, which were later used to calculated the start and end time of each test. With these times the time lapses also have been splitted into the separate test sequences.

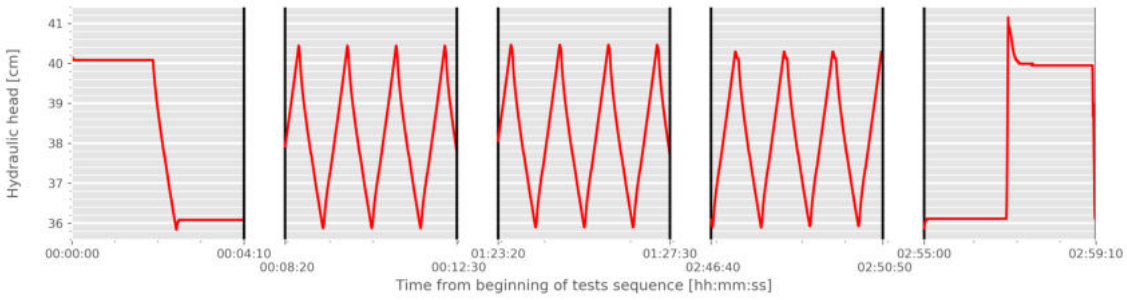

Figure 4.18: The pressure signal from the right pressure sensor during an entire test of three hours. The begining, middle and end of the test are depicted together with the steps prior and after the test.

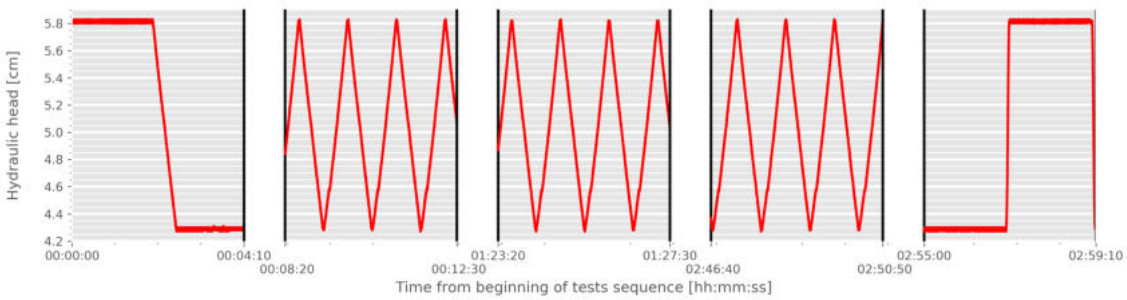

Figure 4.19: Laser signal from the entire test of which the pressure signals are depicted above.

4.10.3. Calculating hydraulic gradients

After the detrending and recalibration of the signals was done, the hydraulic gradients produced by the signals have been calculated. In the parallel setup the hydraulic gradient between the outer pressure sensors in the granular filter layer was governing, while the perpendicular setup used both sensors in the sand layer. For the parallel setup also the parallel gradient could be calculated over the entire setup with the use of the water level gauges, but this was used as a backup if the pressure sensors failed.

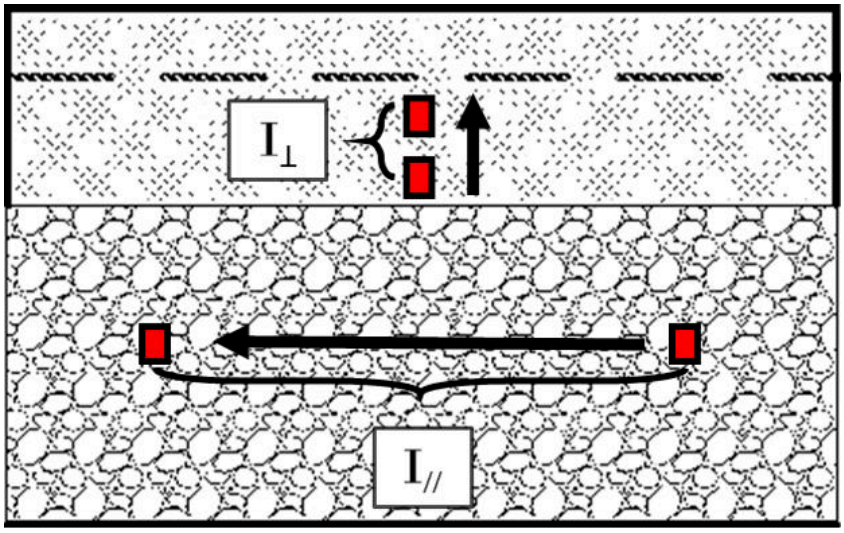

Figure 4.20: Cut out of section B of the model setup, where the granular filter was located. The pressure sensor locations for both parallel and perpendicular flow are depicted together with their positive direction.

The hydraulic gradient has been calculated by the difference between these sensors divided by the distance between the sensors. That calculation delivered a signal similar to the signal in Figure 4.4b. As most tests took 2-3 hours to complete, the hydraulic gradients were calculated at the begin, middle and end of each test and were analysed for accuracy.

The gradients have been determined at the moments where these gradients were constant. Which meant that the velocity in the filter layer was constant. These constant gradients were considered to be the governing loading on the filter layer. This gradient was usually reached at the last part of a half period of the gradient.

4.10.4. Finding critical gradient

The timelapse sequences have been analysed to determine the critical gradients. The videoclips from both sides of the sand trap were analysed, to check whether sand entered this sand trap (see Figure 4.16 and 4.17 for the locations of the sand trap). For the determination of the critical gradient, only boxes 2,3,4 and 5 were used as there might be in and outflow effects around these boxes.

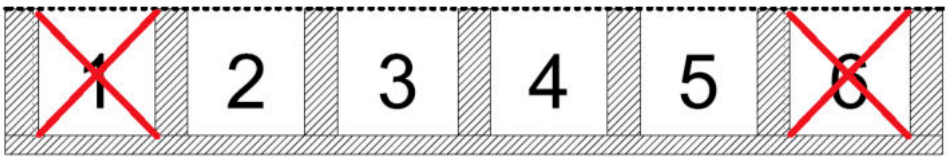

Figure 4.21: Schematic overview of the boxes inside the sand trap, the two boxes where crosses are drawn over were not used for the determination of the critical gradient

Each sequence has been checked for erosion. Erosion was determined as the movement of sand in one of the boxes, which meant that a critical gradient was obtained even when there was erosion in only one box. In this manner, the critical test, which is determined as the test where there is just no erosion, was found. With the measurements of the critical test, the critical gradient has been calculated.

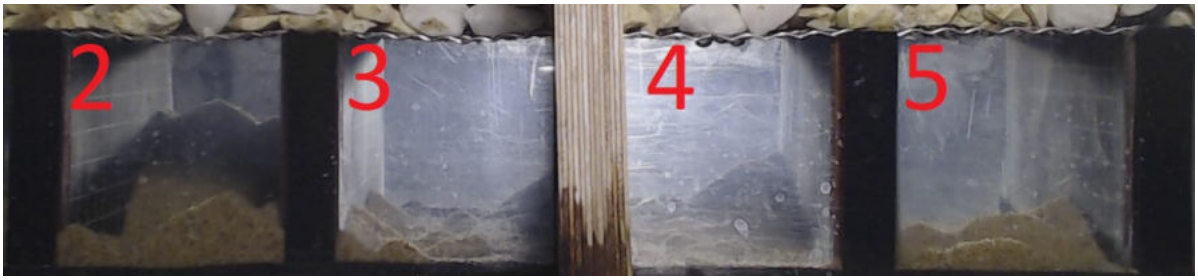

(a) Before critical gradient

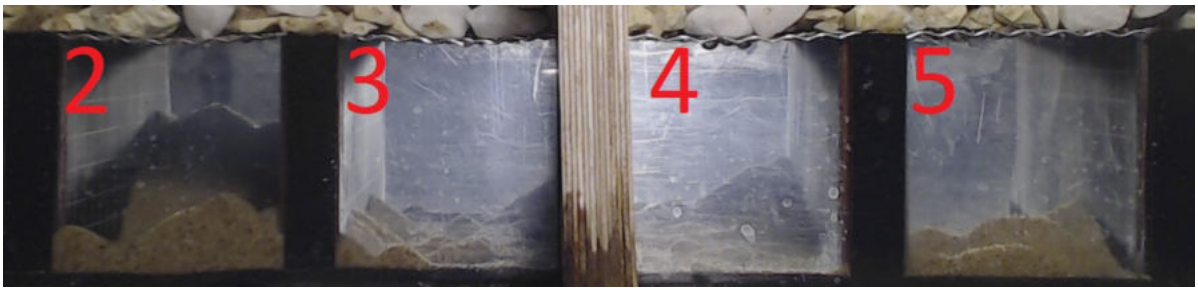

(b) After the three hours of critical gradient

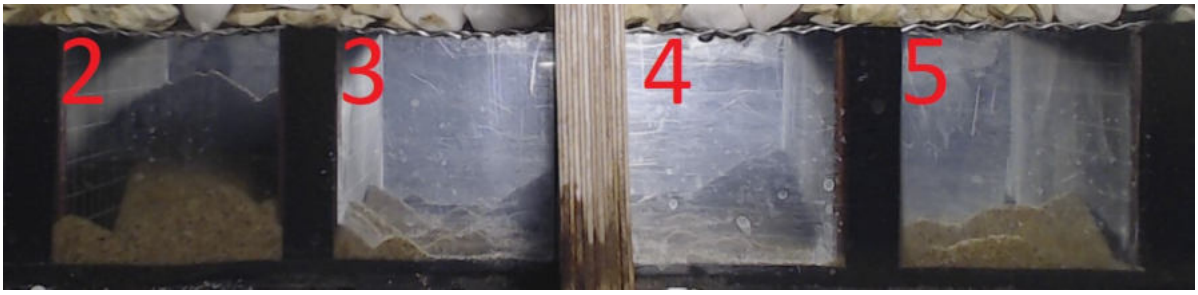

(c) After the three hours of flow larger than critical gradient

Figure 4.22: Critical gradient, for test Ref_8.0_4, the erosion can best be seen in box 2.

In Figure 4.22 three photos of the middle boxes are shown. These boxes were photographed with three hour intervals. The first photo has been taken after a test of three hours were no erosion was visible. The second photo was after the test which was determined to be the critical gradient, since in that photo also no erosion was visible, while in photo three erosion was visible. The erosion can be seen in box 2.

5

Results

In this chapter, the results from the model tests are analysed. Results from each separate test can be found in Appendix D. In this chapter, the outcome is summarized. The chapter is split into three parts. In the first two parts, the consistency of the setup is analysed, with the results from the reference tests. In the first part, the consistency of the forced hydraulic gradients is determined, and in the second part, the consistency of the erosion over the reference tests is analysed. Thirdly the results from the final tests and the special test cases are analysed with a conclusion about the critical gradients.

5.1. Hydraulic gradients over multiple tests

The forcing on the physical model setup has created the hydraulic gradients ($I_{\parallel}$ and $I_{\perp}$), for both the parallel and perpendicular configurations. To see whether these hydraulic gradients were constant over tests these have been checked on consistency during the reference tests on the following

- Forced velocity versus hydraulic gradients
- Development over time
- Influence of grain size granular filter layer
- Phase lag and consistency of the signals

For the final comparison only three reference tests have been used, Ref_8.0_4, Ref_8.0_5 and Ref_8.0_6, because these tests were executed in the same building steps, the same granular material and the same forcing steps on the setup.

5.1.1. Velocity to parallel hydraulic gradients compared

During the last three reference tests, the velocity on the plunger was increased over eight steps. The hydraulic gradients were measured with this increase in velocity. The tests showed a gradual increase of the hydraulic gradients inside the granular filter layer. The forced velocities can be found in Table 5.1 together with the acceleration and waiting time of each velocity step. The explanation of these can be found in Paragraph 4.2.

Test sequence code	VE_005	VE_010	VE_012	VE_015	VE_018	VE_020	VE_025	VE_030
Velocity [rps]	0.05	0.10	0.12	0.15	0.18	0.20	0.25	0.30
Acceleration [rps/s]	0.167*	0.167*	0.167	0.2	0.25	0.35	0.6	0.8
Waiting time [s]	1	0.5	0.5	0.5	0.5	0.5	0.5	0.5

Table 5.1: The velocities which were used for the reference tests: Ref_8.0_4, Ref_8.0_5 and Ref_8.0_6 .
*For these tests the acceleration 0.167 rps/s was used, this was the lowest possible acceleration

In the two figures below both the positive (Figure 5.1a) and negative highest gradients (Figure 5.1b) are displayed. These gradients were calculated as described in Paragraph 4.10.3. As expected, the

gradients increase with an increase in plunger velocity. Since a higher velocity increased the water level quicker, if the permeability stays the same, this would increase the gradient. This could be calculated with the Forcheimer equation (Paragraph 2.1.1).

It was also expected that with the parallel flow, the negative and positive gradients would be equal. Although previous research showed that during overload conditions, these gradients would not match (Polidoro et al., 2015), the research in this thesis has been based on a symmetrical granular filter layer. This symmetry was thought to give a symmetrical gradient, as also seen by Tutein Nolthenius (2018), but the positive and negative gradients were found to be different in magnitude.

The difference of the gradients over multiple tests was found to be large. This has been expected as the gradient was influenced by small phenomena, such as sorting of the rock, placement of the bubble wrap and infill of the granular filter layer. These phenomena were difficult to quantify but can have an influence on the permeability of the granular filter layer. For this research, the occurring gradient that is calculated afterwards is more of interest than the forced velocity on the container, as it directly describes the hydraulic load that works on the granular filter-sand interface. This inconsistency means that the forcing can only be used to give an estimate of the gradient.

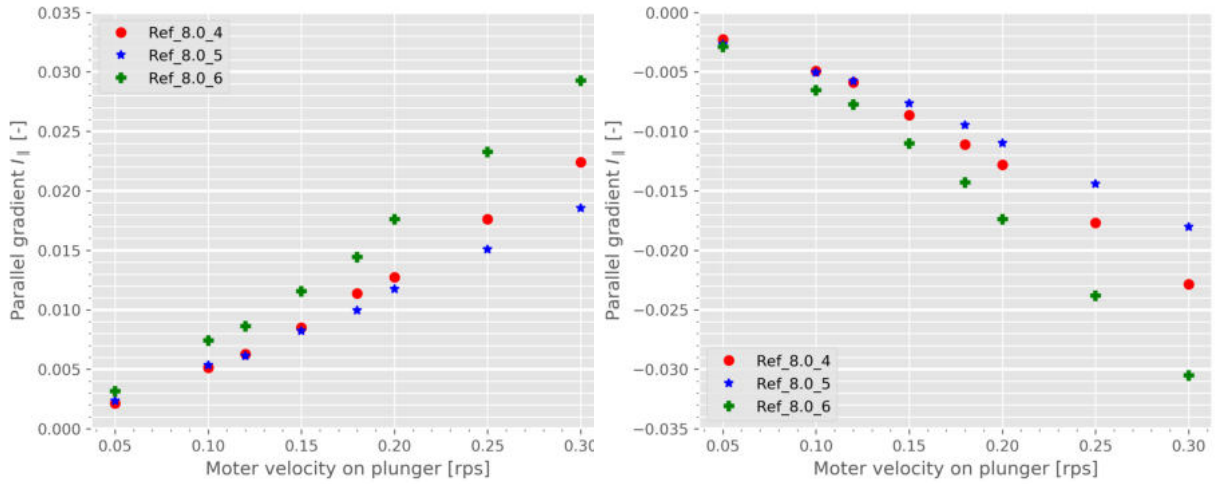

(a) Positive gradients

(b) Negative gradients

Figure 5.1: Maximum parallel gradients over three reference tests: Ref_8.0_4, Ref_8.0_5 and Ref_8.0_6

5.1.2. Ratio between plunger velocity and hydraulic gradient over one test

As a test program was executed, the sand protruded into the granular filter layer. Also, due to settlements in the stone layers, the permeability of the granular filter might have changed slightly. To see whether this had any effect on the gradient that was forced on the granular filter the test program, with the eight velocities described, was ran another time on the same setup after the first test was finished. This test is done with test Ref_8.0_6. The results are plotted in Figure 5.2. The test was first run like any other reference test which had as output the blue plusses. These points are also plotted in Figure 5.1 as blue stars. After all test sequences were finished, the setup was set to rest for 10 minutes, to be sure that all movement inside the granular filter layer had stopped. Afterwards, the test was started again with the same velocities, except for VE_0.12 and VE_0.18. The results of this secondary test are depicted with the red crosses in Figure 5.2a and 5.2b.

It was seen that the difference between the two tests has been minimal. The gradient was just a small fraction lower in the second test than in the first test. The signals of both gradients are also compared. No large differences between these two tests were visible. the signals can be found in Appendix D.1.

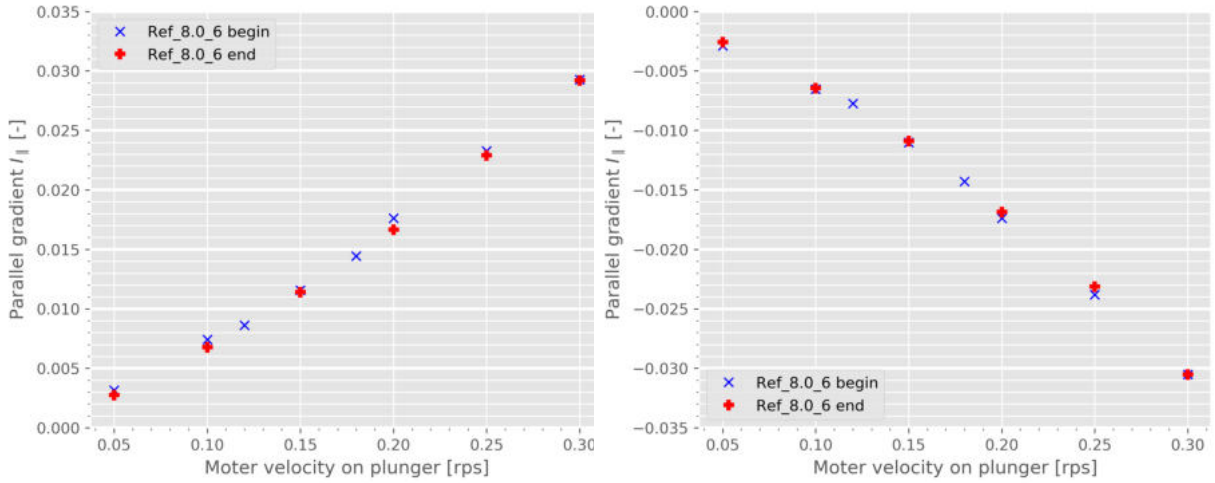

(a) Positive gradients (b) Negative gradients

Figure 5.2: Maximum parallel gradients of test Ref_8.0_6 at the beginning of the test and the end of the test

5.1.3. Difference in hydraulic gradient for other granular filter layers

Because the shear stresses induced by the granular filter layer on the flow induced the gradient, due to a small permeability of the granular material, the use of a different granular filter layer would cause other gradients, if it had a different permeability. The second granular filter that has been used in this research was tested with the same sequences as the reference tests (see Table 4.2). Because the second granular filter had smaller grain sizes it was expected that the gradients on this granular filter layer were higher with the same forced velocity. The gradients from this test were compared with the means of the gradients from the reference tests and are depicted in Figure 5.3a & b

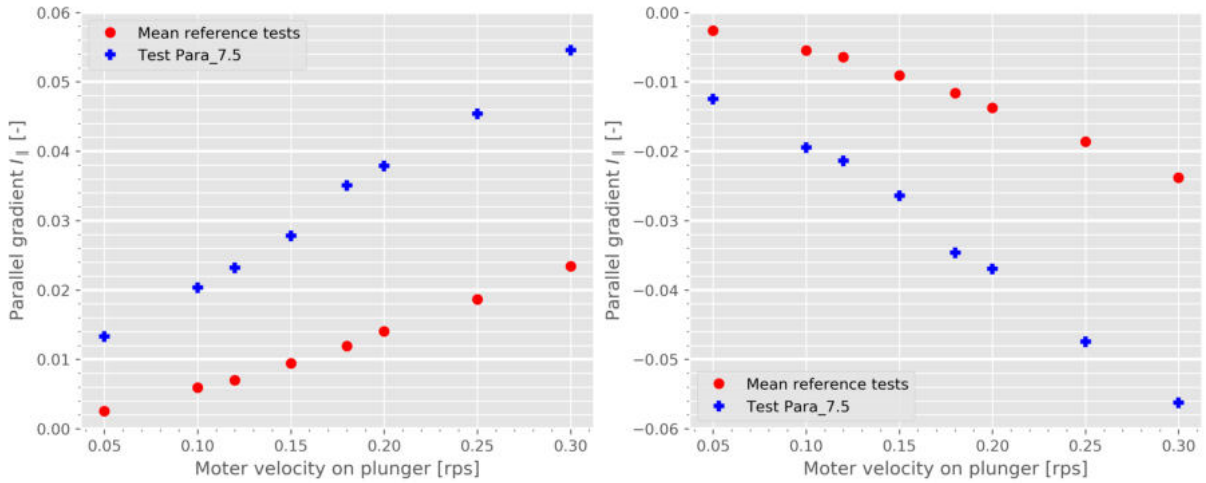

(a) Positive gradients (b) Negative gradients

Figure 5.3: Parallel gradients over two tests, one with granular filter layer with D_{50} 8.8mm (mean of Ref_8.0_4,5 & 6) and one with D_{50} of 3.8mm (Para_7.5).

It can be seen that the gradients that have been induced by the smaller granular filter size were much larger, as described above this was expected, due to the difference in permeability which was caused by the different granular sizes.

5.1.4. Consistency of gradient signal

To see whether this forced velocity still gave a constant gradient, in the form of the desired block signal, this gradient signal of an entire test with all velocities as described in Table 5.1 is plotted in Figure 5.4. In the lower graph, it can be seen that the amplitude of the plunger is not changed, while the period of the plunger is changed. The upper graph displays the gradient signal. As required in this research, the signal was a block type signal, meaning that the gradient was constant for most of a period.

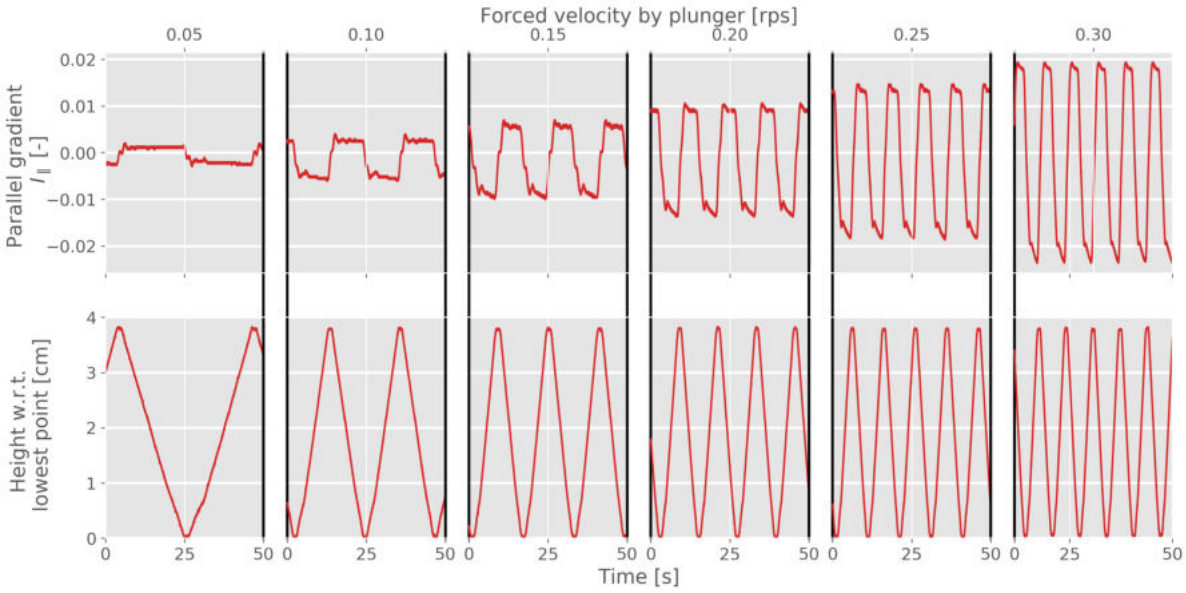

Figure 5.4: Gradient signal for the different consecutive forced velocities. In the upper graph, the gradient over the granular filter layer is depicted. In the lower graph, the motion of the plunger can be seen. The signal between two black bars is 50 seconds cut out of the 15 minute signal of one test sequence

It can be seen that with larger velocities of the plunger, the gradients were larger as also seen in Paragraph 5.1.1. The higher gradients had a stronger influence of the peak since, the acceleration of the higher velocities was also larger, which was necessary to reach the target velocity.

5.1.5. Phase between forcing and pressure sensors for parallel flow

The plunger induced a water level difference over the filter layer, which resulted in the gradient on the setup. The origin of this parallel gradient was a phase lag between section C & A for parallel flow. This phase lag originated from both inertia and friction of respectively the water and the granular filter layer. In the graphs in this paragraph, the pressures are plotted against the time. When the change in pressure over time ($\frac{\partial P}{\partial t}$) was equal between two points and the conveyance width was constant between the points, the velocity between these points would be constant due to the conservation of mass between these points. This furthermore indicated a constant gradient between these points as can be calculated with the Forcheimer equation, see Paragraph 2.1.1. The gradient signal as was calculated with the pressure difference between two points is given in the third graph in each figure. On the right of each graph the location of the signal is shown in a schematized setup, which is from top to bottom; the location of the plunger, the locations of the pressure sensors and the locations of the gradients.

Two figures are shown to see the different behaviour for different forced velocities of the plunger. In Figure 5.5, the results with a velocity set to VE_012 are depicted. In Figure 5.6 the same is plotted, but with a velocity of VE_030. In this paragraph, only the phase lag and the consistency of gradients are analysed. In the next paragraph, the individual characteristics of the gradient signal are explained.

For both velocities, the parallel hydraulic gradient during the downward movement of the plunger, which was the positive parallel gradient, was constant. This constant gradient meant that the velocity in the filter layer was constant during this period. This constant velocity was expected as described above. For both velocities, the parallel hydraulic gradient during the upward movement of the plunger was increasing. This increase in gradient might be due to the difference that the forcing was not equal on both sides.

The amplitude of the water level change in section C, where the plunger is located, was larger than the amplitude of the water level difference in section A. This difference in amplitude meant that the forcing of the water level from section C to A has been larger than the forcing from A to C. This difference in velocity created the difference in gradients during the upward movement of the plunger. The gradient was slowly increased towards the gradient that was reached during a downward movement. The gradient was therefore not constant but slowly reached the intended gradient.

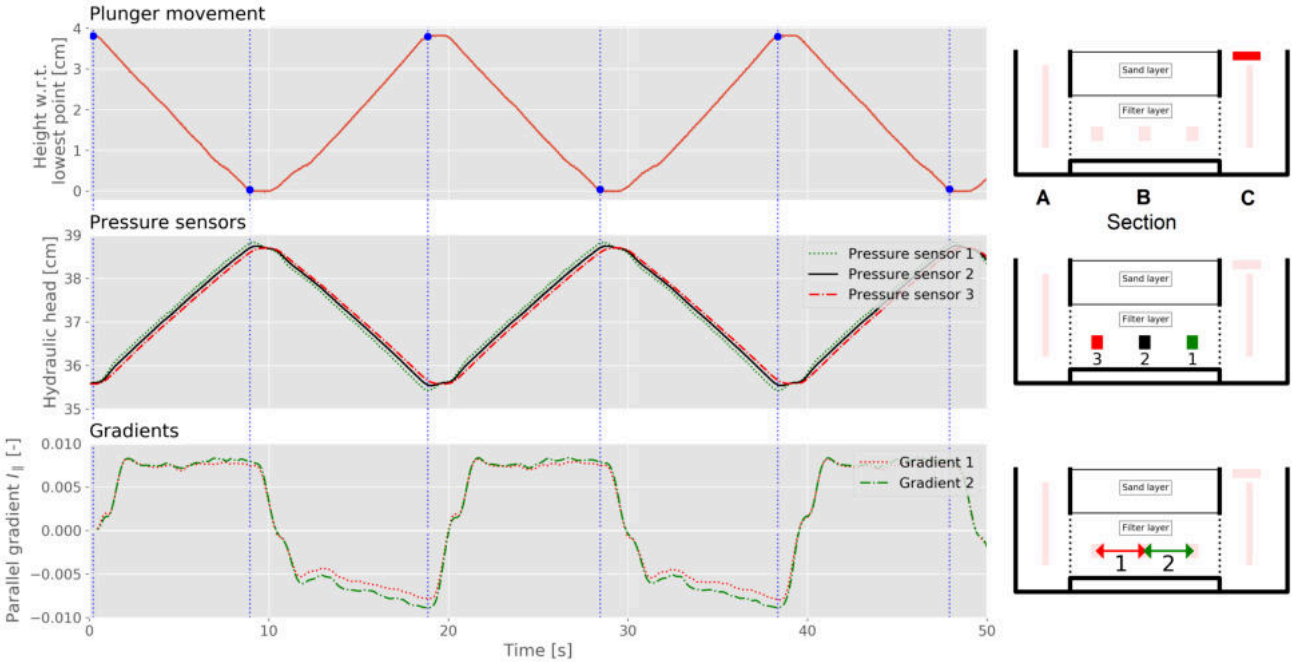

Figure 5.5: 50 seconds of signal from all three pressure sensors (Ref_8.0_6 with VE_012)

The amplitude difference originated from the permeability of the granular layer. The water level on the left had this delay which could be seen as the phase lag in both figures. The water level on the left was still changing when the plunger movement was changing direction. This could be mitigated with the waiting time added by the plunger, but the 0.5 seconds of waiting time were not sufficient to cancel out this effect.

Also, the phase lag over the filter layer is depicted for both plunger velocities. The phase lag for the lower plunger velocity was more constant over the entire period than the phase lag for the higher plunger velocity. The physical process behind this is that with the higher plunger velocity, both the friction played a larger role with the flow through the filter and the water was accelerated faster.

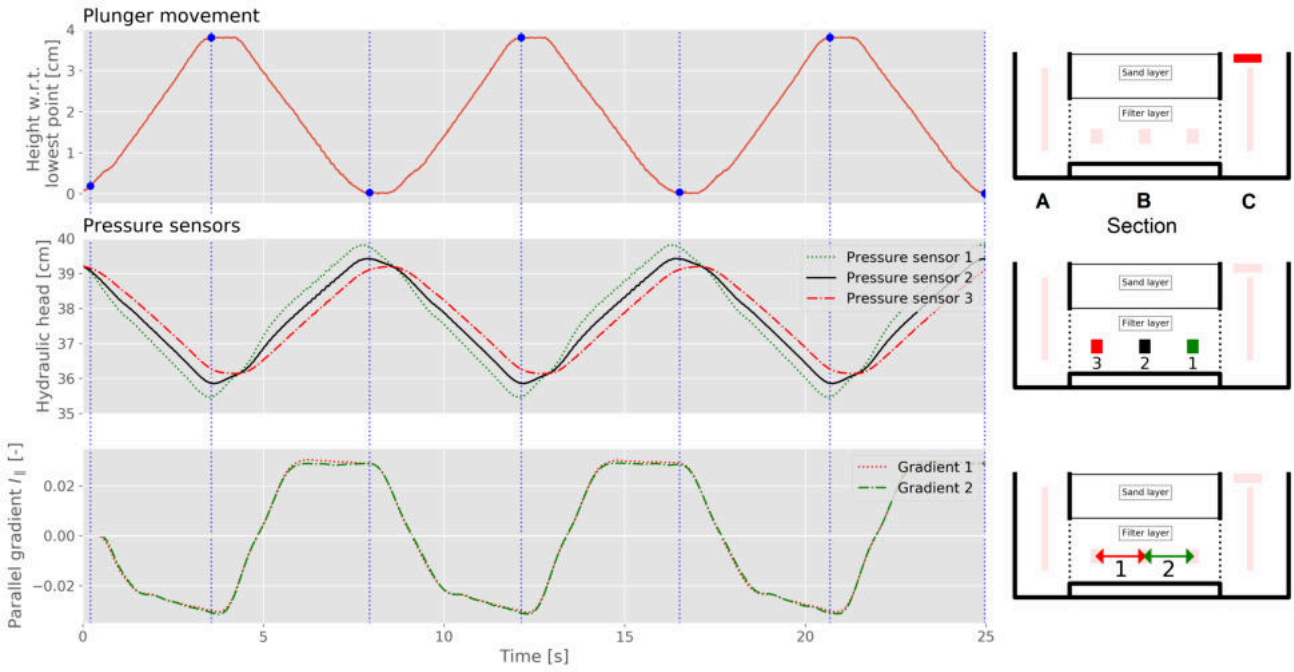

Figure 5.6: 25 seconds of signal from all three pressure sensors (Ref_8.0_6 with VE_030)

5.1.6. Hydraulic gradients created by plunger

As described in the previous paragraphs, the plunger has been programmed to produce the desired block signal. It was however seen that sometimes the gradient signal deviates from the desired signal. In the upcoming paragraphs, these deviations are described together with their origin. Vibrations also had an effect on the gradient signal. First, the parallel gradient signal was analysed, and secondly, the perpendicular gradient signal was analysed. Both gradient signals were compared to the pressure sensor signals, water levels and the movement of the plunger.

Parallel hydraulic gradient

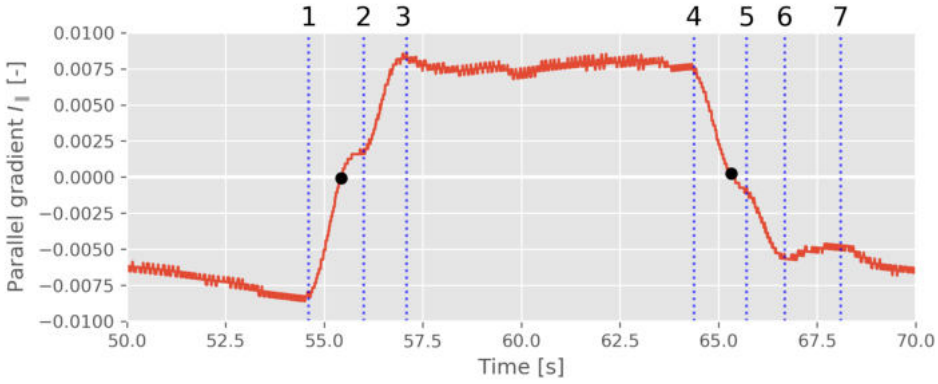

Figure 5.7: Parallel gradient signal from Ref_8.0_6 VE_012, with vertical lines at the points of interest. On the two zero crossings, black dots are placed. The gradient is calculated with the difference between pressure sensors three & one which are located on both sides of the granular filter layer.

The parallel gradient signal that has been analysed is depicted in Figure 5.7. In this graph, seven vertical lines are plotted at the points of interest. The two black dots depict the locations where the gradient changes sign. The gradient signal has been created with Ref_8.0_6 and VE_012. The gradient created by this signal resembles the constant block signal that was desired, see Paragraph 4.2. The period of the signal was around 19s.

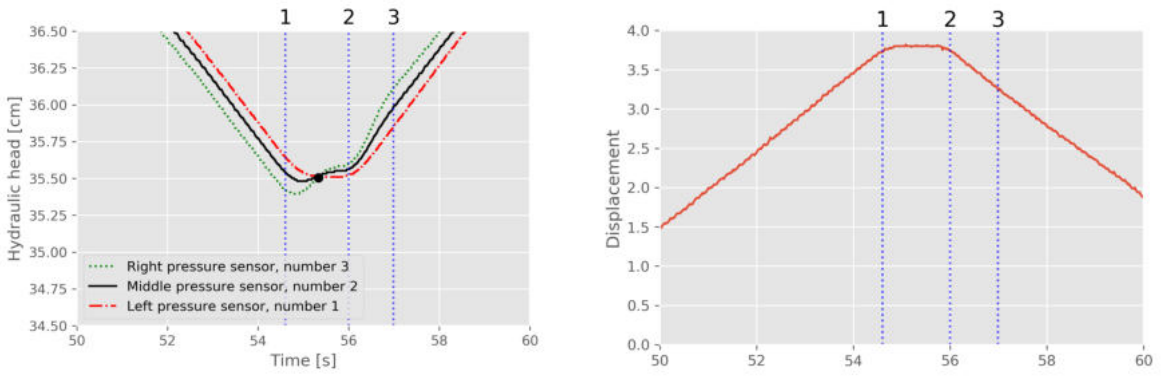

(a) Pressure sensors

(b) Plunger movement

Figure 5.8: Signal from the sensors in Ref_8.0_6 during which the highest point of the plunger was reached.

In the figures above the first 10 seconds are plotted of the pressure sensors and the movement of the plunger. In both figures, the lines are plotted that correspond to the lines plotted in Figure 5.7. The processes that influenced the gradient signal were:

1. Deceleration of the plunger
   The deceleration of the plunger lowered the velocity in the entire container. The deceleration from the plunger was from the target velocity to a complete stop of the plunger. The sensor that was the closest to the plunger reacted almost immediately to the stopping of the plunger, while the other sensors reacted more slowly due to inertia of the water.

2. Acceleration of the plunger
   During acceleration of the plunger, the water levels started moving. The pressures in the entire filter layer reacted simultaneously; the reason for this is that the velocity of the water during the acceleration was much lower than the velocity during deceleration.

3. Reaching the target velocity
   After the acceleration to the target velocity, the velocity of the plunger has been constant. The water inside the filter layer did not react instantaneously. It could be seen in Figure 5.8a that the change in pressure was larger at the right side of the filter than the change of pressure at the left side. This difference was due to the inertia of the water, which meant that the water needed time to react to the forcing. This effect could only be seen during the downward period of the plunger.

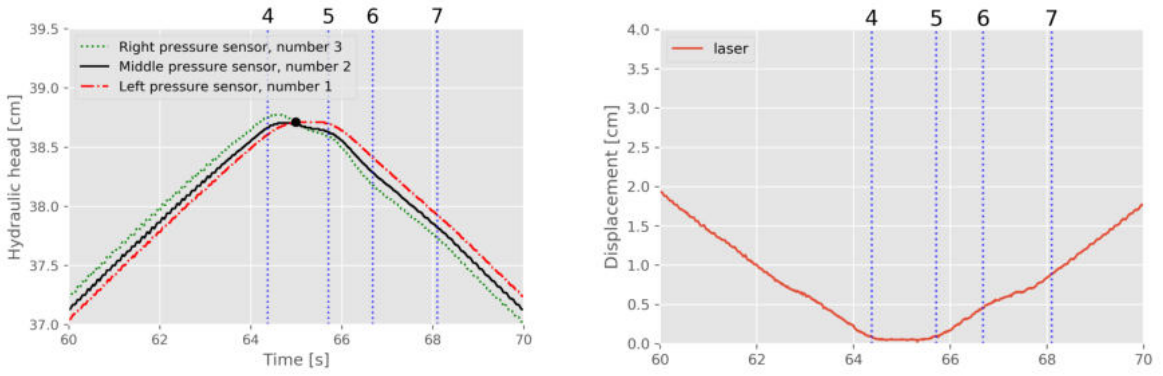

(a) Pressure sensors

(b) Plunger movement

Figure 5.9: Signals from the sensors in Ref_8.0_6 during which the lowest point of the plunger was reached.

During the second interval of 10 seconds the pressure signals showed a similar behaviour as described above. Line 4 is the same as line 1, line 5 can be compared with line 2 and finally line 3 and 6. The only difference is line 7, which is described below.

7. Vibration in plunger
   During the upward motion of the plunger, there was friction inside the plunger, which slowed the movement of the plunger for a short amount of time. This slower velocity induced a slightly smaller gradient during part of the upward movement. The target velocity was nevertheless reached after the plunger moved higher, which ensured that the target gradient was reached.

The conclusion of this signal was that the setup had been highly affected by inertia. The inertia was present during the change of flow direction. The influence of friction on the pressure distributions along the filter layer was low as the velocities of the water inside the filter layer was low during most tests. The setup might have been not completely sealed at the top of the sand layer, as it seemed that pressure was lost in the filter layer. Nevertheless, there was a vast region in which the hydraulic gradient and therefore the velocity in the granular filter layer were constant, which meant that the hydraulic parallel gradients that were produced by the setup were sufficient to be used as the actual occurring loads on the granular filter-sand interface, for the parallel configuration.

Perpendicular hydraulic gradient

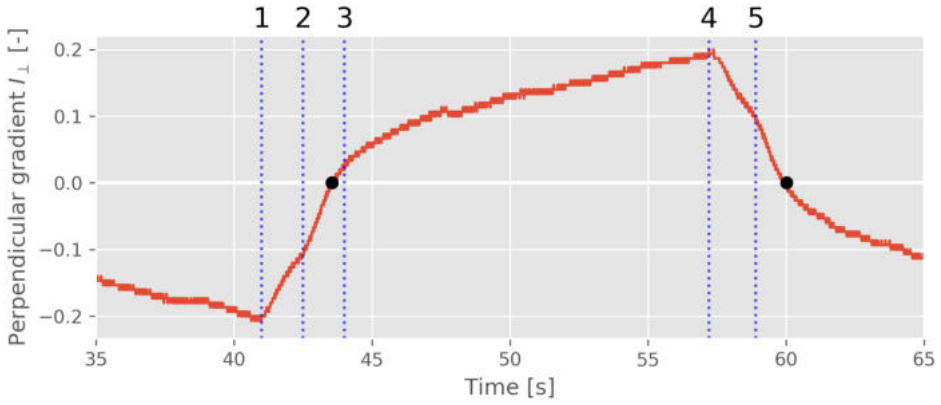

Figure 5.10: Gradient signal from Perp_8.0 with vertical lines at the points of interest. The gradient of this signal has been calculated with pressure sensors, one & two of which two was the top sensor and one the bottom sensor. Both sensors were placed in the sand layer. The duration of oscillation is around 30s

The perpendicular gradient signal was also checked for consistency and to describe the physical processes. Compared to the signal from the parallel gradient, Figure 5.7, the perpendicular gradient was less constant. The gradient signal for the perpendicular case has been slowly increased until the top was reached when the gradient was decreased rapidly.

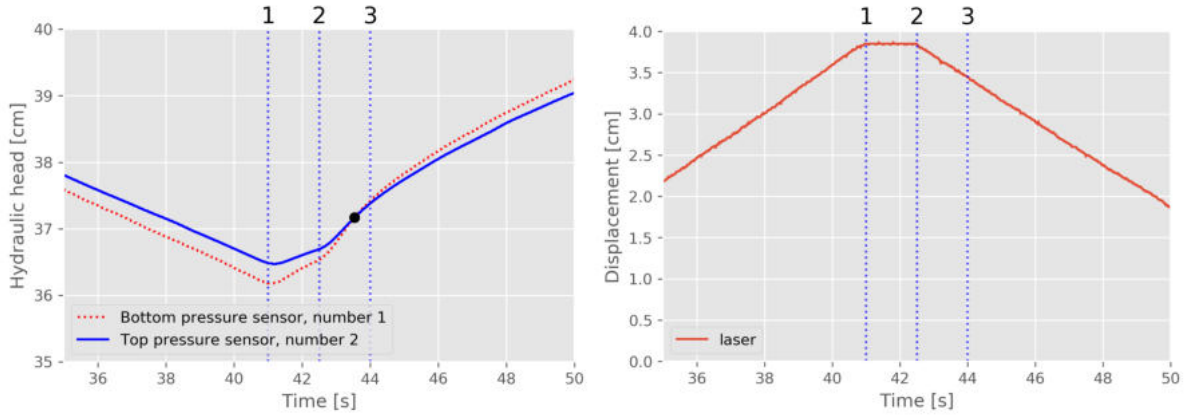

(a) Pressure sensors

(b) Plunger movement

Figure 5.11: Signals from all sensors in Perp_8.0 during which the highest point of the plunger was reached.

The first 15 seconds of the sensors are plotted in the graphs in Figure 5.11 together with the first three lines of Figure 5.10. These three lines have the same origin as the lines in the parallel gradient; Deceleration of the plunger, acceleration of the plunger, and reaching the target gradient.

1. Deceleration of the plunger
   The reaction to the deceleration has been instant for both pressure sensors. The gradient signal also had a clear through at this line in Figure 5.10.

2. Acceleration of the plunger
   The acceleration increased the hydraulic gradient even more. After the deceleration, the pressures were already increased in the system but were more increase after the acceleration starts.

3. Reaching the target gradient
   The target velocity of the water has never been reached for perpendicular gradients. It could be seen that the hydraulic head lines in Figure 5.11a were curved along the entire downward motion of the plunger. The physical process behind this was that the perpendicular gradient had been determined as the overpressure in the filter layer divided by the length to the pheatric surface inside the sand layer. With an increase in pressure, this pheatric surface also increased, but as the sand layer had a low permeability, the increase in pheatric surface has been much lower than the increase in pressure.

During the second interval as depicted in Figure 5.12, the same processes as described above were relevant, with line 4 the deceleration as described at point 1 and line 5 the acceleration as described in point 2. In this second interval also the target velocity and gradient were not reached, which has the same explanation as point three above.

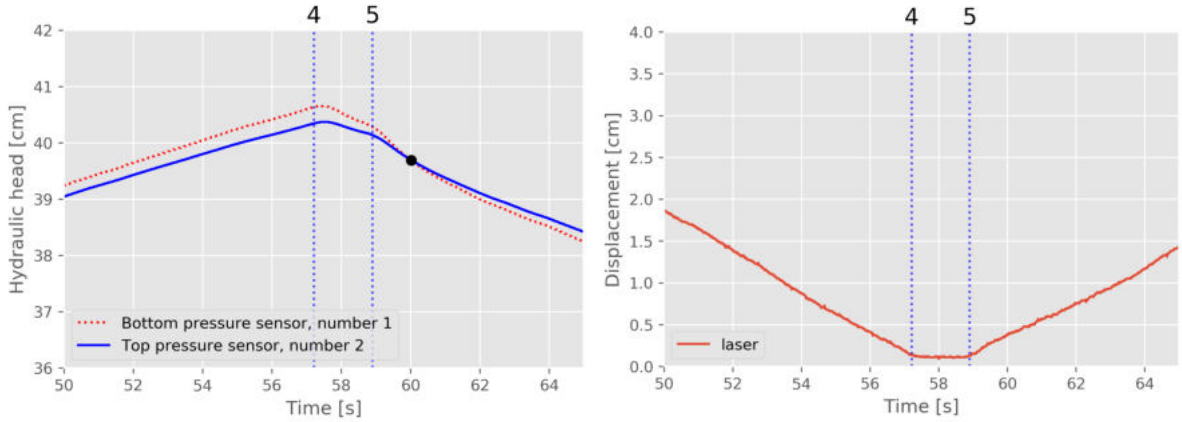

(a) Pressure sensors

(b) Plunger movement

Figure 5.12: Signals from all sensors in Perp_8.0 during which the lowest point of the plunger is reached.

The conclusion is that the perpendicular gradients were not constant. The perpendicular gradients increased in magnitude during an entire period. This increase meant that there was not a single value that could be used to characterize the gradient, which induced a large error for the critical perpendicular gradient, which have been determined during the final tests.

5.2. Erosion during reference tests

Besides the consistency in gradients along different tests, the erosion also had to be consistent to be able to draw conclusions from the used model setup. To check this the erosion over three reference tests has been monitored. Both the magnitude of the erosion and the critical gradient of these tests are compared to see the consistency of the physical model setup. As described before the reference tests were tested with the parallel configuration. But it was believed that the consistency of erosion is independent of the direction of flow as it depended amongst other processes on the spreading of the granular filter layer, which should have been equally important in both configurations.

5.2.1. Spreading of granular filter layer

It was difficult to see whether the spreading of the granular filter layer was different over the tests. Not only did the bubble wrap block the view into the container. Also, the width of the container was large compared to the granular filter size(10-20 times the D_{50}). This meant that the sorting in the middle was only visible during the building of the physical model. Because it was almost not possible to quantify the spreading, this was seen as a major uncertainty. This uncertainty could be less because a large part of the filter was used to determine the critical gradients. The width over which the gradients were determined was much wider than, for example, the physical model used by (Tutein Nolthenius, 2018), which should decrease the influence of the spreading.

5.2.2. Allocation of sand in sand trap

As can be seen in the figures below the initial infill changes a lot over the different reference tests, although the amount of erosion was reasonably constant over the tests, the spread of sand was very different over tests. In test Ref_8.0_4 the erosion was mainly located at the rear side of the sand trap, which could be due to wall transport. In test Ref_8.0_5 the erosion was more evenly spread over the boxes but showed large heaps of sand at the outer edges. In test Ref_8.0_6 the erosion was more focussed on local spots.

(a) Ref_8.0_4 (b) Ref_8.0_5 (c) Ref_8.0_6

Figure 5.13: Filled sand trap after initial infill prior to test

After the entire test sequence was finished, the erosion of the three tests was photographed again. These photos can be found in Figure 5.14. In test Ref_8.0_4 the heaps located at the rear increased, but also new heaps had formed the wall in the front. Test Ref_8.0_5 showed an increase in the amount of sand in the middle boxes. The outer boxes were less influenced during tests. In test Ref_8.0_6 the erosion was mainly in the outer boxes, with almost no erosion in the second box from the right, even after all tests were finished.

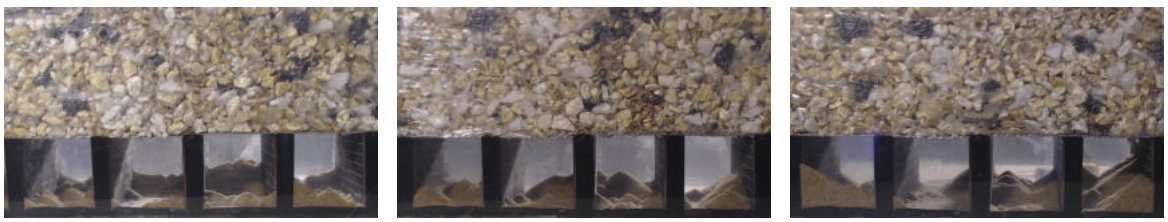

(a) Ref_8.0_4 (b) Ref_8.0_5 (c) Ref_8.0_6

Figure 5.14: Filled sand trap after the entire reference test sequence

The three tests show a different allocation of sand over the tests. This is due to the channelling inside the filter layer. This channelling is the process that the sand finds a ”channel” through the filter layer. The erosion, which is of interest, is located at the interface between the granular filter and sand layer. The results in this paragraph mainly indicate that in all tests, the erosion is located in every box in the sand trap. The magnitudes of the erosion look to be equal over the multiple tests, but only as an estimate.

5.2.3. Critical gradient reference tests

During the reference tests, the critical hydraulic gradients were determined on the velocity steps given in Table 5.1. The steps during the reference tests were only 15 minutes long. The steps between two

consecutive gradients were also larger than during the final test sequence. With a velocity difference of 0.02 to 0.05 rps, this was larger than the 0.01 rps difference that was used during the final test sequence.

The results of both the negative and positive gradients are in Table 5.2. The velocities which were obtained as critical were not similar, but the gradients were. As described in Paragraph 5.1.1, the gradients are the main focus of the research and are more important than the forced velocity. What can be seen in the table is that the critical gradients were constant over multiple tests. The spread over tests was around 10%.

Test	Ref_8.0_3	Ref_8.0_4	Ref_8.0_5	Ref_8.0_6
Velocity	VE_012	VE_018	VE_018	VE_015
$I_{negative,\parallel}$	0.011	0.011	0.011	0.011
$I_{positive,\parallel}$	0.012	0.010	0.011	0.011

Table 5.2: Critical gradients reference tests

5.3. Results final model tests

After the consistency of the physical model was tested and found to be accurate the final tests were run, these final tests were the ten tests that used the five granular filter- sand combinations, with both the parallel and perpendicular configuration as described in Table 4.3. Besides that, additional tests were performed, which were the special test cases described in Table 4.4.

5.3.1. Sensor malfunction

Although measures were taken to extract correct measurements from the pressure sensors, tests have failed due to broken sensors. To be able to calculate the parallel gradient over the granular filter layer, the results of at least two pressure sensors had to be obtained. This requirement was not met for both the Para_9.5 and Para_8.0_super test. The Para_9.5 test had both water level gauges working. These gauges were used as a backup to calculate the parallel gradients. In Appendix D.3 an overview is given of the sensors that were and were not working during tests.

During the perpendicular tests, two pressure sensors were needed inside of the sand layer. The only test where the two sensors were not working was Perp_4.0, which is excluded from the results for this reason.

The pressure sensors were also placed loosely inside both layers, which made movement possible. The sinking for both configurations is depicted in Figure 5.15. It can be seen from this figure that the influence on the results for the perpendicular configuration was large, while there was no influence for the parallel configuration. As the distance over which the gradient has been calculated was much more influenced for the perpendicular sensor configuration.

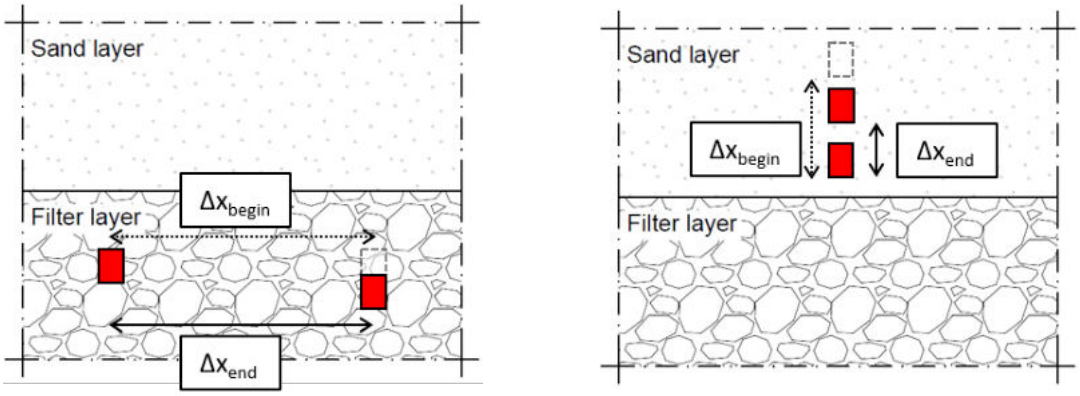

(a) Parallel sensor configuration

(b) Perpendicular sensor configuration

Figure 5.15: Sensor sinking for the two tested configurations together with the difference in distance between the gauges, which is important for the calculation of the Hydraulic gradient.

The video measurements were also vulnerable. The program which was used to record the time-lapses had stalled or crashed multiple times during the execution of the tests. Because two cameras have been used that were connected to two separate computers, the program stalling lead to no loss of data.

5.3.2. Visual observations

Besides the measurements and the video footage, a large set of results has been based on the visual observations of the author during the test sequence. As the total number of tests, including the tests with unfinished models, is around 30 tests. Some patterns were discovered concerning the erosion through the granular filter layer. As these observations have not been measured or filmed, these observations were just used to describe the behaviour of the setup in a qualitative manner.

One observation was the erosion on a layer without hydraulic gradients. Since the tests ran for long times, sometimes even throughout weekends, the plunger was not always moving. At the moments when the plunger was not producing any gradients, the footage from the physical model setup was checked for erosion. During all tests, no erosion during periods without gradients could be seen. This included the most open cases (Para_16.5 and Perp_16.5).

The erosion of the sand through the granular filter was seen to have a delay due to the sorting of sediments inside the filter layer. After the initial infill had stopped and a gradient was exerted on the physical model setup, there was erosion. This erosion was believed to originate from the sediments that were located in the granular filter layer but did not fall al the way through this granular filter layer. This erosion did not influence the strength of the interface but could influence measurements. For this reason, the plunger was run with the minimal gradient to empty the residual sediments in the filter layer.

Inducing large gradients and large vibrations to the model setup. The container was hit with a hammer numerous times both with and without plunger movement. It was seen that the vibrating caused much erosion a short time after the impact, but that the erosion also stopped within a minute, independent of the plunger movement.

The last observation can be seen in Figure 5.16. In this figure, clear heaps of sand are visible inside the sand trap. These heaps originated from channels that have been formed through the granular filter layer. This channelling lead to erosion hotspots in the granular filter layer; all tests showed this type of erosion. The channelling happened after the erosion has occurred. The channelling did influence the measurements as the erosion was more difficult to quantify, but did not influence the erosion on the filter-sand interface.

Figure 5.16: Heaps of sand inside the sand trap, which are due to channelling in the granular filter layer

5.3.3. Relations granular filter-base ratio to critical gradient

The main goal of this research was to look for a relation between the forcing ($I_{crit,\perp}$ & $I_{crit,\parallel}$) and the grain size ratio ($\frac{D_{15F}}{D_{85B}}$). In this paragraph, the results of each test are plotted with the forcing (critical hydraulic gradients) on the y-axis and the grain size on de x-axis (stability ratio), analogue to the figures from previous research discussed in Paragraph 2.3. In Figure 5.17 the results of the parallel test are plotted. In Figure 5.18, the results of the parallel tests are plotted. In both figures also, the closed filter limit is depicted as this is the region where no erosion should be possible.

In both figures, three dots are plotted, which depict the three critical gradients that were determined. Also, two triangles are plotted (only one for the perpendicular gradient), which depict gradients that were measured, but that were no critical gradients. This was due to limitations of the plunger. For the upward pointing arrow, this meant a gradient which was to low to be the critical gradient and for the downward pointing arrow these depict a gradient that was too large to be the critical gradient. Besides these points also errorbars are plotted which depict the steps where the gradient was located in-between.

Parallel gradients

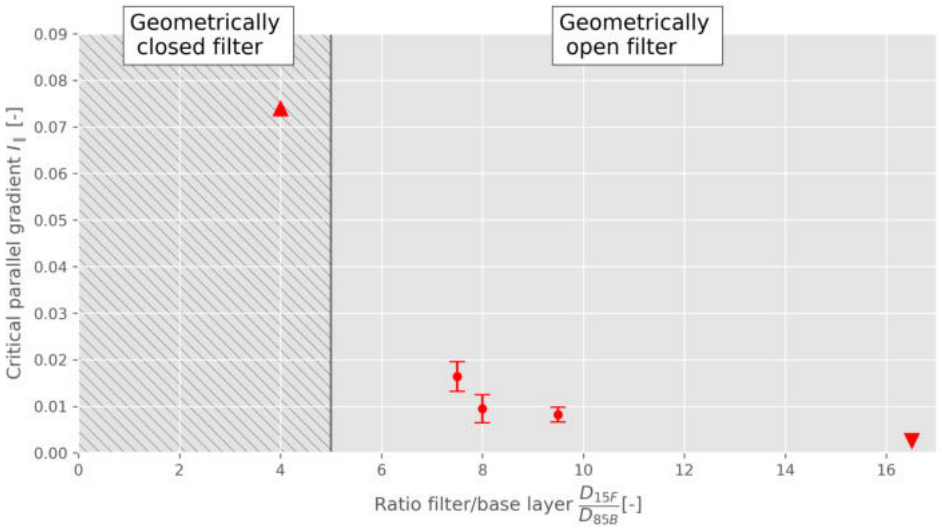

Figure 5.17: Relationship between the stability ratio of the base layer and granular filter layer and the parallel critical gradient.

The three dots, which originate from tests: Para_7.5, Para_8.0 and Para_9.5. were not sufficient to produce a formula of any kind, but clearly gave the region in which a granular geometrically open filter-base layer could be stable. The main result of this test was therefore that a granular filter-base layer with a D_{15F}/D_{85B} between 7.5 and 9.5 had a critical parallel gradient of around 0.008-0.02

Perpendicular gradients

For the perpendicular setup, the same graph is created as Figure 5.17. The perpendicular gradient for the closed filter test (Perp_4.0) is left out of the graph. As discussed above this test did not produce any reliable measurements, but no erosion was visible during the entire test, so it has also been closed during the highest gradients the plunger was able to produce. Similar to the parallel gradients, the three dots which are from tests: Perp_7.5, Perp_8.0 and Perp_9.5, give the region in which a granular filter base layer could be stable for perpendicular gradients. The main result of these tests was therefore that a granular filter base layer with a D_{15F}/D_{85B} between 7.5 and 9.5 had a critical perpendicular gradient of around 0.1-0.2.

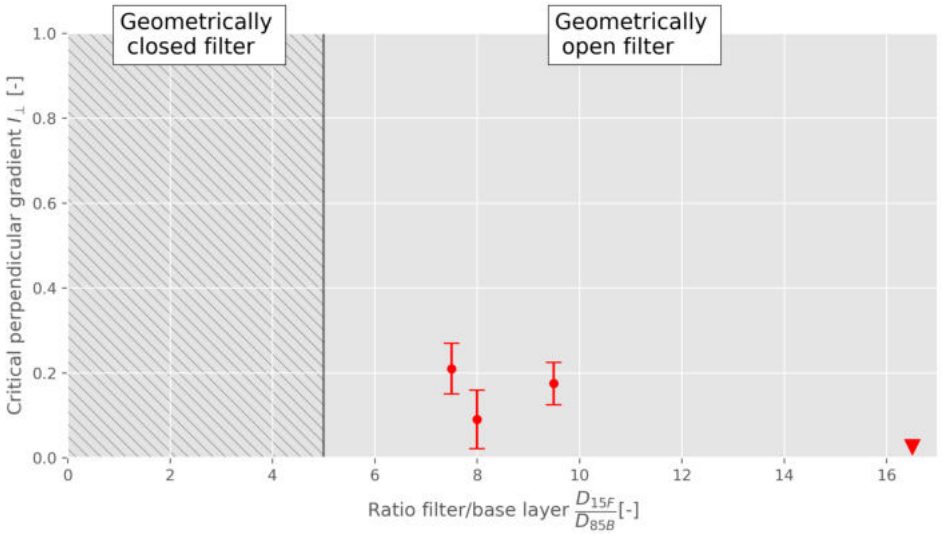

Figure 5.18: Relationship between the stability ratio of the base layer and granular filter layer and the critical perpendicular gradient

Critical gradient versus grain size

Previous granular filter research pointed out that not only the stability ratio between the layers was a factor of influence for the critical gradient, also the grain size of the base layer had a large impact on the stability (de Graauw et al., 1983). To see whether this was also the case with the granular filter base layer considered in this research the critical gradients of both the parallel and perpendicular tests were plotted against the median grain sizes of the sand that was used as base layer in these tests. Note that for both directions only the three tests in which a critical gradient was determined are used. The test that were used, with the corresponding grain sizes are:

- Para_7.5 & Perp_7.5: Sand 2 $D_{50} \approx 0.20mm$
- Para_8.0 & Perp_8.0: Sand 1 $D_{50} \approx 0.40mm$
- Para_9.5 & Perp_9.5: Sand 3 $D_{50} \approx 0.55mm$

The grain size distributions of these tests can be found in Paragraph 4.3.

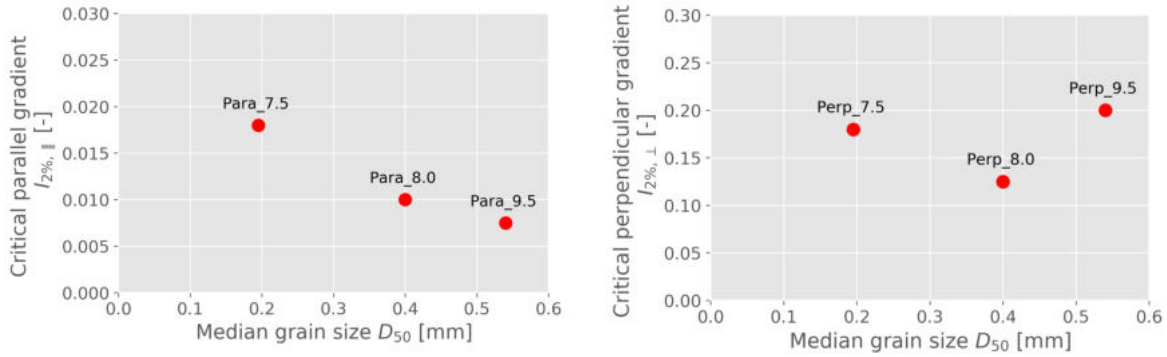

(a) Parallel gradient

(b) Perpendicular gradient

Figure 5.19: Relation between median grain size of the base layer and critical gradient, both parallel and perpendicular.

For the parallel gradients the three points seem to have a linear relation, the perpendicular gradients does not seem to have any relationship.

5.3.4. Special test cases

In this paragraph, the results from the special test cases as described in Paragraph 4.9.3 were described. All three tests did not produce accurate results due to measurement errors. All tests, however, gave a qualitative understanding of the occurring processes.

Influence superimposed load

Both the parallel and perpendicular configurations were tested with the superimposed load. For test Para_8.0_super the pressure sensors stopped working during the tests. The forcings on the container were compared to give an estimate of the occurring gradient, with the help of Figure 5.1a. It was seen from this comparison that the superimposed load did not increase the gradient during parallel testing. Also, visual observations of the model setup, for example, during shaking of the container, did not show any increase in stability.

Test Perp_8.0_super showed an increase in the critical gradient between the critical gradient and the erosional gradient. This increase was due to a programming error of the plunger. The perpendicular gradient with a superimposed load has been slightly larger than the case without superimposed load, but the gradient after the critical gradient was five times larger. For this reason, together with visual observations, it was expected that superimposed load would have an influence on the perpendicular critical gradient, but it could not be quantified with the available results.

Long term behaviour

The long term behaviour of the system has been checked with a test: Para_8.0_long. As breakwaters are usually built for the long term, it was important to see the long term reaction to a critical gradient. The test duration was a week. During this week the granular filter sand combination was loaded with a single parallel gradient. During this long test, it was checked whether the long term did influence the erosion. The test was filmed, similar to the other tests, but with a photo every ten minutes instead of 30 seconds. After the test was completed, the results could not be compared. There was some form of algae that formed a layer on the plexiglass walls. The results of this can be seen in Figure 5.20b. The erosion could be analysed visually, as that was easier to see through the algae. The erosion was compared with the erosion after the initial infill, which is depicted in Figure 5.20a. It looked like there was not much erosion during the week, but the uncertainties are too large to draw conclusions.

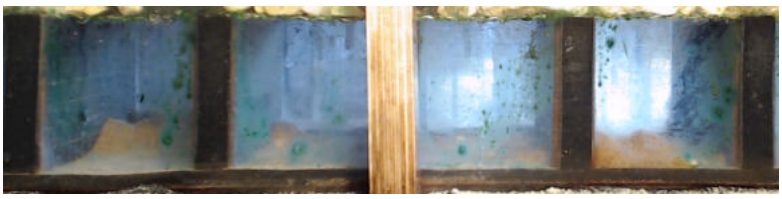

(a) Begin of the test

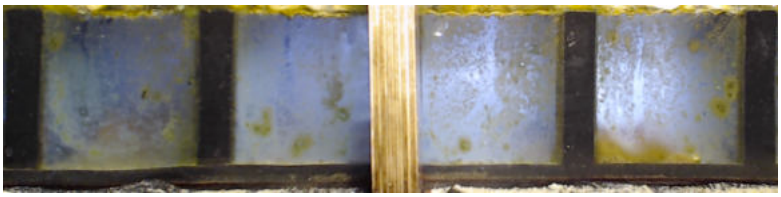

(b) End of the test

Figure 5.20: Results of long term test Para_8.0_long

5.4. Critical gradients compared to case study

In Chapter 3, the gradients of a case study are determined. To see the relevance of the final figures in this chapter, the mean values of the critical gradients are plotted in the graphs in this paragraph.

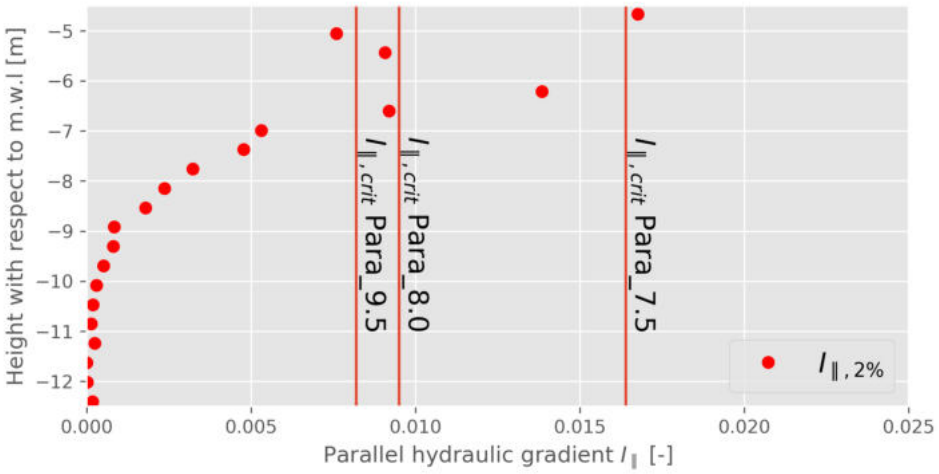

Figure 5.21: Parallel gradients as determined for the case study with OpenFOAM. The vertical lines in these graphs depict the critical gradients determined with the model tests. The graphs do not include the error bars, these bars can be seen in Figure 5.17

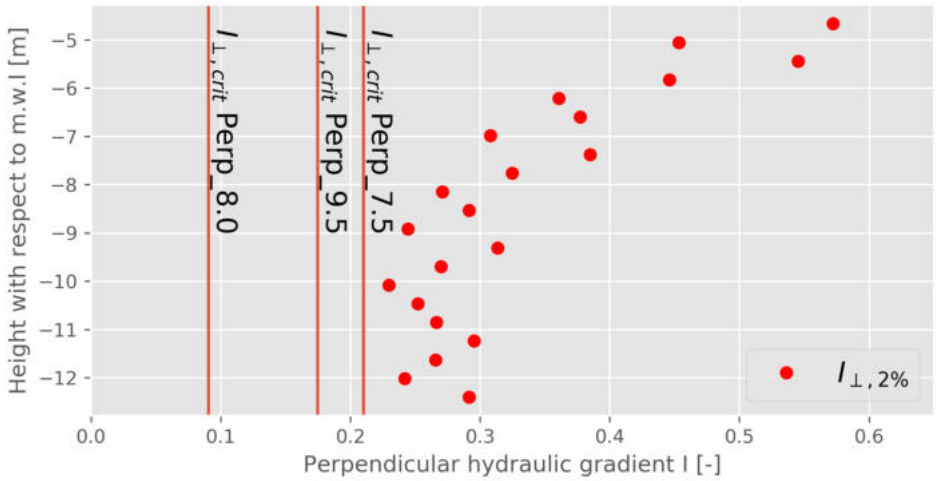

Figure 5.22: Perpendicular gradients as determined for the case study with OpenFOAM. The vertical lines in these graphs depict the critical gradients determined with the model tests. The graphs do not include the error bars, these bars can be seen in Figure 5.18

What can be seen from these graphs is that the parallel hydraulic gradients obtained from the case study were lower, in some parts of the filter than the critical gradients, which would result in a stable system. The perpendicular gradients were always larger in the case study, meaning that there was never a stable situation.

5.5. Conclusions results

In this paragraph, the conclusions of each separate part of this chapter are summarized. The main conclusion of this chapter is that it is possible to have a stable geometrically open hydraulically closed filter layer which is placed below a sand layer.

- The reference tests showed that the setup could be built with good accuracy. The tests also showed that the plunger velocity could only be used for a first rough estimation of gradients. Which meant that all gradients have to be measured inside the correct layer; Granular filter for parallel and sand layer for perpendicular.
- The plunger itself created reliable gradients that were constant over tests. The gradients had the same signal and magnitude during an entire test of three hours.
- The parallel model configuration created constant gradients that were constant over the upward and downward movement of the plunger, which gave reliable results. For the perpendicular configuration, the gradients increased the entire upward and downward movement, which made it more difficult to characterize the gradient by a single value.
- Two graphs have been made that show a relation between the forcing and the resistance. These graphs show a region in which a granular open filter layer can be hydraulically closed for both directions. The parallel gradient shows a linear correlation with the grain sizes of the base layer, while the perpendicular gradients do not show this correlation.
- It can be concluded that the erosion does not increase if the duration of a test is increased. If a critical gradient is exerted on the granular open filter layer, this will not lead to erosion over a long time.
- The critical perpendicular gradient seems to be influenced by the superimposed load. The critical parallel gradient does not seem to increase.

6

Discussion, conclusions and recommendations

6.1. Discussion

Before this thesis, limited research was conducted on the topic of the placement of a filter in between a land reclamation created from dredged sand and a breakwater core with the core partially below the sand reclamation. Although it is possible to create a sand tight interface, this chapter discusses the uncertainties that exist and the applicability of the results.

6.1.1. Measurement inaccuracies

Since a physical model is always a representation of reality, errors could have been present during physical model testing. In this paragraph, the errors that were present are discussed.

- **Accuracy of pressure sensor placement.**
  The placement of the pressure sensors was critical for correct measurements. The sensors had to be placed on the same location during every test to create the same results. As the sensors were loosely placed in the granular material for the parallel configuration, loosely place in the sand for the perpendicular configuration, and had to be injected with water prior to each test, the exact placement was difficult to control. The sensors were aligned correctly in the container before each test; on the centerline of the container above the partitions of the sand trap for the parallel model and the centerline in the middle of the filter for the perpendicular setup. The distance between sensors was not always equal over different tests, which has lead to measurement errors. However, the largest errors due to placement were mitigated, as the distances between the sensors were measured prior to each test, which made the calculation of gradients more reliable.

- **Movement of pressure sensors**
  When the tests were analysed, some measurements showed an increase in the signal from the pressure sensors. This increase in signal was often only seen coming from one of the pressure sensors and had nothing to do with a change in water level as the water level gauges gave a consistent result. The difference in the signal could be caused by the sinking of the sensor into either the filter layer (parallel flow) or the sand layer (perpendicular flow).

  The signal that came from the sensor was de-trended in the analysis, which decreased the error produced by the sinking of the separate pressure sensors. However, the sinking did also change the distance between the pressure sensors, which was used to calculate the gradient.

  For the parallel flow the change in distance, over which the hydraulic gradients were calculated, due to sinking was small. The sinking of a sensor was perpendicular to the distance line, with a few centimetres of sinking compared to a distance of 15-16 centimetres. This meant that a sensor that sinks 1 centimetre only increased the distance between the sensors with 0.04 centimetre,

which is an increase of 2.5%.

The sensor sinking in the perpendicular case had a much larger impact; not only was the sinking in line with the distance line, but also the distance between the sensors was a lot smaller. As the sand layer eroded during initial infill, the sensors, that were placed inside this sand layer, sank already before the plunger did induce gradients. A sinking of one centimetre for a pressure sensor in the perpendicular case meant a difference in sensor distance of one centimeter which is around 20% for a sensor distance of around 5cm, as the sinking was parallel to the distance line between the sensors.

- **Selection of critical gradients.**
  Except for the cases where no critical gradient could be found, which were Para_4.0, Perp_4.0, Para_16.5 and Perp_16.5, a single gradient was chosen to be the critical gradient. This gradient was determined from the time-lapses of that test. Some tests showed a sudden increase in erosion which made it both easy and reliable to determine the critical gradient. Other tests showed a more gradual increase in erosion, which made it harder to determine a gradient in those tests. That uncertainty made the gradients less accurate and therefore, the outcome of the research less accurate. The errors given by these inaccuracies are plotted as error bars in the final figures in Chapter 5.

- **Consistency of perpendicular setup**
  The parallel setup is extensively tested with the reference tests. The perpendicular setup is only tested with the regular tests, so no information regarding the consistency of these tests has been obtained. It is assumed that the consistency of the parallel tests is comparable to the consistency of the perpendicular configuration, but no further information was gained regarding this consistency.

- **Influence of inclination of filter layer**
  The considered breakwater in this research has an inclined granular filter. The granular filter in the physical model setup that was used in this research does not have this inclination. As it is believed that the erosion through the filter layer is always downwards the incline is not necessary to describe the occurring processes. A physical model without inclination gave a more accurate symmetrical representation of the processes.

- **Sloshing of water**
  During testing with higher gradients, the velocity of the plunger was much larger than the water was able to react, due to inertia. This leads to the sloshing of the water inside the right part of the model setup, section C. This sloshing did not move the water inside the filter layer, but did induce peaks in the gradient signal. These peaks did not contribute to erosion but were still visible.

- **Airtightness**
  The airtightness of the physical model setup was also a point of concern. The analysis of the gradients produced by the reference tests showed that there might be some gaps through which some air could leak. This leaking will cause the gradient to change over the filter layer. Another outcome of this leaking could be that the gradients were not purely parallel during testing with the parallel configuration.

- **Calibration**
  Before each test, the sensors were calibrated. The visual checking of the water level was done by holding a ruler onto the right section of the container parallel to the water level and noting this water level on another ruler that was taped to the side of the container. This method was thought to be the most reliable, however, was still inaccurate due to visual measurement inaccuracies, adhesion of the water to the container and the horizontal level of the container which changed slightly throughout tests due to wood warping.

  The intermediate calibration did only decrease the spreading between sensors. It made sure that the sensors gave identical results between themselves for each test. As the gradient is calculated with the difference between sensors, the accuracy of the gradients was less influenced by these measurement inaccuracies.

- **Overall measurement inaccuracies**
  The last type of inaccuracies came from the laboratory. Since it was very hot during the execution of some tests, those tests suffered from large evaporation. Also, vibrations due to construction works or even people passing by the model setup could have an influence on the measurements. These were all difficult to quantify as the author was not always present at the laboratory, and the tests were too long to check the entire test for vibrations. The influence of these vibrations is, however, believed to be negligible as the duration of such vibration would be very short compared to the three-hour duration of an entire test.

- **Numerical model inaccuracies**
  As discussed in Chapter 3, the gradients that were computed with the OpenFOAM model are only used to determine an order of magnitude. The influence of erosion through the filter layer is not computed by OpenFOAM. This erosion might influence the gradients along the interface. For this research, the occurring hydraulic gradients were only of interest to see whether the results were applicable in a prototype case. The gradients exerted on the test setup were in the same order of magnitude as the gradients extracted from OpenFOAM.

6.1.2. Comparison to existing guidelines and research

Previous research is done on the topic of granular geometrically open filters. To put this research into perspective and also to see whether the configuration tested in this thesis shows resemblance with the other configuration, the results are compared with previous research.

- **Tutein Nolthenius (2018)**
  The research in the subject of the reversed open filter was started as an alternative on the method designed in the research by Tutein Nolthenius (2018). The research by Tutein Nolthenius (2018) is focussed on the same problem, but a different interface. The research is about a rubble mound land reclamation in which no filter is used. Without the filter, the sand will infiltrate the core. Tutein Nolthenius (2018) looked at the stability along the interface inside the core, to compare the research about the reversed filter with the research by Tutein Nolthenius (2018) it is assumed that the gradients at the interfaces considered in both studies were equal, in reality, the gradients would be large for the research by (Tutein Nolthenius, 2018), as the distance towards the seaward side is smaller meaning less attenuation of pressures. For the hydraulic gradients that were found using the numerical model, both situations would be stable for parallel gradients. For perpendicular gradients, Tutein Nolthenius (2018) has no measurements.

  For design, one configuration is governing. If a reversed filter is used, this infill will not be present or will wash away. This means that only one of two situations is governing, depending on the design of the rubble mound.

- **Wolters et al. (2012)**
  The formula created by Wolters et al. (2012) is the current guideline for the construction of open filters, the formula created in the research links the erosion through a filter layer to the thickness of that layer, together with the grain sizes and a lot of empirically determined parameters. The formula is created for a situation where the filter is on top of the base layer. Due to gravity, the thickness will add to the strength of the layer. It is not expected that the critical gradients, determined in this thesis, would be anywhere near the ones calculated with the formulas that were created in the research.

- **De Graauw et al. (1983)**
  The guideline by de Graauw et al. (1983) was more in line with the reversed filter research, although the formula was unable to calculate the erosion. With the gradients that were used in this thesis ($I_{\parallel} \leq 0.02$ and $I_{\perp} \leq 0.2$), the filters would be hydraulically closed independently of the used grain sizes, as calculated by de Graauw et al. (1983). The arching proposed in the research is believed to be the actual erosion mechanism that increases stability.

- **Schürenkamp et al. (2015)**
  Although this thesis was about geometrically open filters, also a geometrically closed filter was

tested, since this research showed that even those filters were not always closed for sand transport. This was, however, not the case, even with the highest plunger velocity possible.

These researches showed that the comparison between the layout where the base layer is below the filter layer and the filter base layout considered in this thesis is difficult. It is concluded that the filter-base layer configuration tested in this thesis cannot be compared with the available guidelines. Moreover, only the arching mechanism as proposed by de Graauw et al. (1983) can be used to give an estimate of the stability, especially for the use of a superimposed load.

6.1.3. Hydraulic gradients in reality

In this paragraph, the comparison between both the physical model setup and the hydraulic gradients that are present at a prototype rubble mound land reclamation is discussed. The used physical model setup is simplified to be able to fit inside the small container. The model setup was designed as a small cut-out of the granular filter and sand layer. This simplification induces model effects. These model effects are believed to be small but have to be analysed before the results can be used for construction.

- **Combination of parallel and perpendicular gradients**
  The flow inside the container was one-directional, meaning only parallel or perpendicular to the filter-base interface. This separation made it possible to see the behaviour of the granular filter - sand layer for the particular flow directions, which made it possible to extract the relevant data for these directions. There is, however, no research performed in which both gradients were present at the same time. Below a comparison is made between the hydraulic present in the physical model and the hydraulic gradients that occur in reality

  A combination of both flow directions could be present in reality. The numerical model showed that the largest parallel gradients occur at the same time as the largest perpendicular gradients. In the case both gradients are large, it might be that the critical gradients are not altered, meaning that the stability is similar to one-directional flow with the same gradient. More likely could be that stability is decreased. As both gradients might have the same failure mechanism, breakage of the arching, the gradients might decrease the stability.

- **Symmetry of gradients**
  The symmetry of the flow is also something that is rarely seen in reality. In reality, the filter is inclined and placed at the rear end of a breakwater. This rear end can be schematized with a triangle of which the filter is placed in the corner. Due to this shape, the flow patterns in this rear side are difficult to predict. An estimate is given by the numerical model, which calculated the downward gradients to be larger than the upward parallel gradients. The perpendicular gradients that were determined with the numerical model were also asymmetrical. The perpendicular gradient inward into the sand layer was larger than the perpendicular gradient outwards of the sand layer.

- **Irregular gradients**
  The wave pattern that was forced on the physical model consisted of regular waves, which also means that the critical hydraulic gradients are determined for a regular wave pattern. In reality, the hydraulic gradients could be forced to the breakwater by an irregular wave climate, which means that the results might be different. The gradients produced by an irregular wave pattern are also irregular as seen with the numerical model. Previous research saw that the irregular wave loading produced similar results as a regular wave loading (Ockeloen, 2007). For the failure mechanism considered, which is arching, the irregular wave pattern might decrease the critical gradient, due to breaking of the arches by the largest gradients.

  The wave pattern was characterised by the maximum wave during the numerical simulation. Since the largest waves are considered to be governing for the erosion, this would be a good estimate for the wave forces. The maximum wave height which was used to compare the results to was 5.1m.

- **Currents**
  Also, currents through the breakwater and land reclamation could occur. These currents could

originate from the tides, inland rivers or precipitation on the land reclamation. The currents might have an impact on the strength, but that is dependent on the direction of these currents. There could be two influences of this current. The first effect is the influence on arching. An inward current, meaning coming from a higher water level in the breakwater and a lower water level in the land reclamation, might decrease the critical gradients as it might break the arching of the sand layer. An outward current might increase stability by increasing the strength of the arches. The other possibility could be that the current influences the individual sand grain. If that is the case, the stability could be increased with an inward current, by forcing the grains into the sand layer. The stability for an outward current would be less in that case as the current could convey the sand grains through the filter layer.

Combination of both effects is also possible, an outward flow will give a fragile situation as the arches are strengthened due to the current, but if the arches are broken the currents will convey the sand through the filter layer (de Graauw et al., 1983).

6.1.4. Uncertainties in application

It should be possible to put the knowledge that is gained by this research into practice. As stated in the introduction of this research, land is becoming more scarce, and land reclamations are needed to facilitate population growth. This research can contribute to the build-ability and cost-effectiveness of these reclamations by removing the need for a geotextile on the lower rear end of the breakwater. However, before it can be built, some uncertainties should be addressed.

- **Pressures through breakwater**
  As discussed in Chapter 2, no research is conducted to calculate the gradients that are present along the rear side interface. It is however seen that the perpendicular gradient can be estimated by the linear pressure attenuation through the sand layer behind the breakwater. Which is calculated by the excess pore pressure in the filter layer divided by the distance to the pheatric surface.

  A breakwater, in reality, is subject to waves and flow. To be able to use the results from the physical model tests for construction it is needed to determine the relationship between the forcing on the breakwater, which can be characterised by H_s and T_p, and the hydraulic gradients that affect the filter layer. A possibility is to create a numerical model, similar to the model used in this research. This is, however, time-consuming and therefore not preferable. A calculation similar to the empirical model by Vanneste and Troch (2012) would be more time and therefore cost-effective. As concluded in both Chapters 2 and 3, it is not possible to calculate the pressures with the empirical models created for a closed rear side breakwater.

- **Oblique wave attack**
  A difference in wave climate can also be found in the direction of the hydraulic gradient. This gradient could be, besides the perpendicular and parallel gradients, a longshore gradient. Such a longshore gradient would originate from the oblique wave attack. As the infiltration length into the breakwater on an angle is always larger than the perpendicular infiltration length through the core, the pressures at the rear side of the breakwater will always be lower (Losada et al., 1991).

  Besides the lower pressures and therefore the lower gradients, the longshore gradient will have no influence on the perpendicular hydraulic gradients in the sand layer, as the smallest distance to the phreatic surface, which determines the gradient, will always be perpendicular to the axis of the breakwater. The parallel gradients, as considered in this research will also be lower due to a longer infiltration length, but the gradient in the filter layer will also be influenced due to the oblique wave attack. As the oblique wave attack creates a hydraulic gradient parallel to the axis of the breakwater, there will be another hydraulic gradient on the interface of the filter-sand reclamation. That hydraulic gradient will be the longshore gradient. This longshore gradient will act as a parallel gradient to the interface but in a different direction.

- **Influence wave length**
  A variation in wavelengths can also produce different hydraulic gradients in the filter layer. Longer waves could protrude further into the breakwater and could, therefore, have a larger influence on

the gradients. Very long waves could have the same impact as the currents described above. Longer waves might influence the arching by applying force on the grains with a longer duration. This longer duration could eventually decrease stability, but this is highly uncertain.

- **Top load on sand layer**
  Another uncertainty is the influence of the top loads on the granular filter-sand interface. The physical model tests in this thesis showed a visual increase with a superimposed load on the sand layer. In the application, the sand that is placed on top of the filter layer induces a larger load than is tested. This could have an additional influence on stability. The critical gradients could be influenced by this superimposed load as it increases the strength of the arches. The critical parallel gradients might also be increased by this additional superimposed load.

6.1.5. Preliminary guideline for design

In this paragraph, a guideline to design a structure that uses the reversed open filter considered in this research is proposed. The guideline can only be used for preliminary estimates and should not be used for a final design.

Loads

First, the loads that work on the filter layer have to be determined. These loads have to be approximated, which is preferably done with an empirical model because a numerical or physical model would be too time-consuming for the preliminary design.

The hydraulic parallel gradients could be estimated with the research by Polidoro et al. (2015). This research only gives the range of magnitudes for the gradients, but that will be sufficient for a preliminary guideline.

The hydraulic perpendicular gradients can be estimated with the pressure attenuation over the sand layer. As discussed the overpressure along the rear side of the breakwater is almost linearly attenuated over the sand layer. This means that a first estimation can be made with the overpressure along the rear side. This overpressure cannot be calculated with the method by Vanneste and Troch (2012), as concluded in Chapter 2. A method as proposed by Burcharth et al. (1999) or the Transmission formula from (CIRIA, CUR, 2007) gives a better estimate of the local pressures.

Stability

The loads can be used to estimate the stability of the reversed filter with the use of the final graphs (Figures 5.17 and 5.18). For the perpendicular gradients, the gradient is believed to be influenced by the superimposed load on the sand layer. This superimposed load consists of the weight of the sand layer on top of the filter layer. The critical gradient can be increased because of this superimposed load. A first estimate can be made with Figure 2.16 (de Graauw et al., 1983).

The granular open filter can be unstable at two boundaries; as the granular filter layer will be placed in between the rubble mound core and the sand of the reclamation. In this thesis, only the interface between the granular filter and the sand is considered. The interface between the granular filter and the core can also be either geometrically open or closed. Based on the uncertainty whether the critical gradients of this interface are lower or similar to the gradients of the filter-sand interface, it is recommended to use the closed filter rules on this interface.

If the interface between the sand and the open filter cannot be geometrically closed along the rear side of a breakwater, a geotextile can be added. This geotextile can be combined with the open filter to remove the need for the geotextile in the lower part of the breakwater while ensuring a sand tight boundary. The only limitation is the depth over which the geotextile can be placed, which is dependent on the equipment used to place the geotextile.

6.2. Conclusion

Is it possible to create a filter layer in between a rubble mound breakwater and a sand reclamation? That question was answered in this thesis. The research consists of a review of other literature concerning the filter research, a calculation of the hydraulic behaviour of a case study with a numerical model and tests of the physical phenomena with a physical model. In this paragraph, the conclusions of the subquestions as described in Chapter 1 are explained.

6.2.1. Hydraulic gradients from numerical and empirical models

The gradients that are responsible for the erosion through the filter layer are determined with the help of a numerical model. This numerical model showed to be an excellent tool to describe the order of magnitude. The numerical model showed a wave attenuation through the core of the breakwater, similar to the research by Vanneste and Troch (2012). Inside the sand, there was almost no flow as the hydraulic conductivity of the sand is very low. The flow inside the breakwater was two-directional as the water flowed into the filter from the top during high water levels inside the breakwater and into the bottom of the filter to the top during low water levels inside the breakwater.

The gradients that were obtained using the numerical model were in the same order of magnitude as the parallel gradients found from the literature. The parallel gradients were 0.02 in the top of the filter layer and decreased quickly to zero. The perpendicular gradients were around 0.6 in the top part and decreased to 0.2-0.3 in the lower part of the filter layer. As can also be seen in the figures below.

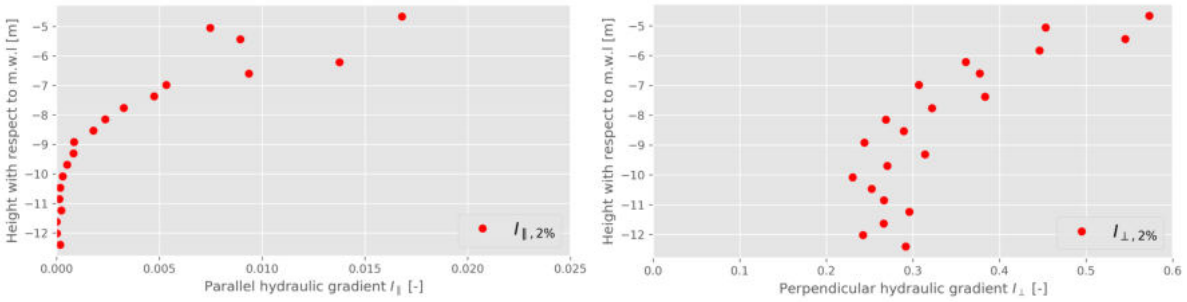

(a) Parallel gradients

(b) Perpendicular gradients

Figure 6.1: The 2% highest gradients plotted against the height with respect to mean water level, is a result from the numerical model for the two directions. T

6.2.2. Magnitude of critical hydraulic gradients from physical model

The physical model setup produced critical hydraulic gradients in both directions for three stability ratios, calculated with D_{15F}/D_{85B} , between the granular filter and the base layer on top of the filter layer.

For the parallel flow configuration, the gradients with a stability ratio between 9.5 and 7.5 were determined to be around 0.005-0.02, with the smaller stability number giving the higher critical gradient. The gradients are depicted in Figure 6.2.

The perpendicular flow configuration had a larger error, but also three critical gradients in the same region of stability ratio were determined, which was between 9.5 and 7.5. The critical gradients were determined to be around 0.1-0.2 but did not show any correlation, which can also be seen in Figure 6.3.

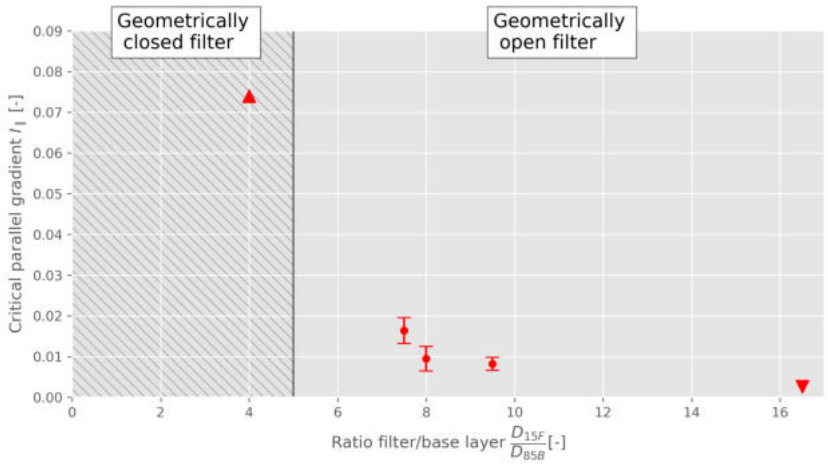

Figure 6.2: Critical parallel gradients plotted against base to filter ratio

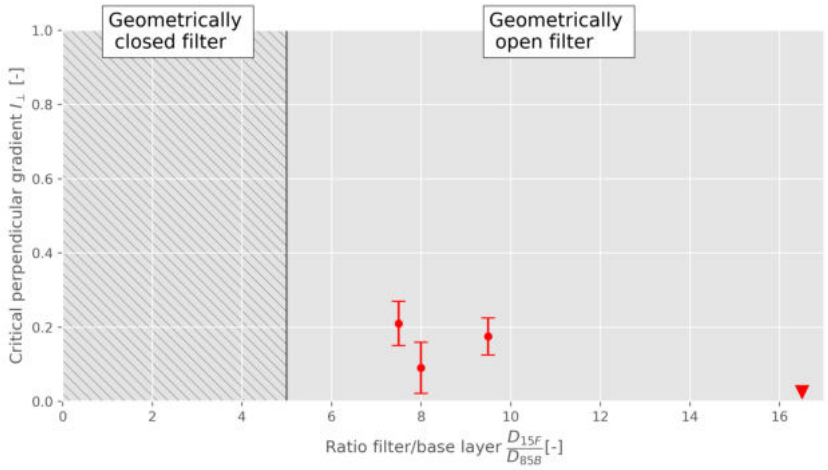

Figure 6.3: Critical Perpendicular gradients plotted against base to filter ratio

Both configurations did not show any erosion during testing with a geometrically closed filter, with a stability ratio of 4.0. For a very open filter, stability ratio of 16.5, both configurations showed erosion with even the smallest hydraulic gradient that could be forced to the setup by the plunger.

6.2.3. Special test cases

The special test cases both did not show reliable results due to measurement errors and sensor failing. The results from the superimposed test seemed to increase the critical gradient as was expected. The critical parallel gradients were not measured, so no results for that are obtained. As it was concluded that the arching effect is the governing effect for the erosion, the superimposed load could have an influence on the stability of the reversed filter.

The long test did not show any increase in erosion over time, meaning that the long term behaviour of the filter is concluded to be stable.

6.2.4. Comparison critical gradient with case study

The gradients on the filter sand interface are separated in two directions. These directions are described separately in the entire report. Both gradient directions are tested with different configurations of the physical model. In reality, both gradient directions are present at the same time, meaning that the stability also has to be a combination of both. In comparison, only the gradients are depicted, no information regarding grain size is used. The results of both physical model tests are depicted together

with the gradients obtained from the numerical model of the case study in Figure 6.4.

The parallel hydraulic gradients that are obtained from the numerical model are more significant than the critical gradients in the filter layer. This means that the filter is not sand tight. This is, however, only in the top of the filter layer. From -7m to -12.4m the hydraulic gradients in the case study are lower than the critical gradient indicating a hydraulically closed filter.

The parallel gradients obtained from the case study are higher than the critical gradients along the entire filter layer. This means that with the used grain size ratios, the reversed filter in the case study is not sand tight.

Combined, it can be seen that the perpendicular gradients are governing for the erosion. The ratio between the gradients is influenced by the geometry of the breakwater cross-sections, so it is only governing for this particular case.

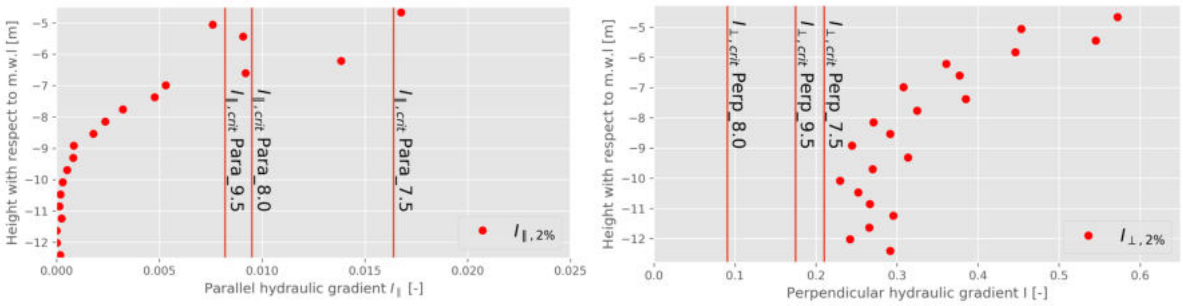

(a) Parallel gradients

(b) Perpendicular gradients

Figure 6.4: The top of the open filter layer is located at the -5m line. The vertical lines depict the critical gradients obtained from the physical model tests.

6.2.5. Main conclusion

The question of this report was: ”How is it possible to create a boundary between a breakwater core and a sand reclamation through which the sand cannot protrude with the use of a single granular geometrically open filter layer?”. The main conclusion is that it is possible to create a granular geometrically open filter layer which is closed for sand transport when the sand layer is on top of the granular filter layer.

The question: ”How is it possible?” is dependent on the local wave climate, if the wave climate is known, the gradients can be compared with the two final graphs in (Figures 6.2 and 6.3). The reversed filter is stable if both hydraulic gradients, which are perpendicular and parallel, are equal to or lower than the critical gradients that are depicted in the final graphs.

6.3. Recommendations

This thesis sparked the interest in the considered ”reversed” open filter layout. The reversed open filter increases the constructibility of these type of rubble mound land reclamations, decreases the cost and simplifies the construction. To be able to use the results for construction, the conclusions have to be quantified, and knowledge has to be widened.

The following paragraph discusses the steps that are recommended to develop the knowledge on reversed open filters further. The paragraph is divided into three parts. The first part describes how it is recommended to increase the accuracy of the model tests. In the second part, recommendations are made to quantify the conclusions, and the last part covers recommendations towards the broadening of knowledge.

6.3.1. Increasing the accuracy

To be able to trust the results, the accuracy of the measurements has to be improved. For further research, it is recommended to improve the following:

- **Increase the stability of pressure sensors**
  Although the accuracy of the pressure sensors was one of the focus points during the measurements for this research, it was still one of the largest sources of inaccuracies of the physical model. The pressure sensors have to be injected with a pipette that is small enough to reach the pressure chamber.

  The sensors also have to be protected against the sand. During tests, some sensors broke down, which was believed to be due to infiltration of sand into the pressure chambers of these sensors. This infill could be prevented by using very fine meshes. This was not used in this research as it might influence the measurements, but if it stops the pressure sensors from failing, this could be an option in further research.

- **Grid of pressure sensors**
  To measure the distribution of gradients along the entire filter layer, a grid of sensors should be placed in the filter layer for parallel flow and inside the sand layer for perpendicular flow. This has to be done to see if the gradient is the same over the entire layer, both vertical and horizontal. Because the erosion is dependent on local hotspots, it could be that the gradients are locally higher.

- **Analyse the effect of the layer thickness on the erosion**
  If the erosion is considered to be not influenced by arching but through the filling of the filter layer, additional research is necessary to quantify this effect. The erosion through the filter layer is the effect of channelling of sand through this layer. This tunnelling effect is thought to be influenced by the thickness of the filter layer. This thickness is, in reality, more than the 20 cm that is tested in this physical model. It can be checked if the erosion decreases with a thicker layer.

- **Airtightness**
  In the physical model rubber seals were used to create an airtight boundary where it was needed; on top of the sand layer for the parallel configuration and left of the filter and sand layers for the perpendicular configuration. This rubber seal might have leaked some air. This caused the gradients to be less constant. In further research, this seal should be improved to ensure nothing can leak through it.

- **Increasing area around plunger**
  The plunger induced waves in section C, where this plunger was located. These waves decreased the accuracy of the measurements. This decrease in accuracy can be mitigated by using a larger section C. With more open water surface around the plunger, there will be fewer waves.

6.3.2. Quantification of results

As this research was purely focussed on the question if there was erosion or not, which was sometimes difficult to determine, a next step would be to quantify the amount of erosion through the filter layer. Two recommendations are made in this paragraph.

- **Visual measurement of the amount of sand inside the sandtrap**
  A start was made in this research to measure the amount of sediment inside the sandtrap visually. To do this, the sides of the sand trap were divided into 1x1cm sections. These sections formed a grid which could be used to divide an entire box into cubes of 1x1cm. This method was not used in this research for two reasons:
  - As this research was focussed on the binary question whether there actually was erosion or not, the boxes were only used to see whether there was erosion, not to quantify this erosion.
  - To use this method, high-resolution photos should be taken from each box prior and after each test sequence. The test sequences began and ended at times that the author was not present in the laboratory, so it was not possible to take these photos.
- **Measuring the erosion**
  To be able to decrease the time needed for a test, it is recommended to measure the erosion through the filter layer. For this research, two methods are briefly investigated, which seemed promising, but were not used due to time and cost restraints:
  - **Measuring the concentration of sediments inside the water.**
    This can be done by the use of conductivity concentration meters. These devices measure the concentration of sediments in the water. These can be placed inside the boxes to see whether there is erosion or not, and in the case of erosion give a quantity. The sensors are available in the TU Delft Fluid Mechanics Laboratory, but the accuracy is questionable (Tutein Nolthenius, 2018).
  - **Extracting water with suspended sediments.**
    Another method is to extract the water from below the filter and let it sink into small containers where the sediment can settle. The accuracy for measuring is very high, but the extraction of water from beneath the filter layer will cause an additional gradient. If this effect can be neutralised by adding the same amount of water, this could be a viable option.
  - **Measuring the weight of the sediment in the boxes.**
    Using a force transducer, the weight of the sediment in the boxes can be measured. This can be used if reliable sensors are found which also work underwater.

6.3.3. Broadening the knowledge

To make the research widely applicable, the knowledge about the reversed filter has to be increased. This can be done in several ways, of which the recommended are described below.

- **Different gradings**
  In this research, only five filter base combinations are tested due to time constraints. These combinations gave an insight into the behaviour of the system but were not sufficient to create a design guideline. More grading could be used to fill the gaps in research between points that are determined in this thesis. More gradings do widen not only the knowledge but also increase the accuracy of the research.
- **Superimposed load**
  In this research, the influence of the superimposed load was checked with only one test. The results seemed promising, but the actual effect still has to be determined. More tests are needed to gain insight into the processes. For this test, the relevant arching has to be determined as there were two length scales of arching that could play a role Chew et al. (2003) and de Graauw et al. (1983).
- **Wet placement**
  In the tests performed in this research, the sand layer was placed on top of the filter layer in the dry. After the sand was placed, the water level was increased until it reached 35cm. In a real-life case, the sand would be placed in the wet. It will be a good idea to test this method if it influences the strength of the filter layer.
- **Overload conditions**
  What would be erosion case of an overload condition such as a storm, would the erosion stop

when the gradients are below the critical gradient or will the erosion continue until the gradients are far below the critical gradient.

- **Assymetrical flow pattern**
  The flow pattern in the considered part of the breakwater is not symmetrical under overload conditions (Polidoro et al., 2015). This asymmetrical behaviour can have an influence on the erosion through the filter layer.

- **Inclination of filterlayer**
  This research is based on the inclined filter layer, but the test setup did not have this inclination. The influence of this inclination is believed to be small but uncertain. This can be tested in future research.

Bibliography

K. J. Bakker, H.J. Verheij, and M.B. de Groot. Design relationship for filters in bed protection. *Journal of Hydraulic Engineering*, 120(9):1082–1088, 1995.

H.F. Burcharth, Z. Liu, and P. Troch. Scaling of Core Material in Rubble Mound Breakwater Model Tests. In *Fifth International Conference on Coastal and Port Engineering in Developing Countries: Proceedings of the COPEDEC V : Cape Town, South Africa*, pages 1518–1528, 1999.

S. H. Chew, H. Tian, S. A Tan, and G. P. Karunaratne. Erosion stability of punctured geotextile filters subjected to cyclic wave loadings — a laboratory study. *Geotextiles and Geomembranes*, 21:221–239, 2003.

CETMEF CIRIA, CUR. *(2007), The Rock Manual. The use of rock in hydraulic engineering (2nd edition). C683, CIRIA, London, ISBN 978-0-86017-683-1*. CIRIA, jan 2007. ISBN 978-0-86017-683-1.

A. de Graauw, T. van der Meulen, and M. van der Does de Bye. Design criteria for granular filters. Technical Report January, Delft hydraulics laboratory, 1983.

V. Heller. Scale effects in physical hydraulic engineering models. *Journal of Hydraulic Research*, 49 (3):293–306, 2011.

N. G. Jacobsen, M.R.A. van Gent, and G. Wolters. Numerical analysis of the interaction of irregular waves with two dimensional permeable coastal structures. *Coastal Engineering*, 102:13–29, 2015.

M. Klein Breteler. Zandtransport in granulaire filters, horizontale stationaire stroming.pdf. Technical report, WL Delft, Delft, 1989.

M. Klein Breteler, H. den Adel, and M.A. Koenders. Taludbekledingen van gezette steen. Technical report, Report number 12, WL Delft, Delft, 1992.

M.A. Losada, P. A. Martin, and R.A. Dalrymple. Reflection and transmission from porous structures under oblique wave attack. *Journal of Fluid Mechanics*, 224(March):625–644, 1991. ISSN 14697645. doi: 10.1017/S0022112091001908.

M. O. Muttray and H. Oumeraci. Theoretical and experimental study on wave damping inside a rubble mound breakwater. *Coastal Engineering*, 52(8):709–725, 2005.

W. J. Ockeloen. *Open filters in breakwaters with a sand core*. Msc thesis, TU Delft, 2007.

A. Polidoro, W. Allsop, and T. Pullen. Exploring the Need for Geotextile Filters for Rubble Bunds Retaining Sand-Fill Islands. In *Coastal Structures and Solutions to Coastal Disasters 2015*, pages 763–773, 2015.

G.J. Schiereck and H.J. Verhagen. *Introduction to bed, bank and shore protection*. VSSD, Delft, 2012. ISBN 978-90-6562-306-5.

D. Schürenkamp, H. Oumeraci, J. Kayser, and F. Karl. Numerical and Laboratory Experiments on Stability of Granular Filters in Marine Environment. *Coastal Engineering Proceedings*, 1(34):17, 2015. ISSN 0589-087X. doi: 10.9753/icce.v34.structures.17.

B.M. Sumer, S. Cokgor, and J. Fredsoe. Suction Removal of sediment from between armor blocks. *Journal of Hydraulic Engineering*, 127(April):2001, 2001.

R.C. Tutein Nolthenius. Sandfill-Retaining rubble mound structures. Msc thesis, TU Delft, 2018.

E. F. Uelman. Geometrically Open Filters in breakwaters. MSc Thesis May, TU Delft, 2006.

M.R.A. van Gent. Porous Flow through Rubble-Mound Material. *Journal of Waterway Port Coastal and Ocean Engineering-asce*, 121, may 1995. doi: 10.1061/(ASCE)0733-950X(1995)121:3(176).

D. Vanneste and P. Troch. An improved calculation model for the wave-induced pore pressure distribution in a rubble-mound breakwater core. *Coastal Engineering*, 66:8–23, 2012.

G. Wolters, J.H. de Vroeg, and M.R.A van Gent. Interface stability of granular filter structures. Technical report, Deltares, 2012.

G. Wolters, M. R.A. van Gent, B. Hofland, and P. Wellens. Wave damping and permeability scaling in rubble mound breakwaters. Technical Report 10, Deltares, 2014.

A. Wörman. Riprap Protection without Filter Layers. *Journal of Hydraulic Engineering*, 115(12):1615–1630, 1989.

List of Figures

1 Example drawing of a considered rubble mound land reclamation cross-section. v
2 The 2% highest gradients plotted against the height with respect to mean water level . . v
3 Side views of both configurations with their open boundaries and directions of gradients. vi
4 Critical gradients of both parallel and perpendicular flow plotted against the base to filter ratio vi

1.1 Examples of land reclamations 1
1.2 Example drawing of a considered breakwater/reclamation cross section. 1
1.3 Installation techniques 2
1.4 Examples of boundaries between breakwater cores and land reclamations. The thick dotted line between the reclamation and the core depicts the geotextile. The cross section displayed here is a small section from the entire cross section as shown in Figure 1.2 3
1.5 The directions of the three gradients 5
1.6 The directions of the two gradients in the filter-base layer region 5

2.1 Example drawings of two different breakwater layout types which are studied for wave attenuation, with incoming wave $H_{incoming}$ 9
2.2 Definitions of zone 1 and 2 as proposed by Vanneste and Troch (2012) 9
2.3 Example breakwater as used by Polidoro et al. (2015) 10
2.4 Lengthward gradients as found by Polidoro et al. (2015) 10
2.5 Lengthward gradients as found by Polidoro et al. (2015) 11
2.6 Depth dependency of the lengthward gradients as determined by Polidoro et al. (2015) 11
2.7 Forces on a grain 12
2.8 Soil arching as illustrated by de Graauw et al. (1983) 13
2.9 Arching by blocking the voids 13
2.10 Original Shield diagram 14
2.11 Breakwater configuration with geotextile shortening 15
2.12 Locations were the gradients are defined 16
2.13 Critical parallel gradients as determined by de Graauw et al. (1983) 16
2.14 Critical perpendicular gradients as determined by de Graauw et al. (1983) 17
2.15 Superimposed load on the filter layer as depicted by de Graauw et al. (1983). 18
2.16 The effect of superimposed load on the critical perpendicular gradient of the base layer 18

3.1 Virtual wave flume and breakwater as modelled in OpenFOAM. 22
3.2 Water level during the numerical simulation 23
3.3 Measurement points used to evaluate the OpenFOAM model 23
3.4 Maximum pressures, from OpenFOAM, at the three lines inside the breakwater core as depicted in Figure 3.3. In that figure also the zero point of the x-axis is depicted 24
3.5 Maximum pressures, calculated with the empirical model by Vanneste and Troch (2012), at the three lines inside the breakwater core as depicted in Figure 3.3. In that figure also the zero point of the x-axis is depicted 24
3.6 Maximum lengthward gradients, as determined with OpenFOAM, at the three lines inside the breakwater core as depicted in Figure 3.3. In that figure also the zero point of the x-axis is depicted 25
3.7 Locations of the numerical sensors 25
3.8 Parallel hydraulic gradients over the granular filter layer 26
3.9 The 2% highest hydraulic parallel gradients through the granular filter layer 27
3.10 Perpendicular hydraulic gradients over the granular filter layer 28

3.11 The 2% highest hydraulic perpendicular gradients in the granular filter layer 29
3.12 Perpendicular gradient calculated with different lengths 29
3.13 Output of the OpenFOAM model during the inflow 30
3.14 Output of the OpenFOAM model during the outflow 30
3.15 Output of the OpenFOAM model for low water inside the breakwater core 31

4.1 Schematic overview of the three sections of the container 33
4.2 Both configurations with their open and closed boundaries 34
4.3 Plunger movement with the sections where the four parameters described below are leading 35
4.4 Example signal 36
4.5 All grain sizes as used in this research 36
4.6 Signals during intermediate calibration steps. 38
4.7 Measurement devices 39
4.8 Water level gauge 39
4.9 Pressure signals filtering 40
4.10 Fast Fourier Transform (FFT) sensors 40
4.11 Webcam 41
4.12 Initial infill of two similar tests 42
4.13 Plunger with motor 43
4.14 Division screen with wire mesh 43
4.15 Plywood rubber seal 44
4.16 Measurement devices parallel setup 44
4.17 Measurement devices perpendicular setup 45
4.18 Entire test 48
4.19 Entire test laser 48
4.20 Direction of gradients 49
4.21 Schematic overview of the boxes inside the sand trap 49
4.22 Critical gradient for test Ref_8.0_4, ... 50

5.1 Maximum parallel gradients over three reference tests 52
5.2 Maximum parallel gradients of test Ref_8.0_6 53
5.3 Parallel gradients over two tests with different granular filter layer 53
5.4 Gradient signal for the different consecutive forced velocities 54
5.5 50 seconds of signal from all three pressure sensors 55
5.6 25 seconds of signal from all three pressure sensors 56
5.7 Parallel gradient signal from Ref_8.0_6 VE_012 56
5.8 Signal from the sensors in Ref_8.0_6 57
5.9 Signals from the sensors in Ref_8.0_6 57
5.10 Gradient signal from Perp_8.0 58
5.11 Signals from all sensors in Perp_8.0 58
5.12 Signals from all sensors in Perp_8.0 59
5.13 Filled sand trap after initial infill prior to test 60
5.14 Filled sand trap after the entire reference test sequence 60
5.15 Sensor sinking for the two configurations 62
5.16 Heaps of sand inside the sand trap 63
5.17 Stability ratio plotted against critical parallel gradient 64
5.18 Stability ratio plotted against critical perpendicular gradient 64
5.19 Relation between median grain size of the base layer and critical gradient 65
5.20 Results of long term test Para_8.0_long 66
5.21 Parallel critical gradients compared to OpenFOAM 66
5.22 Perpendicular critical gradients compared to OpenFOAM 67

6.1 The 2% highest gradients plotted against the height with respect to mean water level . . 75
6.2 Critical parallel gradients plotted against base to filter ratio 76
6.3 Critical Perpendicular gradients plotted against base to filter ratio 76

B.1 The model setup as used by Polidoro et al. (2015) scaled to the geotextile shortening . 95
B.2 The model setup as used by Polidoro et al. (2015) scaled to the sensor lines 96
B.3 Differences between the OpenFOAM case and the Vanneste (2012) model on the first line at z = -2.73m. 97
B.4 Differences between the OpenFOAM case and the Vanneste (2012) model on the lowest line at z = -10.66m. 98
B.5 Flow directions inside breakwater at T=209s 98
B.6 Flow directions inside breakwater at T=216s 98

C.1 Preliminary test tube 99
C.2 Photos of the cylinder that was used for the preliminary tests. 100
C.3 Model iteration 1 100
C.4 Model iteration 2 101
C.5 Model iteration 3 101
C.6 Model iteration 3 photo 102
C.7 Model iteration 4 102
C.8 Model iteration 4 photo 103
C.9 Model iteration 5 103
C.10 Model iteration 5 photo 103
C.11 Dimensions final parallel setup 104
C.12 Dimensions final perpendicular setup 104
C.13 additional measurement devices 105
C.14 Sieving photos 105
C.15 Calibration curves pressure sensors 106
C.16 Calibration curves waterlevel sensors 106
C.18 Final setup TU Delft laboratory of fluid mechanics 109

D.1 Gradient signal difference over one test 111
D.2 50 seconds of signal from all sensors (Ref_8.0_4 with VE_0.10) 112
D.3 FFT of all sensors Ref_8.0_4 with VE_0.10 112
D.4 50 seconds of signal from all sensors (Ref_8.0_4 with VE_0.18) 113
D.5 FFT of all sensors Ref_8.0_4 with VE_0.18 113
D.6 50 seconds of signal from all sensors (Ref_8.0_4 with VE_0.25) 114
D.7 FFT of all sensors Ref_8.0_4 with VE_0.25 114
D.8 50 seconds of signal from all sensors (Ref_8.0_6 with VE_0.10) 115
D.9 FFT of all sensors Ref_8.0_6 with VE_0.10 115
D.10 50 seconds of signal from all sensors (Ref_8.0_6 with VE_0.18) 116
D.11 FFT of all sensors Ref_8.0_6 with VE_0.18 116
D.12 50 seconds of signal from all sensors (Ref_8.0_6 with VE_0.25) 117
D.13 FFT of all sensors Ref_8.0_6 with VE_0.25 117
D.14 Critical gradient for test: Ref_8.0_3 VE_012 119
D.15 Critical gradient for test: Ref_8.0_4 VE_018 119
D.16 Critical gradient for test: Ref_8.0_5 VE_018 119
D.17 Critical gradient for test: Ref_8.0_6 VE_015 120
D.18 Critical parallel gradient for test: Para_4.0 120
D.19 Pressure sensor signal for the critical parallel gradient test: Para_4.0 120
D.20 Critical gradient for test: Para_7.5 121
D.21 Pressure sensor signal for the critical parallel gradient test: Para_7.5 121
D.22 Critical gradient for test: Para_9.5 121
D.23 Pressure sensor signal for the critical parallel gradient test: Para_9.5 122
D.24 Critical gradient for test: Para_16.5 122
D.25 Pressure sensor signal for the critical parallel gradient test: Para_16.5 122
D.26 Critical gradient for test: Para_8.0_long 123
D.27 Pressure sensor signal for the critical parallel gradient test: Para_8.0_long 123
D.28 Critical perpendicular gradient for test: Perp_7.5 123
D.29 Pressure sensor signal for the critical perpendicular gradient test: Perp_7.5 124

D.30 Critical gradient for test: Perp_8.0 124
D.31 Pressure sensor signal for the critical parallel gradient test: Perp_8.0 124
D.32 Critical perpendicular gradient for test: Perp_9.5 125
D.33 Pressure sensor signal for the critical perpendicular gradient test: Perp_9.5 125
D.34 Critical gradient for test: Perp_16.5 125
D.35 Pressure sensor signal for the critical parallel gradient test: Perp_16.5 126

List of Tables

3.1 Overview of the comparison between the Polidoro et al. (2015) test results and the Vanneste and Troch (2012) empirical calculation, for each test performed by Polidoro et al. (2015), two estimated distances are used, which can be found in Appendix B.1.2. The outcomes give the ratios between the calculated lengthward gradients and the measured gradients with the physical model. . . . 22
3.2 Layer input coefficients for the used OpenFOAM model . . . 23

4.1 Overview of the different gradings. . . . 37
4.2 Code names for the reference tests . . . 46
4.3 The entire test sequence . . . 47
4.4 Special test cases . . . 47

5.1 The velocities which were used for the reference tests . . . 51
5.2 Critical gradients reference tests . . . 61

A.1 Grainsizes and other parameters as used by Klein Breteler et al. (1992) . . . 92

B.1 Gradients of the third case by Polidoro et al. (2015) . . . 96
B.2 Gradients of the ninth case by Polidoro et al. (2015) . . . 96

C.1 Standard deviation and mean difference between the calibration tests . . . 106
C.2 Standard deviation and mean difference between the calibration tests for the water level tests . . . 107
C.3 Additional parts . . . 109

D.1 All available sensors for every parallel test . . . 118
D.2 Available sensors for perpendicular tests. . . . 118
D.3 Standard deviations of the 4 reference tests. . . . 118
D.4 Standard deviations of the 5 Parallel tests . . . 118
D.5 Standard deviations of the 4 perpendicular tests . . . 119

A

Literature study

A.1. Previous filter research

Muttray and Oumeraci (2005)

Muttray provided an overview of the historic research of both waves through breakwaters. The also created three new functions based on the Forcheimer equation each for a different flow regime. These relations are based on the particle velocities inside the breakwater. This leads to a coeffient κ_v which is determined as the average particle velocity over the local wave height inside the breakwater, noted as: $\kappa_v = \frac{\bar{v_f}(x)}{H(x}$. This κ_v can be calculated with:

$$\kappa_v = \frac{n}{\pi}\frac{\omega}{k'h}\left[1 + \frac{2}{\pi}\left(1 - \frac{coshk'h}{cosh1.5k'h}\right)\right] \tag{A.1}$$

With this velocity coefficient and the hydraulic gradient, which can be described as $\bar{I}(x) = -\frac{2}{\pi}\frac{\partial \bar{P}(x)}{\partial x}$, the Forcheimer equation can be rewritten as:

$$-\frac{2}{\pi}\frac{\partial \bar{P}(x)}{\partial x} = \underbrace{a\kappa_v H(x)}_{A} + \underbrace{b(\kappa_v H(x))^2}_{B} \tag{A.2}$$

With this formula the three different flow regimes can be described:

- Laminar flow:
  For laminar flow only part A from Equation A.2 is used. This leads to a linear damping which can be described with the following equation:

$$H(x) = H_0 exp(-\frac{\pi}{2}a\kappa_v x \tag{A.3}$$

- Quadratic damping:
  For fully turbulent flow the damping can be described with part B from Equation A.2. This leads to the following damping:

$$H(x) = \frac{H_0}{\frac{\pi}{2}b\kappa_v^2 H_0 x + 1} \tag{A.4}$$

- Polynomial damping:
  If turbulent and laminar flow are both present in the breakwater both parts A and B from Equation A.2 have to be used. This leads to the following damping function:

$$H(x) = \frac{a}{(\frac{a}{H_0} + b\kappa_v)exp(\frac{\pi}{2}a\kappa_v x) - b\kappa_v} \tag{A.5}$$

Vanneste and Troch (2012)
As the other calculation methods focussed more on the Forchheimer approach, which is difficult to model for a breakwater as it has multiple layers(armour, filter, core etc.). Vanneste and Troch (2012) tried to find a new formula which was specifically created for the flow through a breakwater.

Vanneste created a new empirical formula that was able to describe the flow through a breakwater with a lot of empirically observed parameters.

For these empirical parameters, Vanneste used not only a new designed model for this method, but also the test data that was obtained in previous research(Muttray (2000)). The research started with a formula that was first proposed by Oumeraci and Partenscky (1990), this formula describes the damping of pore pressure height over the breakwater core.

$$P(x) = P_0 exp(-\delta k' x) \tag{A.6}$$

with: P(x) is excess pore pressure along the horizontal axis of the breakwater [m], P_0 height of pore pressure oscillations at the interface between the core and filter layer, δ : damping coefficient and k' is the internal wave number $[k^{-1}]$.
The damping coefficient is calculated with the following equations.

$$\delta = a_\delta \frac{\sqrt{n} L_p^2}{H_{m0} b} \tag{A.7}$$

with: a_δ: dimensionless coefficient obtained through curve fitting of experiments, n: porosity of the core, L_p: Peak wave length, H_{m0}: Significant wave height at the breakwater toe and b: Total width of horizontal breakwater section[m].

In the research a different method is proposed with a new formula that describes the wave attenuation separately in the two zones which can be seen in Figure 2.2. The pressure attenuation in the second zone, which is of the most interest for this thesis, can be described with:

$$P(x,z) = P_i(z) exp\left(-\delta'(z) k (x - x_i(z))\right) \tag{A.8}$$

For the calculation of the different parameters in Equation A.8 the formula's are given in Appendix A.2. In this research there were also new tests performed to check the calculated coefficients. This results were very promising for the breakwater that was considered.

Polidoro et al. (2015)
The scope of this research was to define the pressure gradients along the rear side interface between a breakwater and a sand fill. Polidoro used the calculation methods by Muttray and Oumeraci (2005) and Burcharth et al. (1999), but found that these were not suitable because the situation for which they were calibrated were different than the case in this paper. Both methods were calibrated for a breakwater with an open end, which means that the pressure difference on the rear side is assumed to be zero. This assumption meant that if these methods are used, the pressure will go to zero along the interface of interest and the transport will be underestimated. For this reason scale tests were performed.

Testing was done in a wave flume on a 1:32 scale. The rear side of the breakwater was constructed with a solid barier made of plywood, which meant that this interface was not permeable. Polidroo found that the gradients along the rear side of the breakwater remained relatively stable during normal conditions, however for the conditons with high wave impact, the negative gradients were a lot larger than the positive gradients. Which can result in a larger sediment transport as the negative gradients have a suction effect.

Tutein Nolthenius (2018)
In the report made by Raoul Tutein Nolthenius the results of the Vanneste model and the Polidoro model were compared. Although the tested parameters were not comparable, the calculations with the Vanneste equation showed a fairly accurate representation at large depth. The accuracy of the Vanneste equation regarding the Polidoro case is checked in Chapter 3.

With all these models it is possible to get a rough estimation of the pressures that work on the considered interface. However the best method for the calculation of these pressures is not tested for a breakwater with a closed rear side. For this reason a numerical model should be used to get an insight of the pressures that work on this rear corner of the breakwater.

These gradients should be compared to the Vanneste equations to see if both the model and the equation are valid for these kind of calculations.

A.1.1. Closed filters

A closed filter is a filter in which the sediments of the base layer cannot pass through the filter layer because the largest particles in the base layer get stuck inside of the filter pores and block the further movement of these sediments. This also means that if a filter is closed it does not matter which loading is exerted on the base layer.

If these rules are obeyed the filter should be closed for all sediment transport through it and will therefore be stable independent of the hydraulic loads that act on the filter/base interface. However as stated before the construction of a closed filter can be unfavourable in some situations, in such a case an open filter can be designed.

A.1.2. Open filters

Because it is theoretically possible for the base grains in an open filter to move through the filter layer an open filter also has to be designed to cope with the loads that are expected to work on this layer. For open filters it is therefore needed to create a clear understanding of the local flow patterns. These flow patterns are investigated for steady flow through a filter layer.However

de Graauw et al. (1983)

De Graauw researched 4 different flow patterns:

1. Steady flow parallel to the interface
2. Cyclic flow parallel to the interface
3. Steady flow perpendicular to the interface
4. Cyclic flow perpendicular to the interface

After scale model tests they came up with a formula which can be seen in 2.8. This formula uses the critical shear velocity as described by Shields. What can be seen from this equation is that it uses the d_{50b} instead of the d_{85b} as used by Terzaghi.

$$I_C = \left(\frac{0.06}{n_F^3 d_{15F}^{4/3}} + \frac{n_F^{5/3} d_{15F}^{1/3}}{1000 d_{50B}^{5/3}} \right) u_{*c}^2 \tag{A.9}$$

For the cyclic flow parallel to the interface it was found that the amplitude of the critical hydraulic gradient was the same order of magnitude as for the steady flow parallel case. However some perpendicular gradients were observed causing some transport.

The third case was the steady flow perpendicular to the interface. This test was performed with the filter layer on top of the base layer and a flow from the base layer into the filter layer. This flow caused no transport if the critical hydraulic gradient was lower than 1. This is due to the fluidization of particles and has to do with the influence of gravity on the particles.

The fourth case with cyclic flow through the filter layer showed a lower critical gradient. What also could be seen from these tests is that the Stability criterion that Terzaghi found (equation 2.7a) Should be no lower that 2-3 for a safe design.

The physical explanation of filter actions are also described in the report. It is concluded that there

is a large difference between perpendicular and parallel flow. These are therefore considered separately. For the parallel flow the resistance for erosion of the base material is found as the Shields criterion. For the perpendicular flow the resistance was found to be dependent on soil arching, see Figure 2.8. This arching improves the resistance for fluidization of the base layer. However it is also found that with reversing flow these arches are broken down and the critical gradient is lower.

de Graauw et al. (1983) also inbestigate the effect of a superimposed load on the filter. It was found that if the arching occured, meaning that: $\frac{n_f D_{15f}}{D_{50b}} = 1-6$, the critical gradient increases for soil A. What can be seen further is that if the filter to base grain size ratio is larger, $\frac{n_f D_{15f}}{D_{50b}} \leq 6$, the critical gradient is less influenced by this load.

Klein Breteler (1989) and Klein Breteler et al. (1992)
Klein Breteler (1989) did some measurements of a flow parallel to a filter, with these measurements and together with other measurments Klein Breteler et al. (1992) created some design formula's for parallel flow along a filter:

$$v_{fcr} = \left(\frac{n_f}{c} \left(\frac{d_{f15}}{v} \right)^m \sqrt{\Psi_s \Delta g D_{b50} \left(\frac{sin(\phi - \alpha)}{sin\phi} - \frac{i_\perp}{\Delta(1-n_b)} \right)} \right)^{\frac{1}{1-m}} \tag{A.10}$$

With this formula the critical gradient can be calculated:

$$I_{cr} = \frac{190}{g n_f^3} \frac{(1-n_f)^2 \nu}{D_{f15}^2} v_{fcr} = \frac{0.13}{n_f^5 D_{f15} g} v_{fcr}^2 \tag{A.11}$$

Both of these formulas are valid for cyclic and steady flow. The results of these tests showed a large variation in critical velocity, however a trend of a larger critical velocity with larger incline could be seen, which meant that if a inclined filter is designed with this equations the design will be conservative. In this research the following parameters were found to use in the formula's above:

D_{b50} mm	c -	m -	Ψ_s -	ϕ °
0,1	1,18	0,25	0,11	60
0,15	0,78	0,2	0,073	60
0,2	0,71	0,18	0,055	60
0,3	0,56	0,15	0,044	55
0,4	0,45	0,11	0,038	55
0,5	0,35	0,07	0,036	55
0,6	0,29	0,04	0,035	55
0,7	0,22	0	0,034	50
0,8	0,22	0	0,034	50
1	0,22	0	0,035	50

Table A.1: Grainsizes and other parameters as used by Klein Breteler et al. (1992)

Sumer et al. (2001)
Sumer et al. (2001) researched the effect of base material removal through a filter layer with steady parallel flow. The suction was called this way as not only the entrainment of material was considered, but with suction the sediments were also transported away from the bed. Sumer et al. (2001) suggested a new equation for the Shields parameter Ψ. This equation is dependent on the filter to base ratio $\frac{D_B}{D_F}$. In this research only a standard size material was used for both the filter and base layer.

$$\Psi_{su} = 0.3 + 3 \left(\frac{D_B}{D_F} \right)^{-0.15} exp\left(-7.5 \frac{D_B}{D_F} \right) \tag{A.12}$$

What can be seen from this equation is that the parameter Ψ_{su} is decreasing with an increasing filter to base ratio $\frac{D_B}{D_F}$.

CUR report 233
The design guidelines that are described in CUR report 233 (Wolters et al., 2012) are discussed in this section. The design guideline is a stability formula that is adjusted from previous research ((Wörman, 1989) and (Bakker et al., 1995)). Wörman started with this research. He investegated the erosion around bridge piers for non-uniform flow. Wörman found a linear relationship between the velocity over the gravitational force and the layer thickness ($\frac{U^2}{g*d_f}$) and the base to filter ratio ($\frac{D_{85B}}{D_{15F}}$) if this ratio was lower than 0.1. Note that this ratio is the inverse of the stabilty ratio used by Terzaghi. This relationship formed the following equation:

$$\frac{d_F}{D_{15F}} = 0.16\frac{\Delta_F}{\Delta_B}\frac{n_F}{1-n_F}\frac{D_{85F}}{D_{85B}} \tag{A.13}$$

Bakker et al. (1995) changed this formula to take some other parameters in consideration that Wörman did not take into account, such as:

- The water depth
- The layer thickness
- The effect of the flow around the pier

Bakker also assumed a couple of coefficients to be constant, like the factor$\frac{\Delta_F}{\Delta_B}$. The new formula he found was:

$$\frac{D_{15F}}{D_{50B}} = \frac{\alpha}{C_0}\frac{R_h}{D_{50F}} \tag{A.14}$$

with: R_h as the hydraulic radius, which is usually taken as the water depth, α= 9.5 and C_0 is a coefficient that scales the average hydraulc gradient to the occuring gradient at the filter layer and is chosen as: 15.

In CUR report 233 these formua's were adjusted for sand-tight filters under steady flow (Wolters et al., 2012):

$$\frac{d_F}{D_{15F}} = 2ln\left(\alpha_k\frac{D_{50F}}{D_{50B}}\frac{1-\gamma V_{GF}}{1-\gamma V_{GB}}\frac{\Psi_{cF}}{\Psi_{cB}}\frac{\Delta_F}{\Delta_B}\right) \tag{A.15}$$

with: α_k coefficient related to turbulence intensity: α_k= 0.05 for low turbulence and α_k 0.5 for high turbulence. γ parameter determining allowable transport of bed material, advised value: 0.625. V_G variation coefficient for non-uniformity of material, determined as: $1-\frac{D_{15}}{D_{50}}$.

A.1.3. Conclusion resistance
For the resistance against erosion through the filter layer that is considered in this research the researches that are listed above have little similarities. The research started with the report by de Graauw et al. (1983) in which a formula was found to describe the resistance of a base layer with a filter layer on top against erosion.

For the filter considered superimposed load could have a large influence. The graauw started with the research and found that a superimposed load actually has a beneficial load on the critical gradient, which was confirmed and extended by Schürenkamp et al. (2015).

A.2. Vanneste 2012

$$\delta'(z) = c_{3,1}(z)(kh)^{-\epsilon c_{3,2}(z)}(H_{m0}/h)^{c_{3,2}(z)} \tag{A.16}$$

$$P_i(z) = P_0(z) + \rho g I_1(z)(1-\kappa(z))z cot\alpha \tag{A.17}$$

$$P_0(z) = \rho g H_{m0} exp\left(c_{1,1}(z) - c_{1,2}(z)kh - c_{1,3}(z)\frac{H_{m0}}{h}\right) \tag{A.18}$$

$$\kappa(z) = \frac{x_i(z)}{z cot\alpha} \tag{A.19}$$

$$I_1(z) = c_{2,1}(z)(H_{m0}/h)^{c_{2,2}(z)} \tag{A.20}$$

with: z: vertical height [m] ,h : waterdepth[m], k: Wave number[m^{-1}], and $c_{1,1}, c_{1,2}, c_{1,3}$ are dimensionless parameters that are estimated from previous research.

The parameters $c_{1,1}, c_{1,2}, c_{1,3}$ were the main scope of this research and were able to estimate the pore pressure attenuation in the breakwater at a higher accuracy than the existing calculation method

A.3. Physical moddeling

Because the above mentioned lacks confident meaning in the manner of a base layer on top of a filter layer a physical model can be used to find a relation between the erosion and the other parameters. A physical model is a representation of reality which is not necessarily scaled.

A scale model is a representation of the real situation but with different length scales. This scale model can be an exact replica, but scaled down. It can also be a simplification of a certain part. In every scale model there is a parameter that is called the scale factor (λ), this scale factor consists of the ratio of a characteristic length scale of both the model and the reality. This scale factor can be written as:

$$\lambda = \frac{L_p}{L_m} \tag{A.21}$$

With λ as the scale factor, L_p as characteristic length in the real life prototype and L_m as the characteristic length in the model

Scaling of a prototype to a model scale always induces scaling effects. These scale effects have to mitigated in a certain way to have the best representation of the reality. For this mitigation dimensionless parameters can be used. Some examples of regularly used parameters can be found in Equations A.22a, b and c

$$Froude = \text{(inertial force/gravity force)}^{1/2} = \frac{V}{(gL)^{1/2}} \tag{A.22a}$$

$$Reynolds = \text{intertial force/ viscous force} = \frac{LV}{\nu} \tag{A.22b}$$

$$Keulegan - Carpenter = \text{drag force/ inertial forces} = \frac{VT}{L} \tag{A.22c}$$

It should also be determined which parameters are the important parameters for the processes (Heller, 2011). The different parameters are discussed below:

Froude number
Froude similarity is especially suited if friction is negligible or if there is a short highly turbulent flow phenomena. If the Froude number has to be equal in both model and prototype, the scaling parameters for both the velocity and the length scale should be: $\lambda_u = \sqrt{\lambda_L}$.

Reynolds number
If the viscous force is dominant a Reynolds similarity should be used. Altough this induces the need for a very high velocity as this forces scales with λ^{-1}. Because the Reynolds number > 2000 means that a flow is turbulent, it is necessary to have the Reynolds number of both the prototype and model above or below this level.

Keulegan -Carpenter number
The Keulegan Carpenter number is a measure of the importance of the drag forces over the inertial forces. For small numbers inertia dominates, while for large numbers the drag force dominates.

B

Hydraulic pressures

B.1. Calculated gradients

B.1.1. Model setup measurements

Because the measurements of the model setup were not included the drawing provided in the paper by Polidoro et al. (2015) was used. Besides this drawing, two times in the text there are measurements placed. The first one was that the geotextile would be shortenend from -9m CD until -5m CD. The drawing was scaled to fit this distance and with this scale some other sizes were determined. The result of this can be seen in Figure B.1

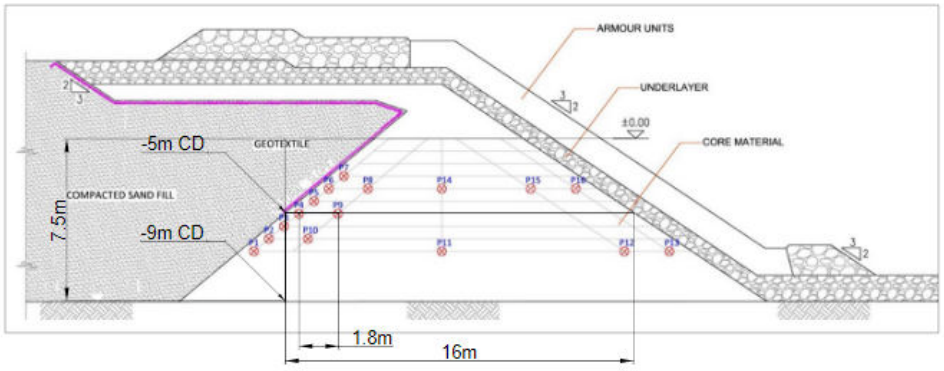

Figure B.1: Image of the model setup as used by Polidoro. The image is scaled related to the shortening of the geotextile from -9m CD to -5m CD

The second scaling was performed with the distance between the upper most sensor line and the lower sensor line, which were placed on respectively -4.5m CD and -8.5m CD. This drawing can be seen in Figure B.2

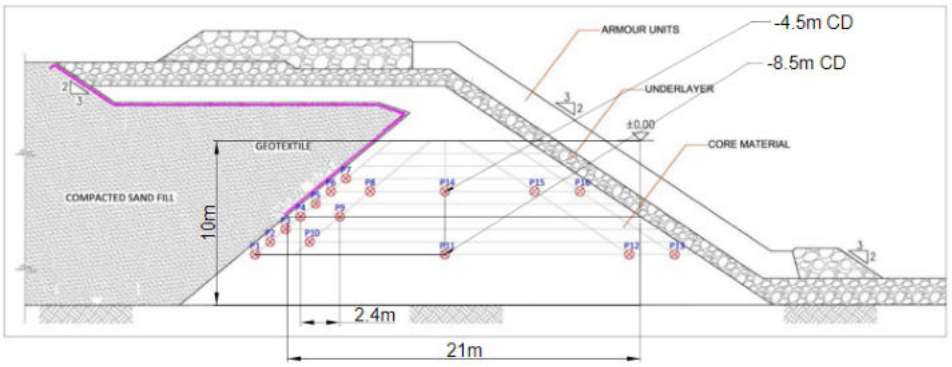

Figure B.2: Image of the model setup as used by Polidoro. The image is scaled related upper and lower sensor lines, which are placed on respectively -4.5m CD and -8.5m CD

Although the 2nd scaling seems to be more correct, both are used in the calculations, which give the range of pressures in Table 3.1

Case 3

The third case of the Polidoro tests can be seen as the base case. The wave conditions were: H_{m0} = 3.00m, T_p = 9.2s and h ≈ 12.4. This case can be seen as the base case. The water level is not exact because the used Chart Datum was not provided. Also the exact locations of the sensors were not provided, but were estimated. This will result in a certain deviation between the results and the calculations.

It can be seen for this case that the error ratio of the results is between 5.5 and 15, this is quit a lot.

Elevation w.r.t waterline [m]	I_{calc}: Parallel gradient calculated method 1 [-]	I_{calc}: Parallel gradient calculated method 2 [-]	I_{meas}: Parallel gradient measured Polidoro [-]	$\frac{I_{meas}}{I_{calc}}$
-8.75	0.006	0.0006	0.009	15-15
-8.25	0.0013	0.002	0.011	5.5-11
-7.75	0.002	0.001	0.016	15-8

Table B.1: Gradients of the third case which was performed by Polidoro et al. (2015). The calculated gradients are calculated with the model proposed by Vanneste and Troch (2012) while the measured gradients are fromPolidoro et al. (2015)

Case 9

The ninth case of the Polidoro tests can be seen as the case with overload conditions. The wave conditions were: H_{m0} = 5.80m, T_p = 10.5s and h ≈ 12.4. For this case also the gradients are not precise with the same reasons as given above (Paragraph B.1.1).

Elevation w.r.t waterline [m]	I_{calc}: Parallel gradient calculated method 1 [-]	I_{calc}: Parallel gradient calculated method 2 [-]	I_{meas}: Parallel gradient measured Polidoro [-]	$\frac{I_{meas}}{I_{calc}}$
-8.75	0.0075	0.0081	0.016	2.0-2.1
-8.25	0.0060	0.0056	0.020	3.5-3.3
-7.75	0.004	0.011	0.027	2.5-6.8

Table B.2: Gradients of the ninth case which was performed by Polidoro et al. (2015). The calculated gradients are calculated with the model proposed by Vanneste and Troch (2012) while the measured gradients are from the Polidoro et al. (2015) paper.

B.1.2. Comparison between OpenFOAM® model and empirical calculations for the lengthward gradient

As the OpenFOAM model setup is not calibrated with a physical model test, it is difficult to extract conclusions from this OpenFOAM model. The OpenFOAM model is therefore only used for a preliminary estimate of the range of pressures that occur in the rear side of the breakwater. Nevertheless, a calculation with both the OpenFOAM model and the Vanneste and Troch (2012) model are performed with the same boundary conditions. In this manner, the OpenFOAM model can be reviewed for its accuracy to represent the wave attenuation.

The methods are compared with the help of numerical pressure traducers, which give the pressure as an output of the OpenFOAM model. The locations are chosen such that these sensors coincide with the sensors for which the Vanneste and Troch (2012) model was calibrated. The water depth of these sensors is -2.73m, -6.6m and -10.66. The approximate points are drawn in Figure 3.3.

The pressure output of these points is plotted in the upper graph of Figure B.4. The pressures are divided by the water density and the gravitational acceleration to have the pressure in meters water-column, just as the pressures are given by Vanneste and Troch (2012), which are located in the lower graph of Figure B.4.

It can be seen from these graphs that the lengthward gradients in the OpenFOAM model start at a higher value than the gradients in the Vanneste and Troch (2012) model. At the landward side of the breakwater, the gradients in the OpenFOAM are a factor 2-3 lower than the gradients that were Calculated with the Vanneste and Troch (2012). This probably has to do with the non-uniformity of the modelled breakwater in OpenFOAM and the overtopping in that model.

Although the results of both models are not similar, the magnitude of both gradients is very much alike. This means that the results of the OpenFOAM model have to be used with caution, as was already expected, but it can give some reasonable results and will be sufficient to provide the first order of magnitude to start the experiments from.

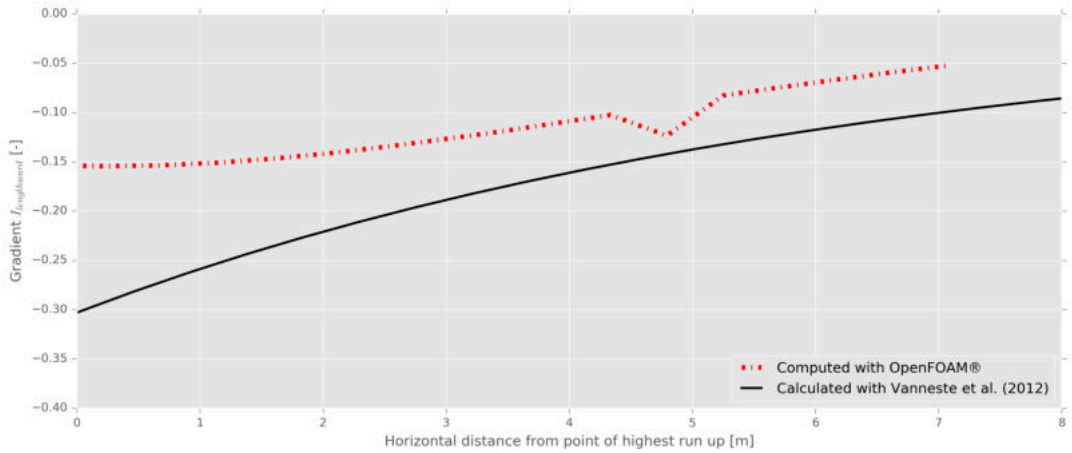

Figure B.3: Differences between the OpenFOAM case and the Vanneste (2012) model on the first line at z = -2.73m.

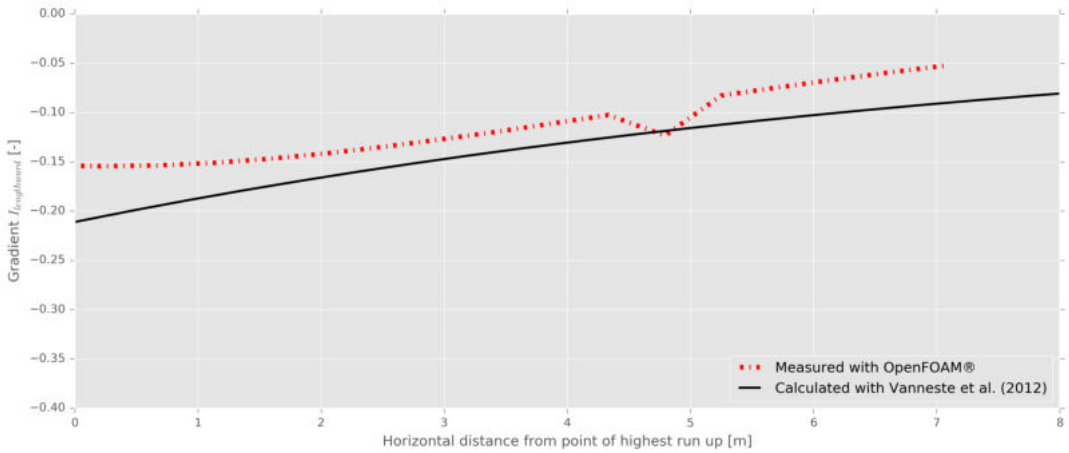

Figure B.4: Differences between the OpenFOAM case and the Vanneste (2012) model on the lowest line at z = -10.66m.

B.2. Direction of flow in breakwater

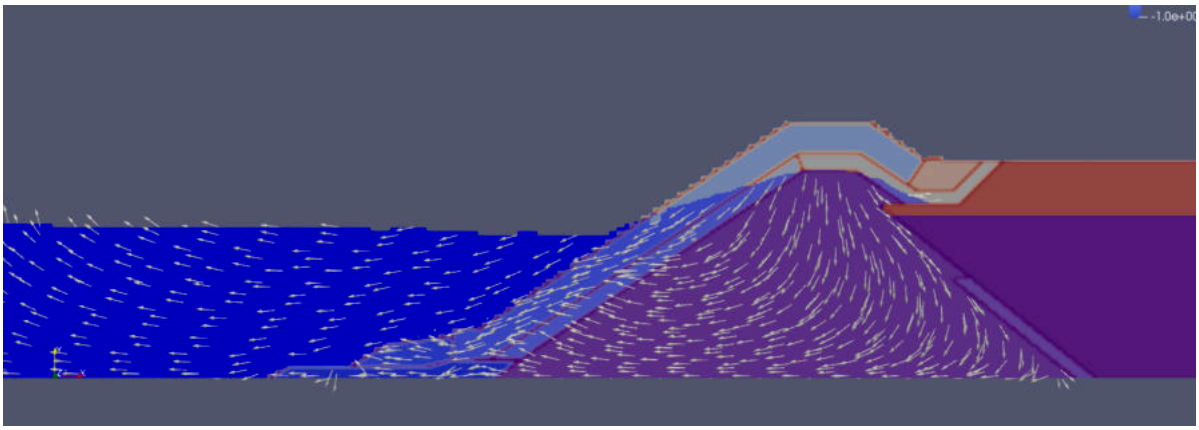

Figure B.5: Direction of flow in entire breakwater at time T=209s

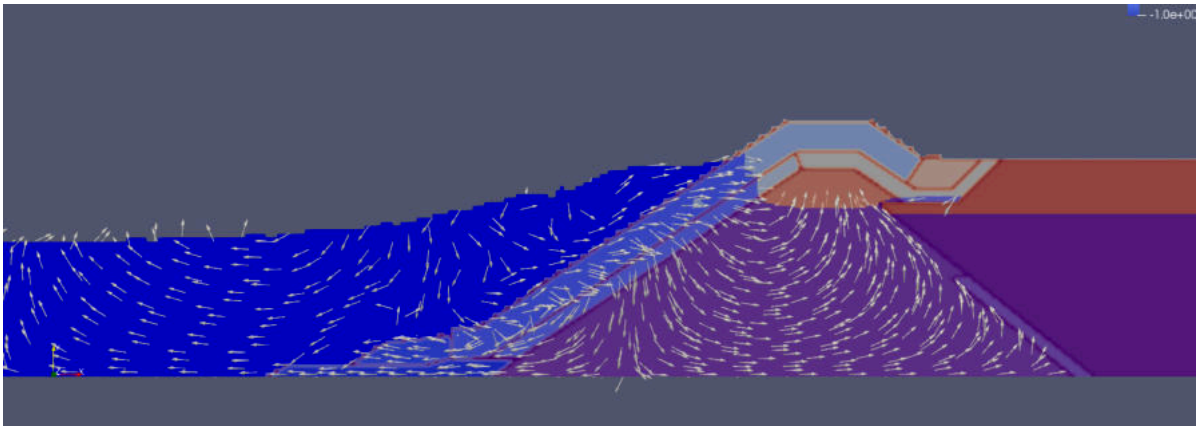

Figure B.6: Direction of flow in entire breakwater at time T=216s

C

Model setup

C.1. Preliminary model test

To get an idea of the erosion through the filter layer a tube filled with the filter material and the sand is used. This tube is used to see if it is at all possible to have the sand on top of the filter material without eroding through this layer.

The tube is filled as depicted in Figure C.1. The first test that is conducted is the filling of the tube. This is done with the following steps analogue to building practice:

1. Filling the tube with water
2. Placing of the stones by dropping in the water
3. Placement of sand layer, by dropping in the water

After this test it was seen that the sand protruded into the filter and was moving downwards through the filter layer. This process stopped after around 10 minutes, but the tube was set aside for 30 minutes until further testing to assure that the equilibrium was reached. Before shaking the cylinder.

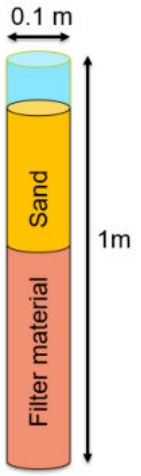

Figure C.1: Drawing of the tube that is used for the preliminary tests.

C.1.1. Preliminary test results

After the placement of the sand on the filter layer the intrusion of the sand into the filter layer was around 10-15cm. This process continued until there was no flow of sediments 10 minutes later. The intrusion of sand into the filter layer did not increase at that moment, but there was some sediment that dropped through the filter to the bottom of the tube.

Next the tube was dropped from 5-10cm height. The sediments protruded much further into the filter, but reached again an equilibrium.

(a) Before shaking (b) After shaking (c) Different filter material after shaking

Figure C.2: Photos of the cylinder that was used for the preliminary tests.

C.2. Model evolution

The final model setup as discussed in the main matter is an evolution of multiple test setups to eventually come to a setup in which both the results are a good representation of reality, but also can be measured with accuracy. The process and individual setups are discussed in the paragraphs below.

C.2.1. Model setup 1

The first setup is designed to have the largest infiltration length into the filter layer as possible inside the container that was available. This setup was discarded as the flow through the granular material would be very difficult to analyse.

Also the disability to close of certain parts of the setup to force the flow into a perpendicular or parallel pattern decreases the usability and accuracy of this setup.

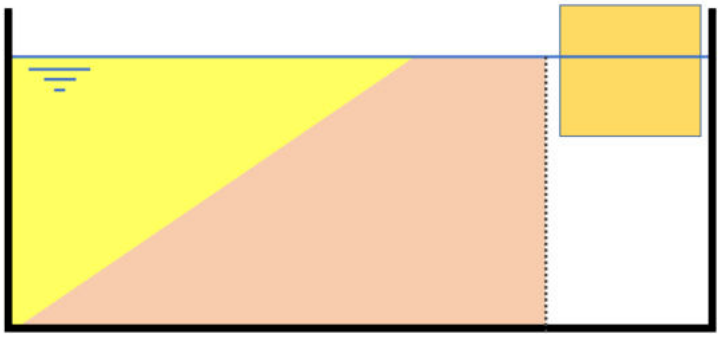

Figure C.3: Model iteration 1. The yellow colored section is where the sand was designed. The pink section is the granular material(Filter layer) and the orange rectangle is the location of the plunger. The waterlevel is indicated with the blue line and the dotted line is a wire mesh

This setup was designed but discarded before it was built, so there is no image of this setup.

C.2.2. Model setup 2

Setup number 2 has the improvement of a open water level on both side of the filter/sand construction. This has the advantage that both the perpendicular and parallel flow can be altered in this setup, by closing of the top of one of the outlets (depicted with 1 & 2 in Figure C.4). The parallel flow can be forced by closing outlet 2, while the closing of outlet 1 forces a flow through the sand layer.

A large disadvantage of this setup is that the thickness of both the sand and filter layer are not the same at every location. This creates a gradient over the filter layer which will increase over the filter layer as the thickness decreases(See Section 2.1.1 for the explanation).

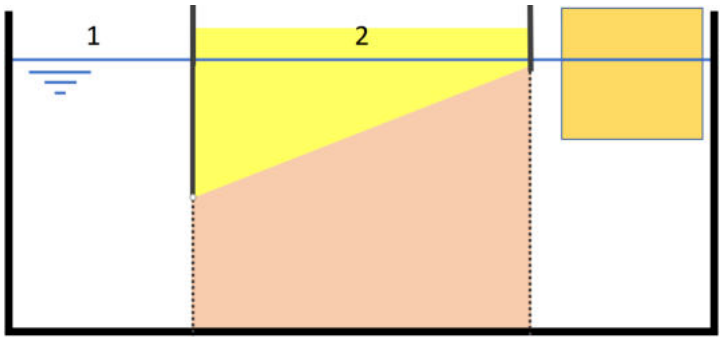

Figure C.4: Model iteration 2. The yellow colored section is where the sand was designed. The pink section is the granular material(Filter layer) and the orange rectangle is the location of the plunger. The waterlevel is indicated with the blue line and the dotted line is a wire mesh

This setup was also not built with a similar reason as setup 1. As the main goal of the setup was to research the relation between the hydraulic gradient and the material used. If the gradient cannot be determined in the filter layer the results cannot be trusted for accuracy.

C.2.3. Model setup 3

The third setup focussed on a hydraulic gradient inside of the filter layer that was equal along the entire layer. To be able to have both the layer thickness constant and the angle of the filter layer as in prototype a piece of wood was placed at the correct angle before filling the container with both the filter material and sand.

Although the hydraulic results of this setup were reliable, the layer thickness of the filter layer was influenced by the size of the container. Because the container is just 450mm high the layer thickness was limited to 100mm with an angle of 1:1.5. What also can be seen in Figure C.5 is that the sand layer has a different thickness, which was a issue for especially the perpendicular tests.

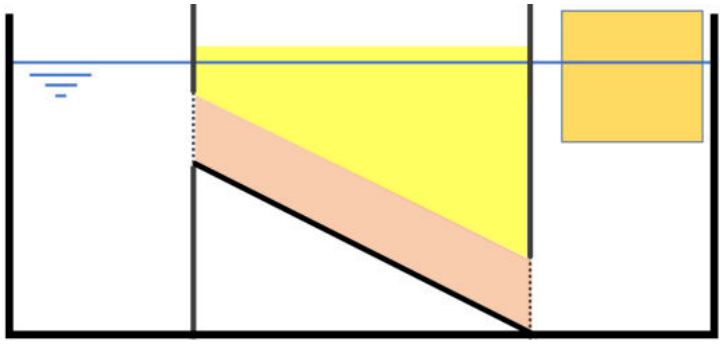

Figure C.5: Model iteration 3. The yellow colored section is where the sand was designed. The pink section is the granular material(Filter layer) and the orange rectangle is the location of the plunger. The waterlevel is indicated with the blue line and the dotted line is a wire mesh

As this setup looked promising it was built for some preliminairy testing. A photo prior to this first test can be seen in Figure C.6. Two things were visible from this test. The first was that the sand penetrated thourhg the layer untill it filled the entire layer. Because in reality the filter is placed on top of the core, which has a higher permeability, the sand that is falls through the filter layer will be swept away by the wave action in the core. The second is that although the filter and flow through the were placed on an angle, the sand was falling down perpendicular to the ground.

Figure C.6: A photo of the third model setup. What can be seen that the interface between the sand and the filter layer has been closed prior to the placement of the sand.

C.2.4. Model setup 4

The fourth setup added a box, with a mesh on top, under the filter layer. This box was divided into 6 boxes to hinder flow through these boxes. The 6 boxes capture the sediment when the sediment erodes through the filter layer, which means that not only the actual erosion through the entire layer can be measured, but it also stops the filter layer from filling up with sediments.

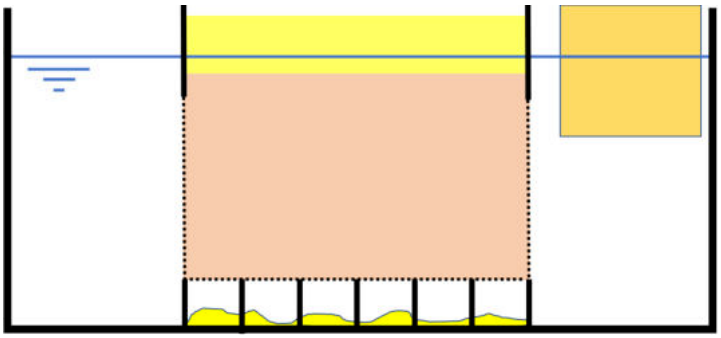

Figure C.7: Model iteration 4. The yellow colored section is where the sand was designed. The pink section is the granular material(Filter layer) and the orange rectangle is the location of the plunger. The waterlevel is indicated with the blue line and the dotted line is a wire mesh

The first time this setup was built it could be seen that the initial infill was larger than expected(Figure C.8). This problem was due to wall transport and is mitigated with the use of bubble wrap. What also can be seen is that the entire sand layer is eroded before the boxes are filled. Because of that more sand is needed, which will lower the height of the filter layer.

Figure C.8: A photo of the fourth model setup. In this setup there was no bubble wrap in place, which cause the large erosion

C.2.5. Model setup 5

The fifth and final setup was very similar to the fourth setup. Only the tickness of the filter layer and the addition of the bubble wrap are different from setup 4. This setup is also the setup that is described in Chapter 4.

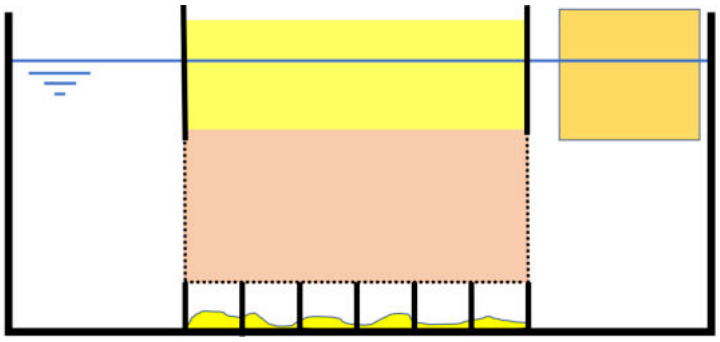

Figure C.9: Model iteration 5. The yellow colored section is where the sand was designed. The pink section is the granular material(Filter layer) and the orange rectangle is the location of the plunger. The waterlevel is indicated with the blue line and the dotted line is a wire mesh

Figure C.10: A photo of the final model setup. The photo is taken after a long test which is why the boxed are filled with sediment

C.2.6. Final model setup

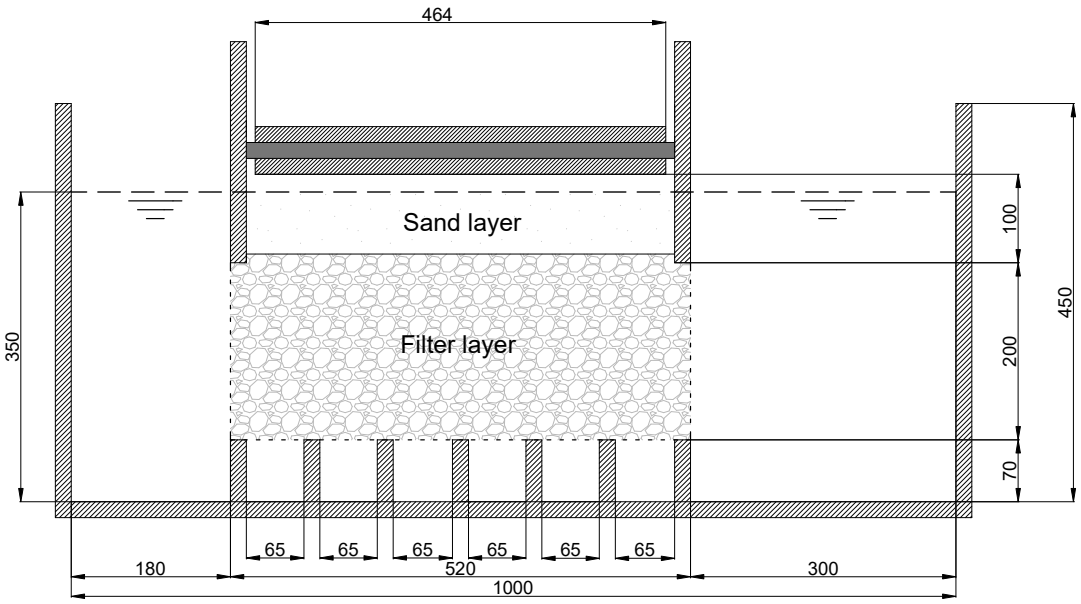

Figure C.11: Sizes of the parallel setup. All sizes are in mm

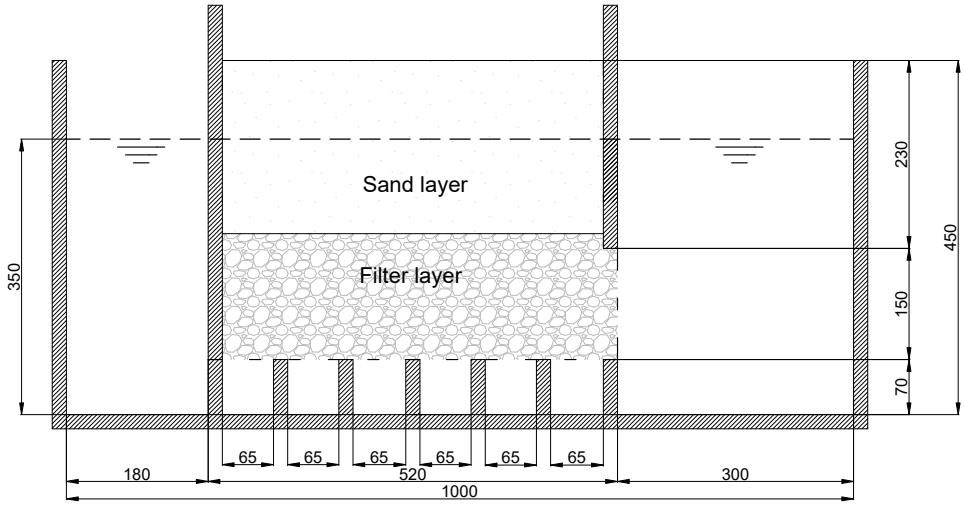

Figure C.12: Sizes of the parallel setup. All sizes are in mm

C.3. Additional measurement devices

(a) DAQ device

(b) Signal amplifier as used with the pressure sensors

Figure C.13: additional measurement devices

C.4. Sieving of sediments

The filter material is created by the author, the stones are sieved (Figure C.14a) and base on predetermined grain size distributions weighted and combined to create the filter material. Afterwards samples were taken from the filter material and weighted stone by stone (Figure C.14c). This was done to check the consistency of the sieving.

The sand samples that were used were sieved (Figure C.14b) and weighted to produce a grading curve. The sands that were used were already available in the TU Delft Fluid Mechanics Laboratory.

(a) Sieving filter

(b) Sieving sand

(c) Weighting stones from filter

Figure C.14: Three ways of determing the grain size distribution of the material.

C.5. Calibration

In this paragraph two calibration cycles are analysed for both the pressure sensors and the water level gauges. For all sensors the mean difference and the standard deviation of this difference is computed. The mean difference is believed to be dependent on a different location where the sensors are placed, while a different standard deviation gives an idea for the accuracy of the calibration. The regression lines of two consecutive tests are depicted in Figure C.15a and b for the pressure sensors and Figure C.16a and b for the two water level sensors.

Pressure sensors

For the tests three pressure sensors were used. During calibration it was seen that two sensors had a similar behaviour, see sensor 1 and 2 in Figure C.15a and b. The third sensor is less sensitive to water level changes as can be seen from the same figures.

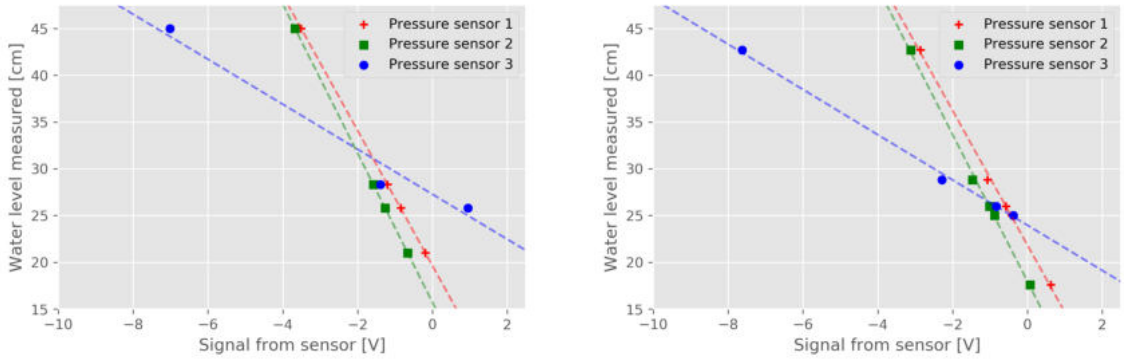

(a) Pressure sensors test 1

(b) Pressure sensors test 2

Figure C.15: Calibration curves pressure sensors

		Pressure sensor 1	Pressure sensor 2	Pressure sensor 3
Standard deviation between tests	[cm]	0.22	0.66	0.081
Mean deviation between tests	[cm]	2.2	2.22	3.31

Table C.1: Standard deviation and mean difference between the calibration tests

Water level gauges

For the waterlevels the lines are also plotted. The results of the two tests can be found below. Because two different types of sensor were used the lines were expected to differ. The results were different, but showed a good correlation.

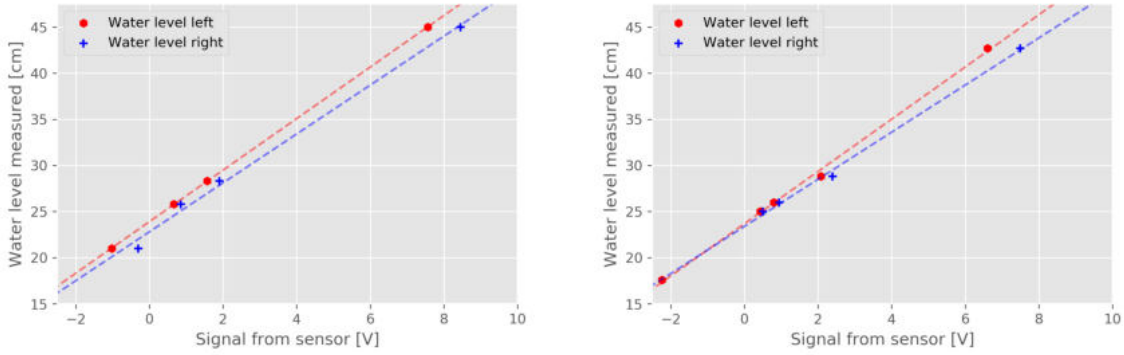

(a) Water level gauges test 1

(b) Water level gauges test 2

Figure C.16: Calibration curves waterlevel sensors

The mean difference between the two tests of the water level sensors is around 1-3 cm, which is because of the loose placement of the sensors inside the granular filter layer. Both water level gauges were mounted on the setup, which is why the mean difference between the 2 sensors is much lower

		Water level left	Water level right
Standard deviation between tests	[cm]	0.57	0.23
Mean deviation between tests	[cm]	0.58	0.22

Table C.2: Standard deviation and mean difference between the calibration tests for the water level tests

C.6. Plunger movement

The water movement in the model setup is produced by the plunger. This plunger is located on the far right of the setup. The consist of a wooden block that is moved in the water to create a pressure difference inside of the container. It is moved by a stepper motor.

The size of the plunger is 140mm wide by 250mm in length. The total height of the plunger is 230mm. During tests the bottom of the plunger is always submerged. This is to make sure that there is no impact on the water surface during the downward movement. The movement is also smaller than 230mm, which means that the plunger is never fully submerged and the effect of a downward movement is always the same.

The movement of the stepper motor is controlled by a computer that is placed besides the model setup. For the tests the total movement is kept the same, only the velocity and acceleration of the plunger is altered. The total movement is given in steps, which is kept to 60000 steps, which is 38mm. The velocity is given in rps. The minimum that can be reached by the moter is 0.025 rps which is 0.001 m/s. The maximum velocity that is used is 1 rps, which was equal to 0.389m/s. The velocity is the leading parameter that is changed for each test. The acceleration is adjusted to give the correct velocity profile.

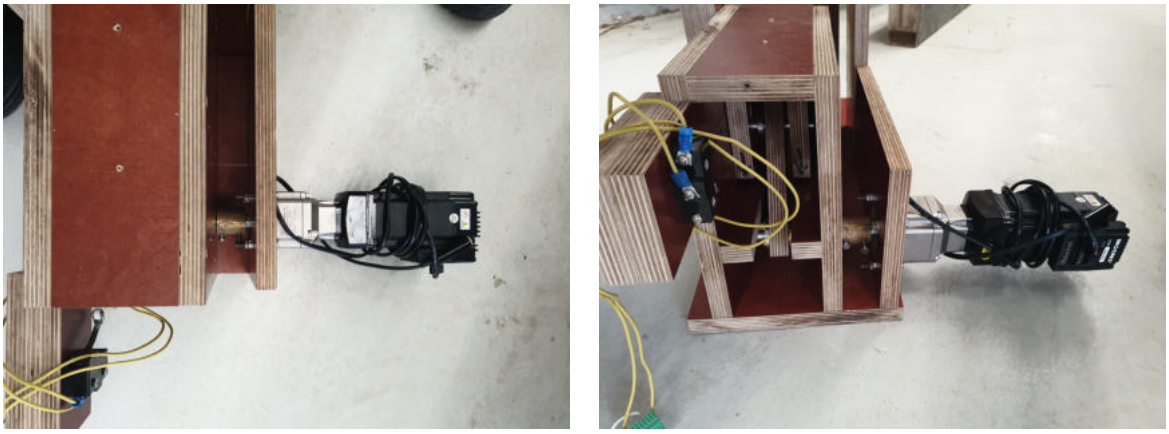

(a) Front view of the motor on the plunger together with the stop switch (b) Top view of the motor on the plunger together with the stop switch

C.7. Parameters of importance

In Section 4.9 an overview can be seen of the tests that are performed and which parameters are used. The most important parameters are given below. Parameters with numbers 1 to 4 are altered, the numbers 5 to 10 are kept equal over the entire test sequence.

1. Sediment grain size

Both the sediment grain size and filter grain size alter the resistance of the layer. The hypothesis is that a larger sediment size, with equal filter grain size, will lead to a smaller transport as the sediments need larger pores to protrude into the filter. Therefore the filter should be more resistant to higher gradients. The opposite applies to smaller sediment sizes, which should lead to higher transport. For normal filters, a smaller grain size with the same stability number leads to a higher gradient (de Graauw et al.,

1983).

The former only applies to sediments without cohesion. All sediments that are tested in this research are classified as sand without cohesion($D_{n50} \leq 100\mu m$)

2. Filter grain size

For the grain size of the filter material, the opposite is true. A larger grain size will mean a lower resistance to hydraulic gradients, while a smaller grain size is more resistant to hydraulic gradients.

This also has to do with the pores, because the pores are larger if the grain size increases, therefore, increasing the volume for sand to protrude through.

3. Hydraulic gradient

As the research is focussed on geometrically open filters there will be some erosion at certain hydraulic gradients. For the case that is considered in this research, the hydraulic gradient is the main trigger for erosion through the filter layer.

4. Direction of flow

To create a reproducible model the flow is split into one direction. This can be perpendicular or parallel over the filter layer. In Chapter 3 the gradients in both the parallel en perpendicular direction are determined. With the use of these parameters, both flows will be tested to see where one is dominant.

5. Thickness filter layer

The filter layer is responsible for the attenuation of pressures over the setup. For an equal gradient over de filter, the thickness should be equal at every point in the setup. Also to compare the results between tests the filter thickness should also be of equal size over different tests.

In reality, the filter layer thickness will be larger than the 200mm that is used during the model tests. Because the research is focussed on the critical gradient this is not of importance as the difference with a thicker filter layer is that the erosion would be measured with a delay.

6. Width of filter layer

Because there will be side effects with inflow and outflow in the filter layer, this layer needs to have sufficient width to be able to have an undisturbed flow in the middle of the layer.This width is kept equal for every test to have the same expected erosion in all boxes below the filter layer.

7. Water level

The water level fluctuations induced by the plunger are responsible for the gradients over the filter layer. The filter layer that is considered in this research is always submerged, which means that there is no influence of air entrainment on the filter-sand interface. For this reason, the water level should be higher than this interface and is kept at the same level for a good comparison.

8. Internal stability number of filter layer

The grain size distribution of a filter layer can be schematized into two value: The nominal diameter (D_{n50}) and coefficient of uniformity ($C_u = \frac{D_{60}}{D_{10}}$)). Both values influence the resistance against erosion. In this research, the coefficient of uniformity is the same in all tests. Only the nominal grain size is altered as described at point 2.

9. Duration of tests

Because breakwaters are built for a time span of 10 to 100 years the long term effect of gradients on a filter has to be investigated. To be able to compare the results of the tests the duration will be the same every test.

10. Thickness of sand layer

For the perpendicular flow case, the thickness of the sand layer on top of the filter layer is of influence on the gradients that are acting on the sand layer. with a thicker layer also piping or blowout can be avoided.

C.8. Setup at TU Delft laboratory of fluid mechanics

The setup used in this research is broken down and stored in the TU Delft laboratory of fluid mechanics, if the research is continued at the laboratory this paragraph will give a small summary of the parts that are stored in the laboratory as well as the location of each part on the setup. All parts are labeled with the code names (See table below), together with the name of the author (Daan van de Ven) and the months it was used (may-sept 2019).

Number	Code	Use
1	Base plate	Create a solid base for the container and holding the standers
2	Top rubber seal	Creating an air-tight seal between the sand and air. Has to be screwed on the rubber seal
3	Rubber seal	Sealing the container. Can be used as a separator for perpendicular flow
4	Container reinforcement beam	Used to strengthen the container
5	Mesh separator 1	Used for both parallel and perpendicular flow. Can be inserted in sand trap and is held in place with clamps.
6	Mesh separator 2	Only used for parallel flow. Is replaced with rubber seal for perpendicular flow
7	Stander 1	Used to strengthen the container
8	Stander 2	Used to strengthen the container
9	Plunger attachment	To increase the height of the plunger
10	SI load top plate	Was used to place the weights on top of the sand layer, while maintainingpermeability
11	WL- sensor left	Used to screw the sensor on. Was clamped in place
12	Black cloth	Used to remove reflections from both sides

Table C.3: Additional parts

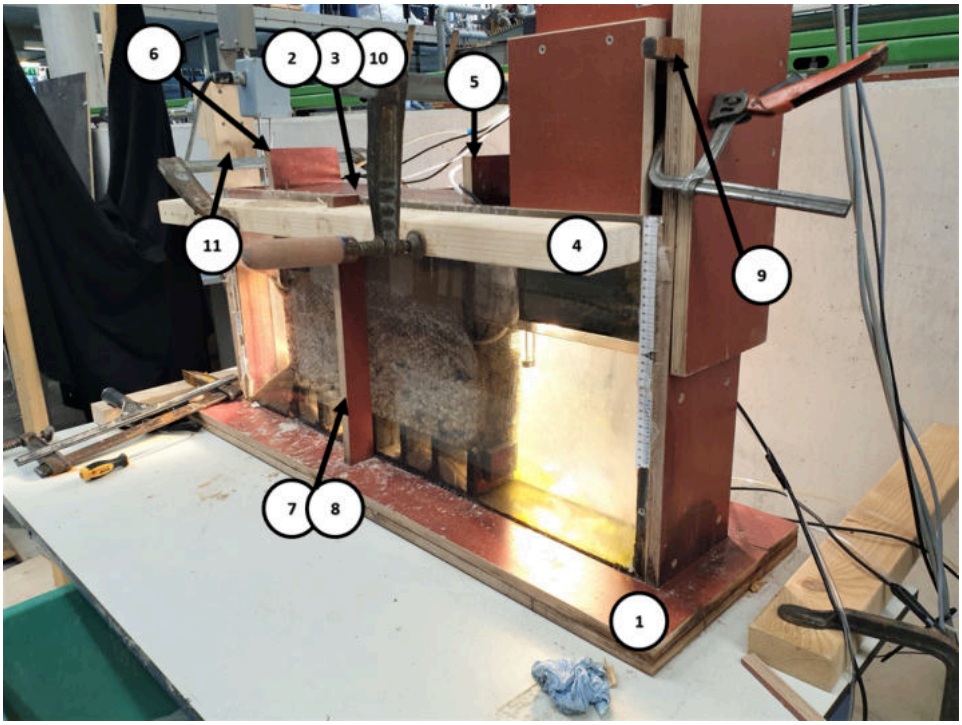

Figure C.18: Location of the parts as described in Table C.3

D

Results model tests

D.1. Consistency of gradient during one test

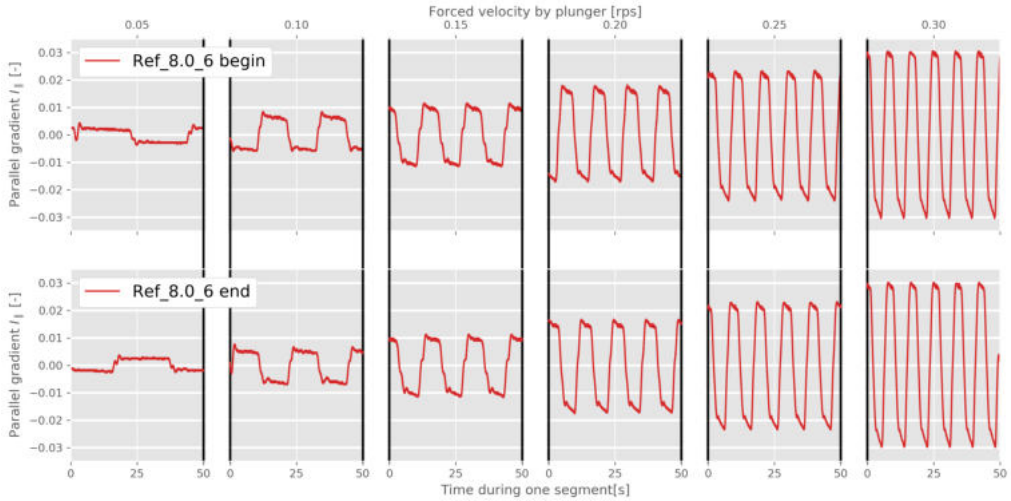

Figure D.1: Gradient signal for two different consecutive tests. The gradient over the granular filter layer is depicted. In the In the upper graph the gradients during the first tests are depicted, while in the lower graph the gradients during the second series of tests can be seen. The signal between two black bars is a 50 seconds cut out of the 15 minute signal of one test sequence

D.2. Phase lag sensors

The phase lag is given in the paragraphs below for 2 reference tests Ref_8.0_4 and Ref_8.0_6. During these tests the phase lag is given for three velocities:

- VE_0.10
- VE_0.18
- VE_0.25

For these velocities also the individual FFT graphs are depicted. Which can be used to give an idea of the oscillations of all the sensors.

D.2.1. Ref_8.0_4

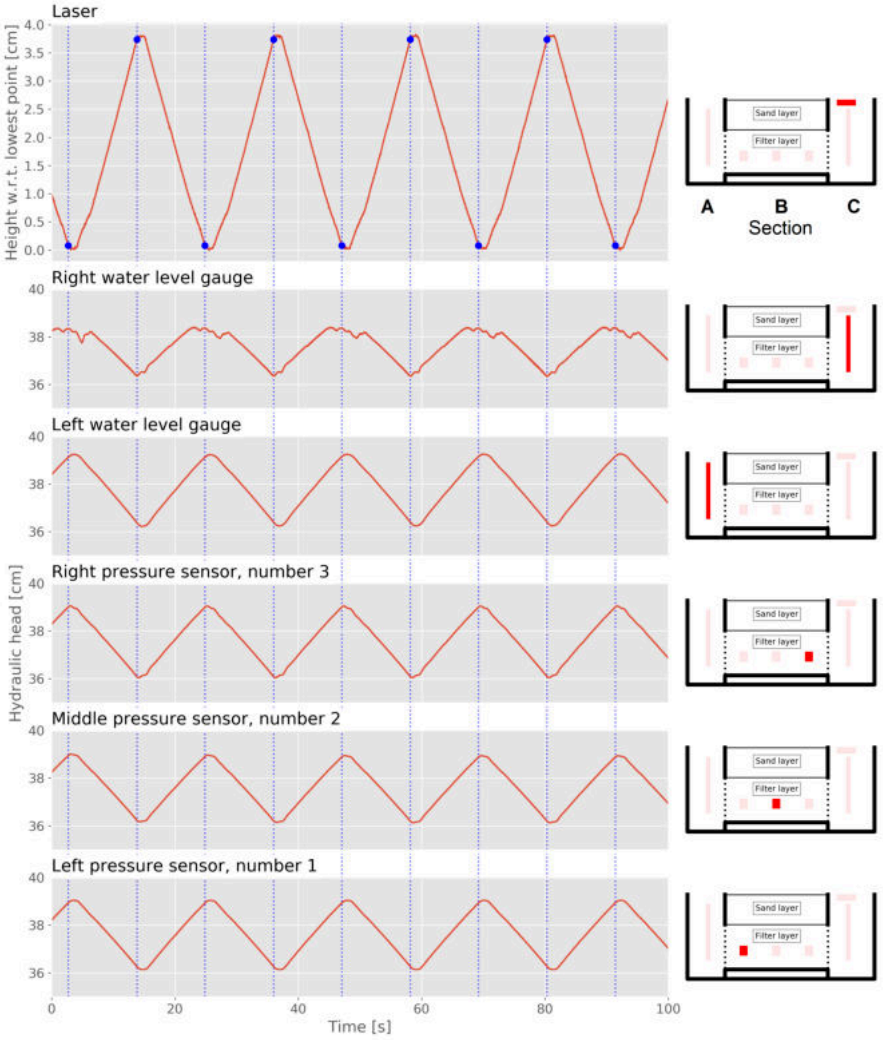

Figure D.2: 50 seconds of signal from all sensors (Ref_8.0_4 with VE_0.10)

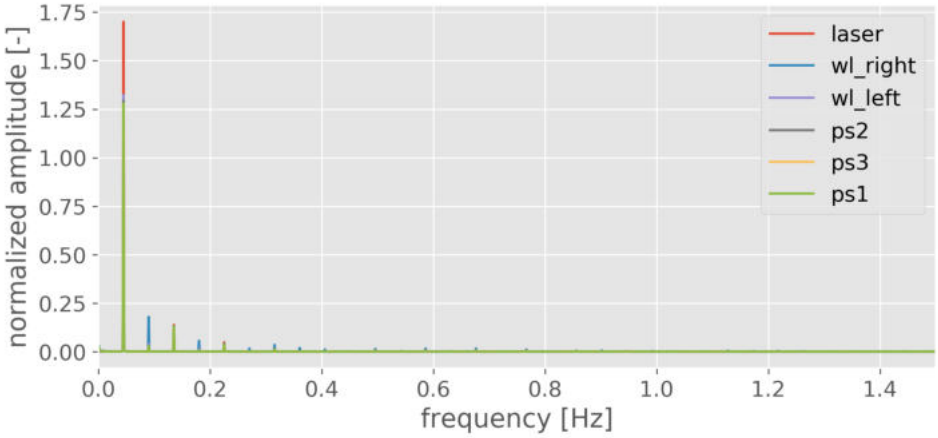

Figure D.3: FFT of all sensors Ref_8.0_4 with VE_0.10

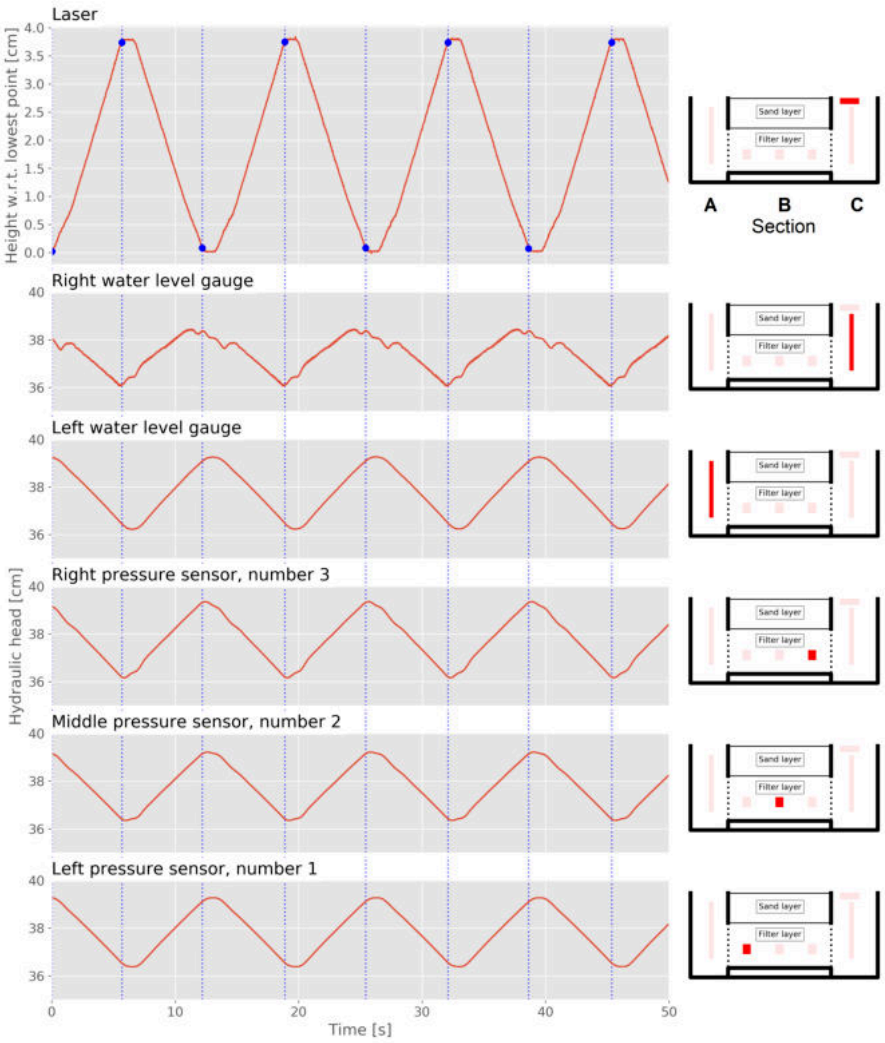

Figure D.4: 50 seconds of signal from all sensors (Ref_8.0_4 with VE_0.18)

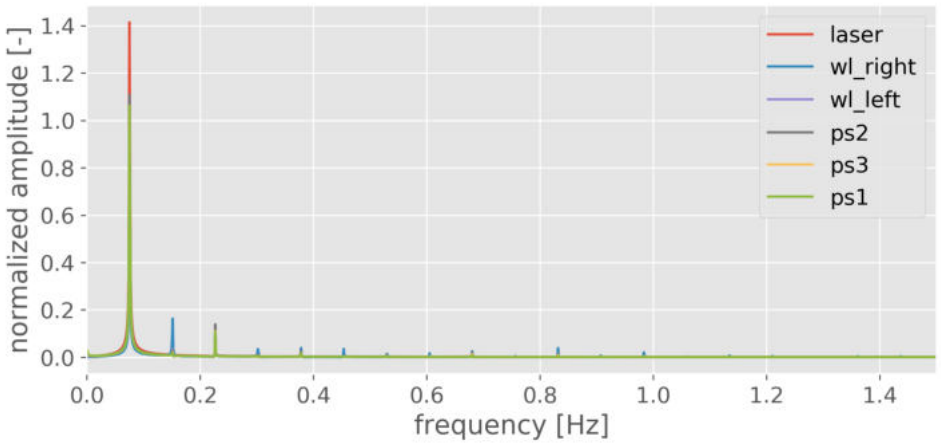

Figure D.5: FFT of all sensors Ref_8.0_4 with VE_0.18

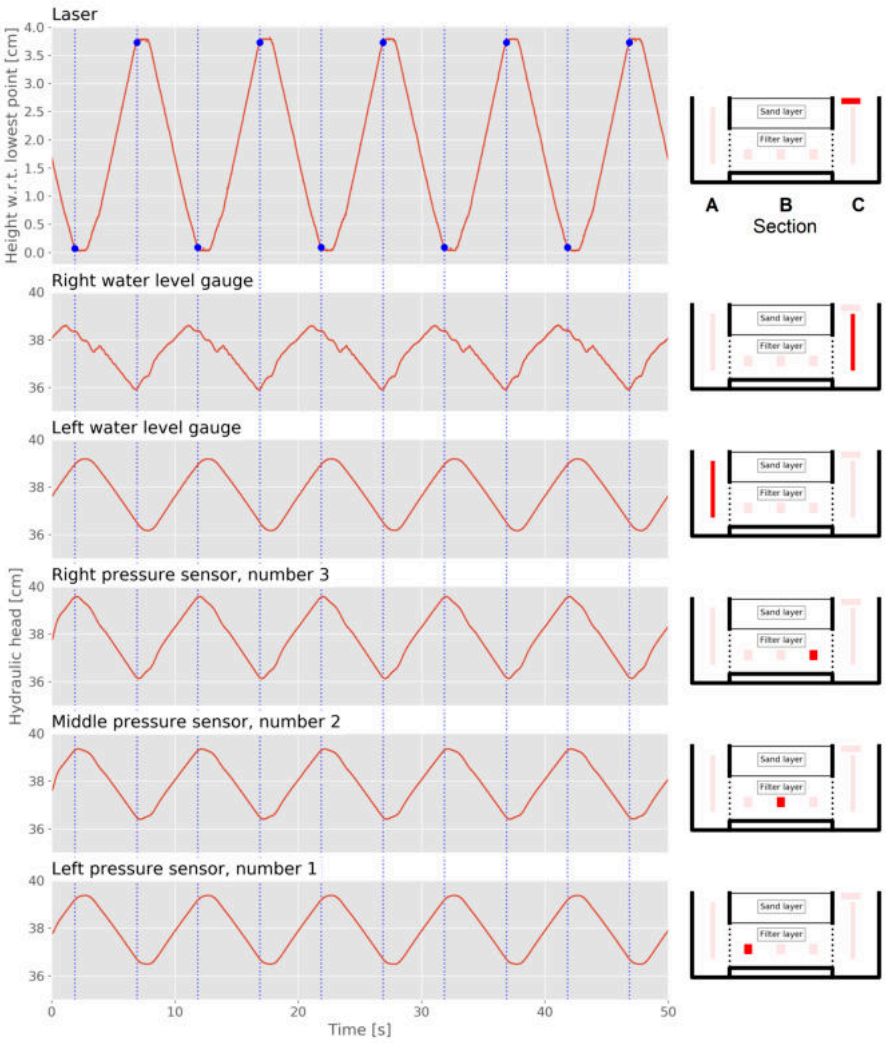

Figure D.6: 50 seconds of signal from all sensors (Ref_8.0_4 with VE_0.25)

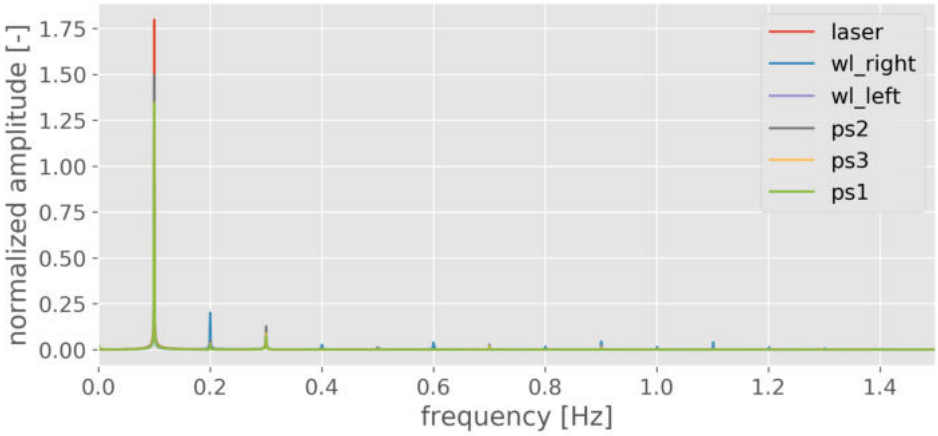

Figure D.7: FFT of all sensors Ref_8.0_4 with VE_0.25

D.2.2. Ref_8.0_6

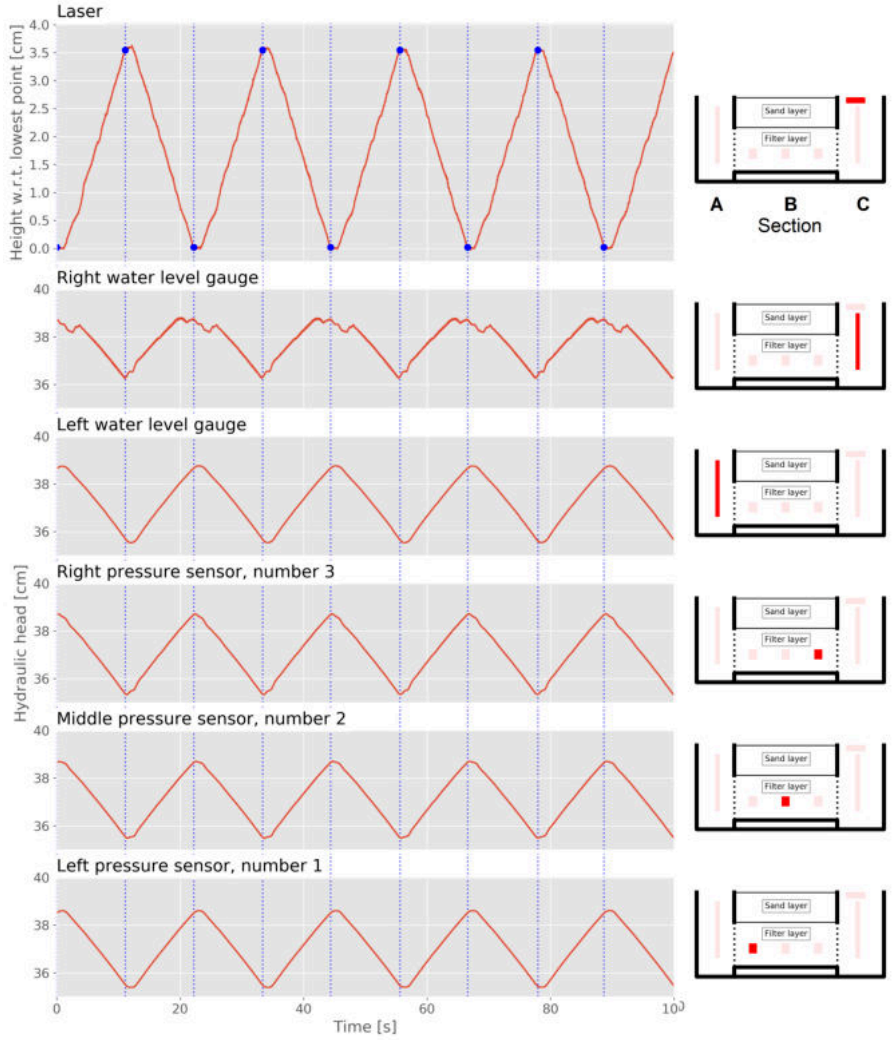

Figure D.8: 50 seconds of signal from all sensors (Ref_8.0_6 with VE_0.10)

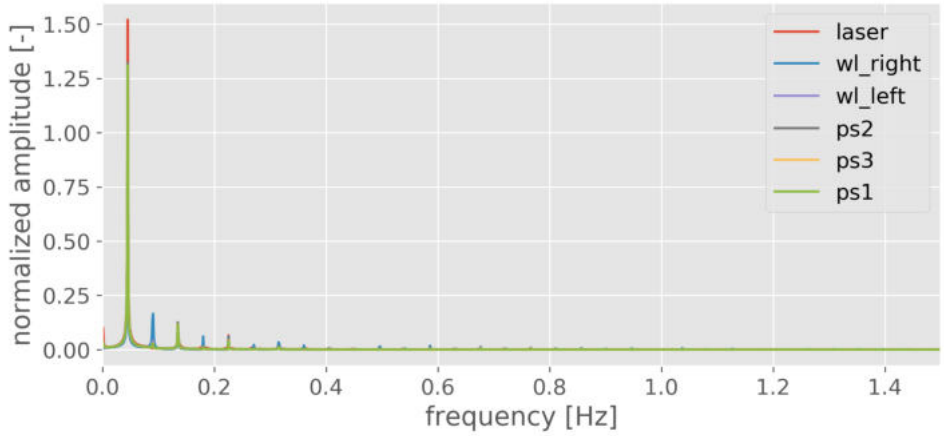

Figure D.9: FFT of all sensors Ref_8.0_6 with VE_0.10

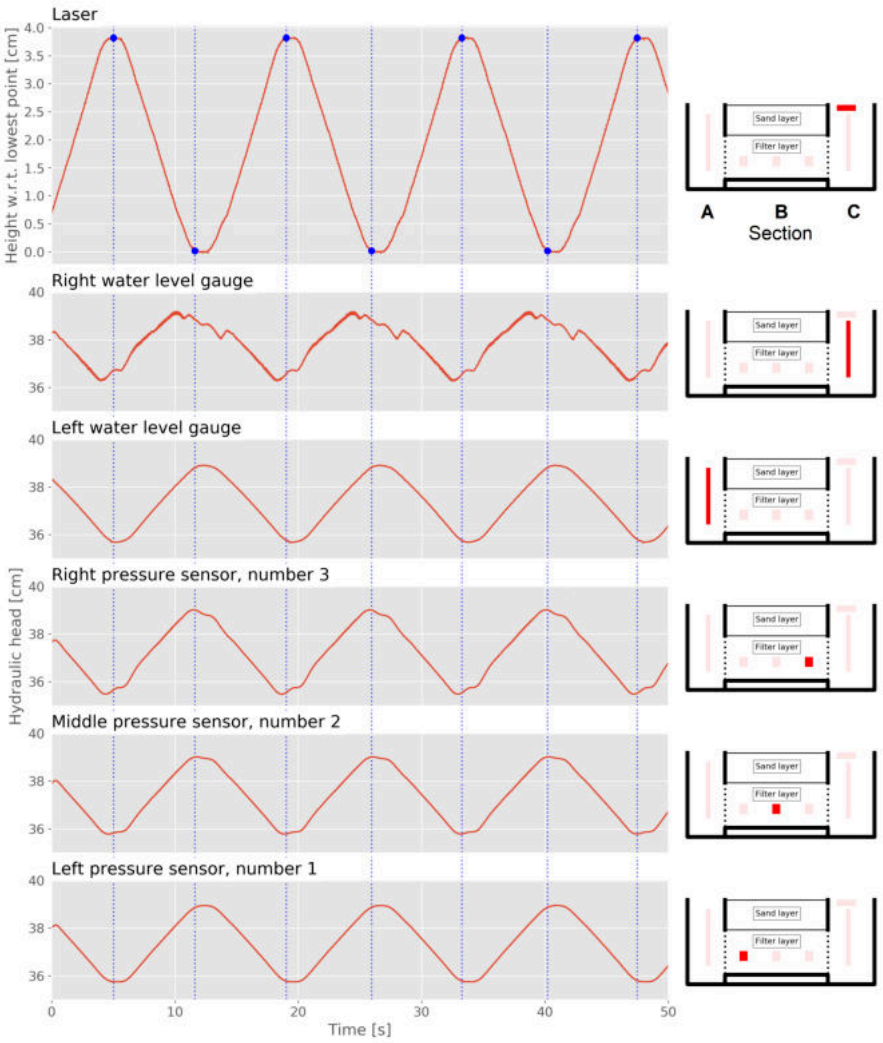

Figure D.10: 50 seconds of signal from all sensors (Ref_8.0_6 with VE_0.18)

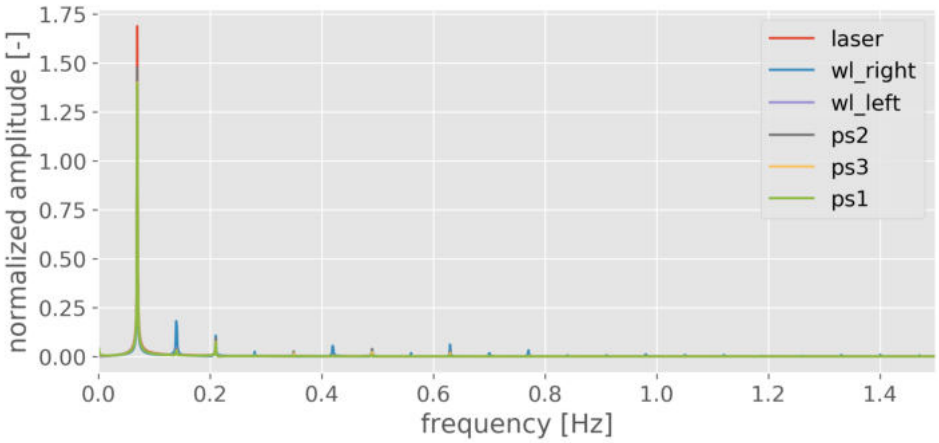

Figure D.11: FFT of all sensors Ref_8.0_6 with VE_0.18

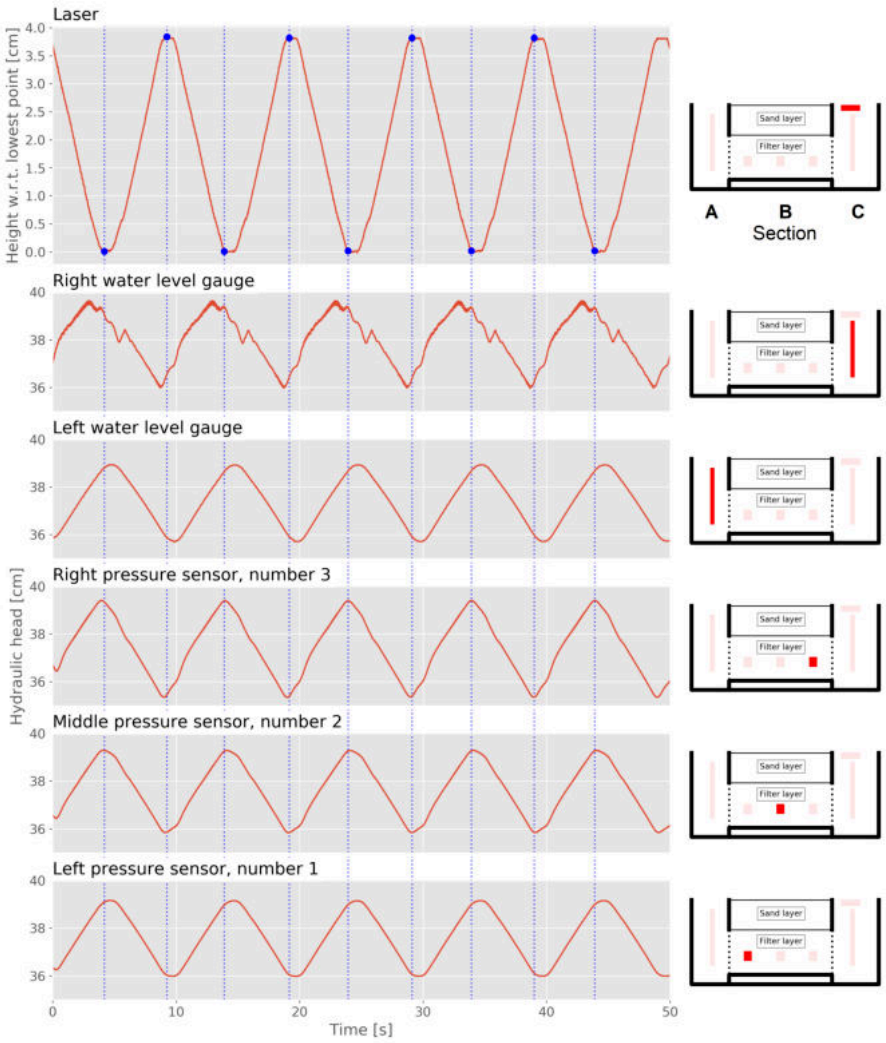

Figure D.12: 50 seconds of signal from all sensors (Ref_8.0_6 with VE_0.25)

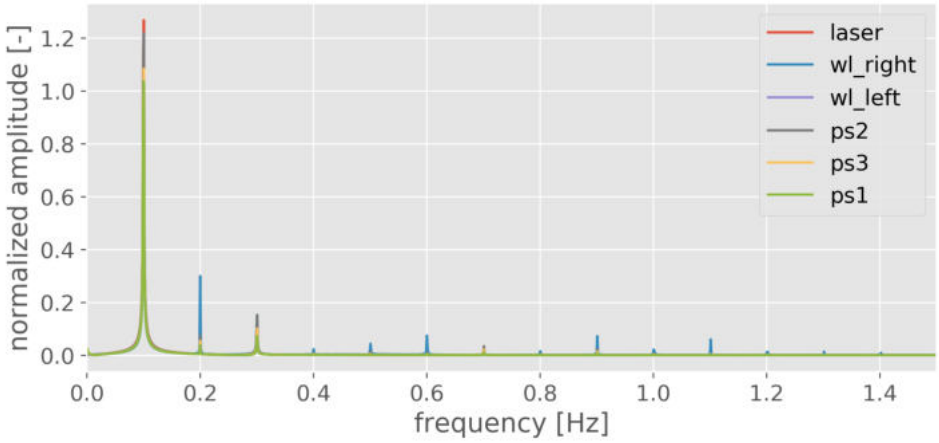

Figure D.13: FFT of all sensors Ref_8.0_6 with VE_0.25

D.3. Sensors malfunction

Sensor	Para_4.0	Para_7.5	Para_8.0	Para_9.5	Para_16.5	Para_8.0_super
Water level guage left		X	X	X		
Water level guage right	X	X	X	X	X	X
Pressure sensor 1	X	X	X		X	
Pressure sensor 2	X		X		X	
Pressure sensor 3	X	X	X	X	X	X

Table D.1: All available sensors for every parallel test

For the perpendicular tests also two sensors were needed, but in the sand layer. The left water level sensor was not used and could not function as backup. For all tests except Perp_4.0 results were obtained.

Sensor	Perp_4.0	Perp_7.5	Perp_8.0	Perp_9.5	Perp_16.5	Perp_8.0_super
Water level guage right	X	X	X	X	X	X
Pressure sensor 1	X	X	X	X*	X	X
Pressure sensor 2		X	X	X	X	X

Table D.2: Available sensors for perpendicular tests.
*For test Perp_9.5 pressure sensor 3 was used instead of pressure sensor 1

The reasons why some tests are perfomed with less sensors are that pressure sensors broke during tests and the water level guages were not connected properly during all tests. Another reason that some tests lack correct measurements is the cutting of power. As the tests ran 24 hours a day the author was not always present at the laboratory. A couple of times the entire power of the laboratory was cut, which made entire tests unusable. Also due to construction works inside the laboratory, power cords were removed during tests, even with warning signs at the power outlets.

Besides the sensor malfunction also the webcam that was used did not work during all tests, for this reason 2 cameras on both sides of the container were used. During Para_8.0_long the application that ran the camera crashed on the first computer, while the hard disk on the second computer was completely filled with footage, for this reason there is no camera footage from the long test.

D.4. Standard deviation tests

Standard deviation		Ref_8.0_3	Ref_8.0_4	Ref_8.0_5	Ref_8.0_6
$I_{negative,\parallel,std}$	[-]	0.00027	0.00012	0.00013	0.00021
$I_{positive,\parallel,std}$	[-]	0.00028	0.00011	0.00019	0.00022

Table D.3: Standard deviations of the 4 reference tests.

Standard deviation		Para_4.0	Para_7.5	Para_9.5	Para_16.5
$I_{positive,\parallel,std}$	[-]	0.00034	0.00031	0.00010	0.00016
$I_{negative,\parallel,std}$	[-]	0.00026	0.00035	0.00018	0.00016

Table D.4: Standard deviations of the 5 Parallel tests

Standard deviation		Perp_7.5	Perp_8.0	Perp_9.5	Perp_16.5
$I_{positive,\square,std}$	[-]	0.0063	0.0073	0.015	0.0073
$I_{negative,\square,std}$	[-]	0.0078	0.012	0.0096	0.0062

Table D.5: Standard deviations of the 4 perpendicular tests

D.5. Reference tests

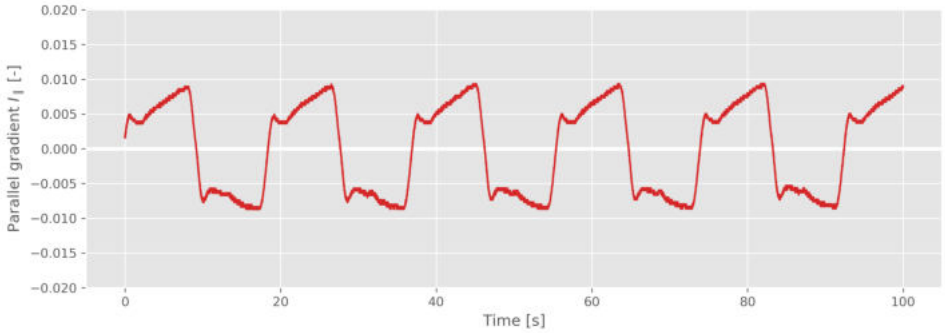

Figure D.14: Critical gradient for test: Ref_8.0_3 VE_012

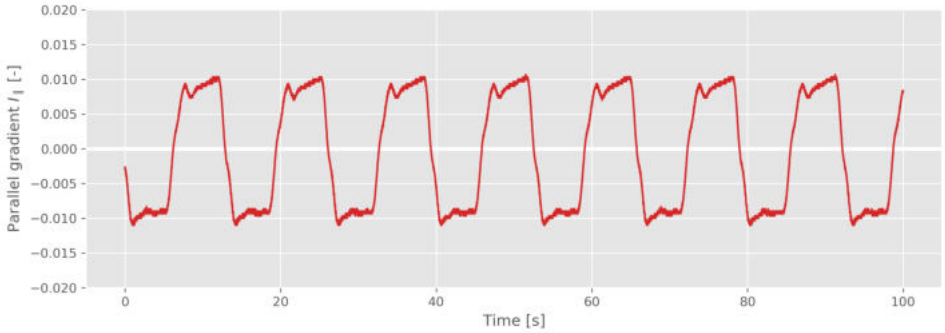

Figure D.15: Critical gradient for test: Ref_8.0_4 VE_018

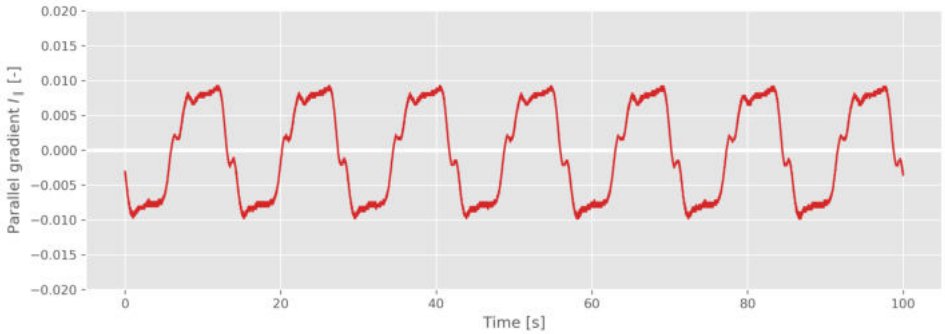

Figure D.16: Critical gradient for test: Ref_8.0_5 VE_018

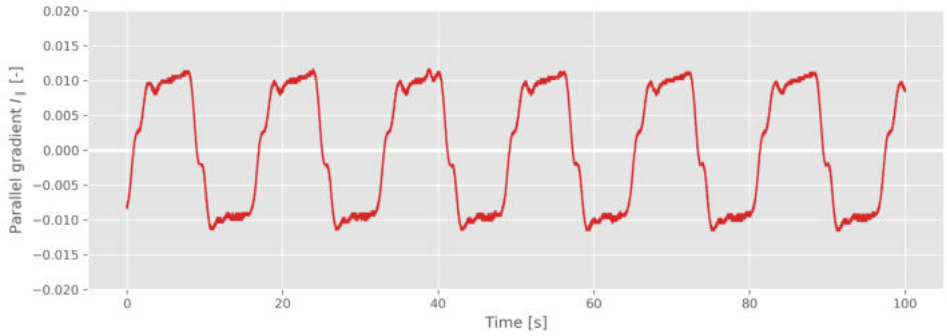

Figure D.17: Critical gradient for test: Ref_8.0_6 VE_015

D.6. Parallel tests

D.6.1. Para_4.0

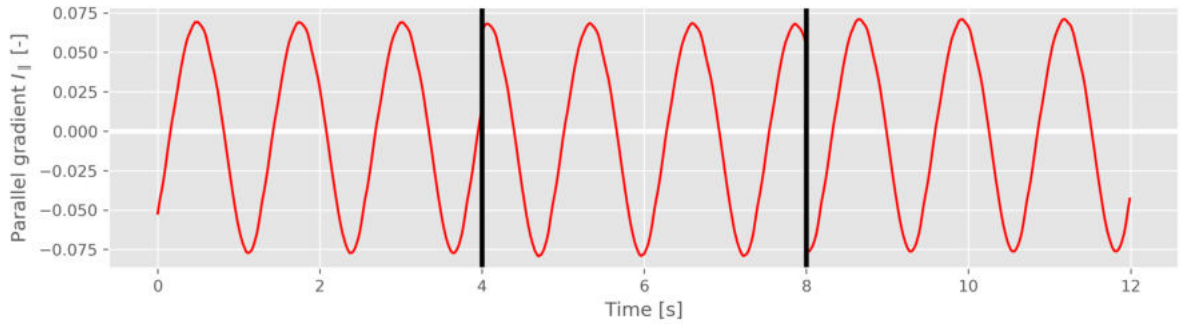

Figure D.18: Critical parallel gradient for test: Para_4.0

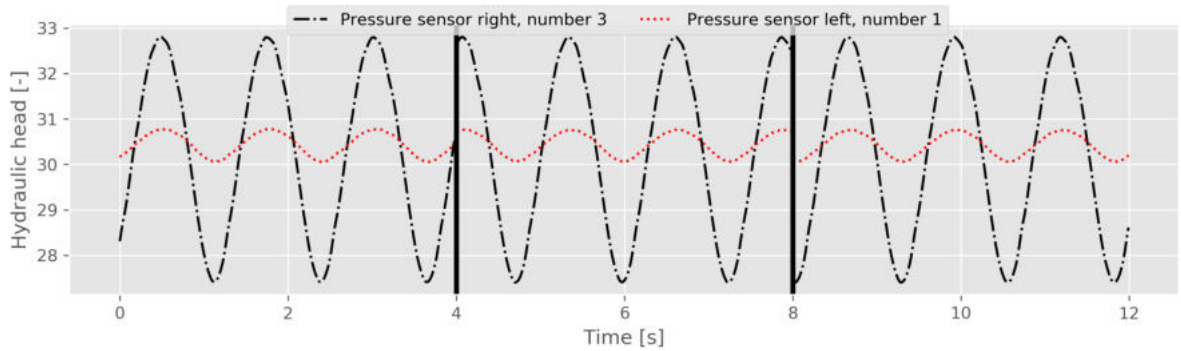

Figure D.19: Pressure sensor signal for the critical parallel gradient test: Para_4.0

D.6.2. Para_7.5

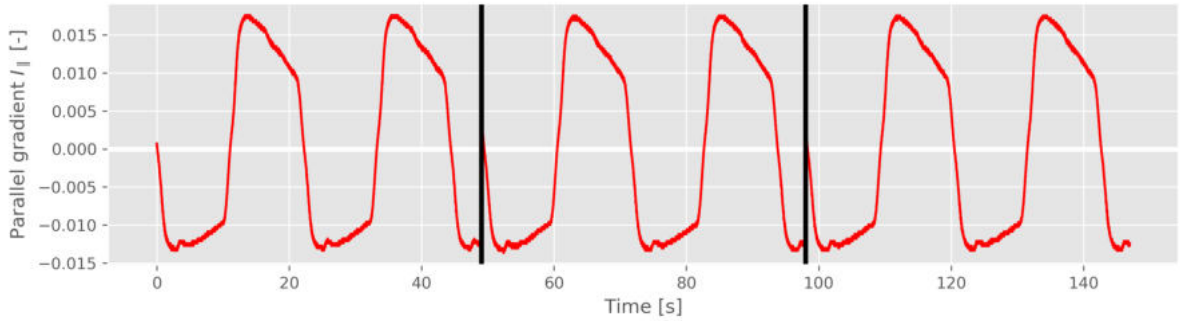

Figure D.20: Critical gradient for test: Para_7.5

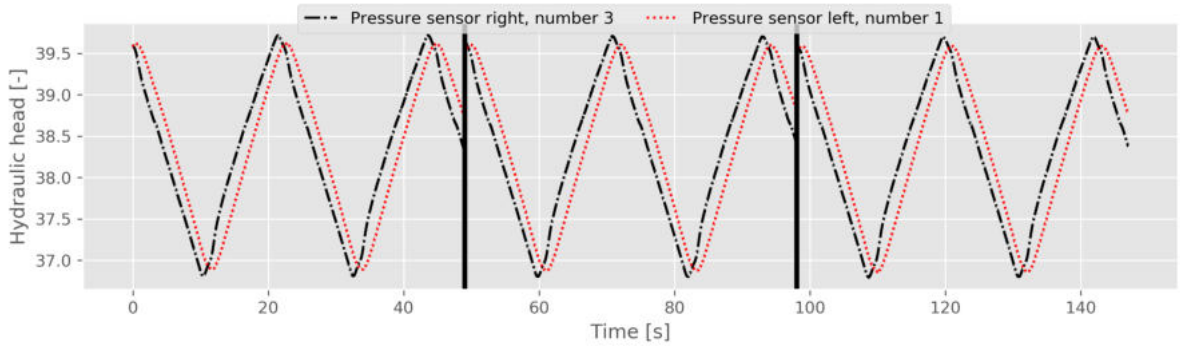

Figure D.21: Pressure sensor signal for the critical parallel gradient test: Para_7.5

D.6.3. Para_8.0

See reference tests for this gradient

D.6.4. Para_9.5

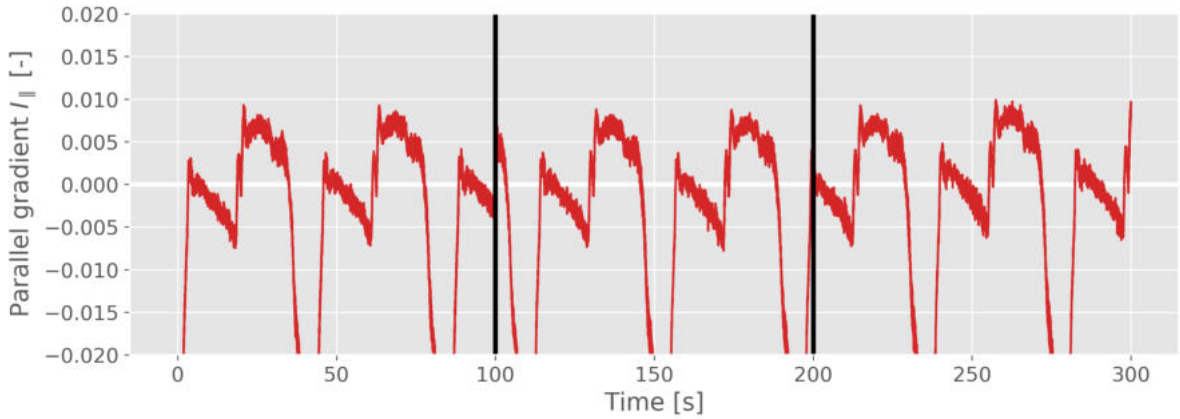

Figure D.22: Critical gradient for test: Para_9.5

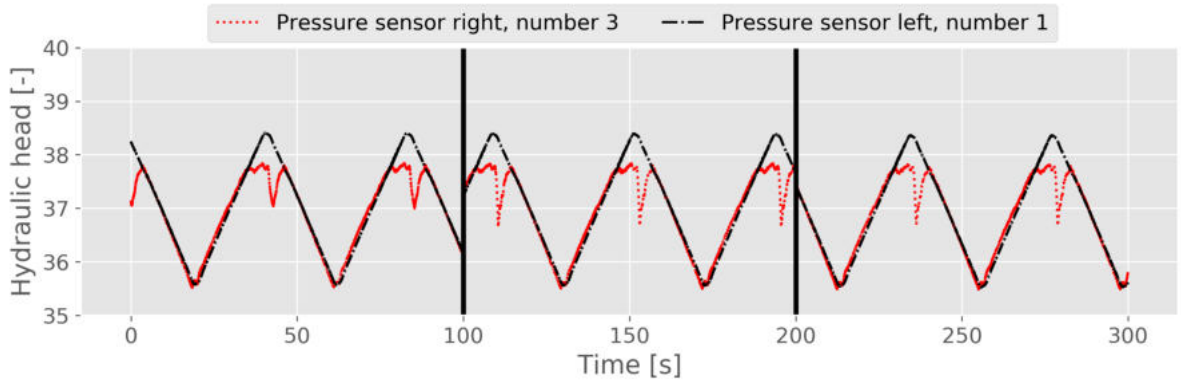

Figure D.23: Pressure sensor signal for the critical parallel gradient test: Para_9.5

D.6.5. Para_16.5

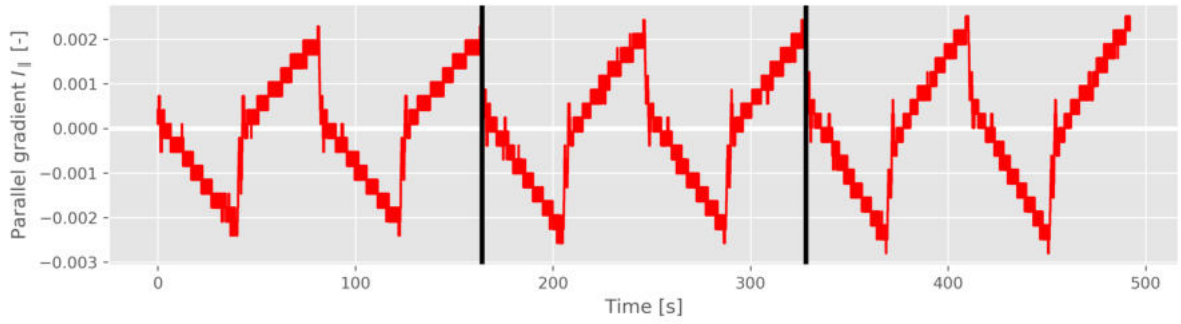

Figure D.24: Critical gradient for test: Para_16.5

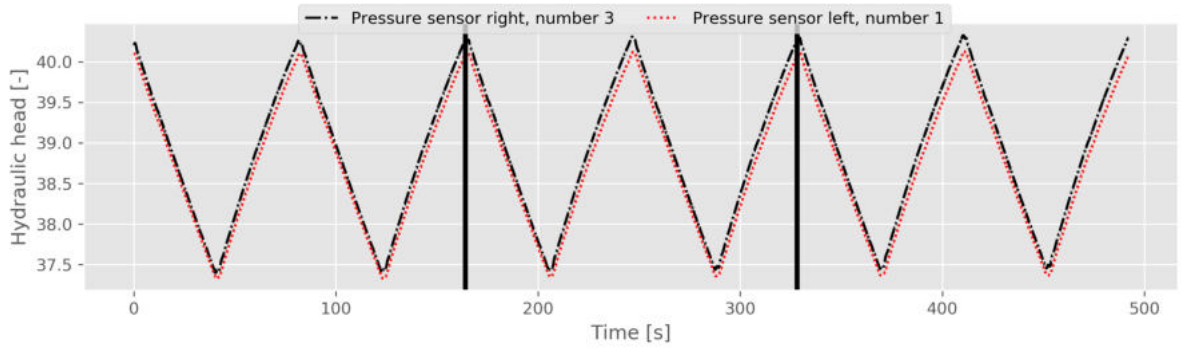

Figure D.25: Pressure sensor signal for the critical parallel gradient test: Para_16.5

D.6.6. Para_8.0_super

No results were obtained during this test.

D.6.7. Para_8.0_long

Critical gradient for the long test, the results of the long test are lost due to the crashing of the computer.

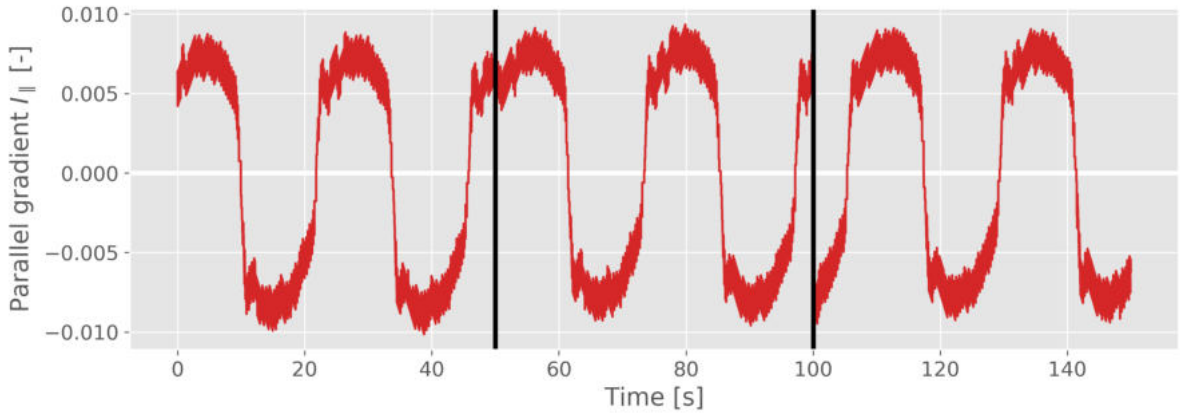

Figure D.26: Critical gradient for test: Para_8.0_long

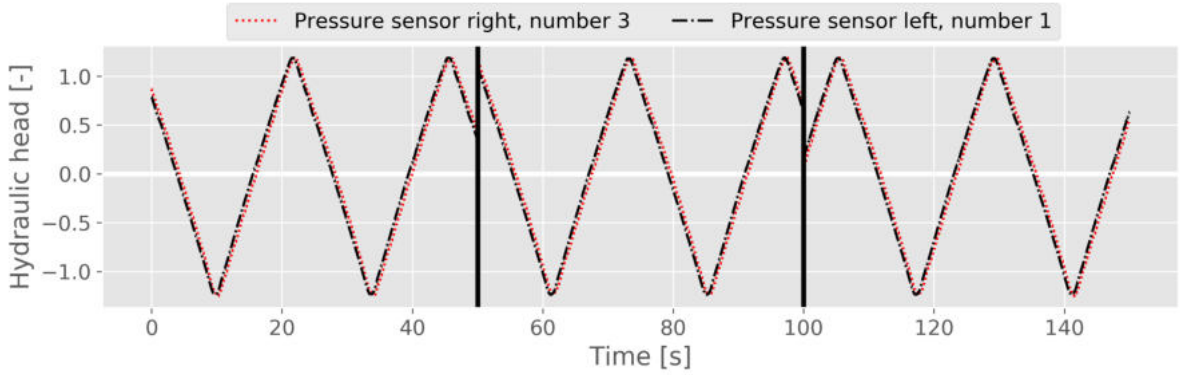

Figure D.27: Pressure sensor signal for the critical parallel gradient test: Para_8.0_long

D.7. Perpendicular tests

D.7.1. Perp_4.0

No results

D.7.2. Perp_7.5

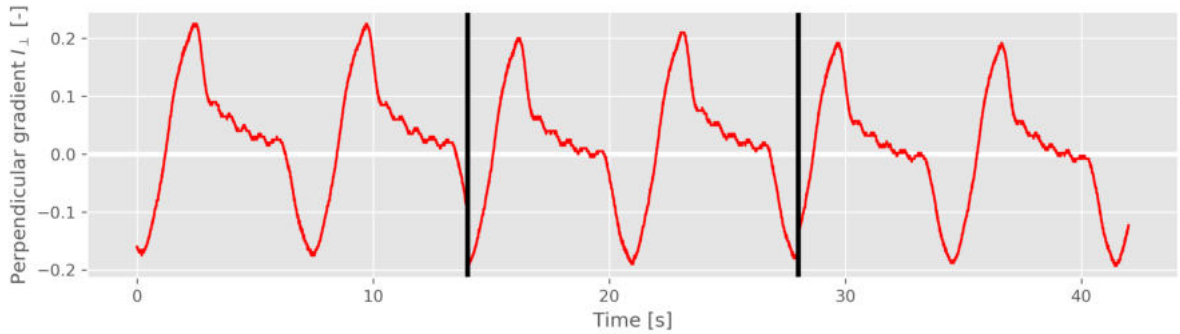

Figure D.28: Critical perpendicular gradient for test: Perp_7.5

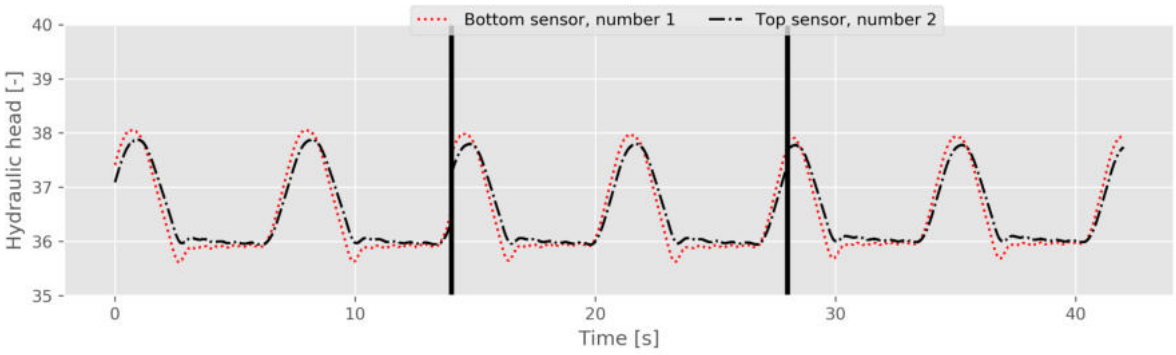

Figure D.29: Pressure sensor signal for the critical perpendicular gradient test: Perp_7.5

D.7.3. Perp_8.0

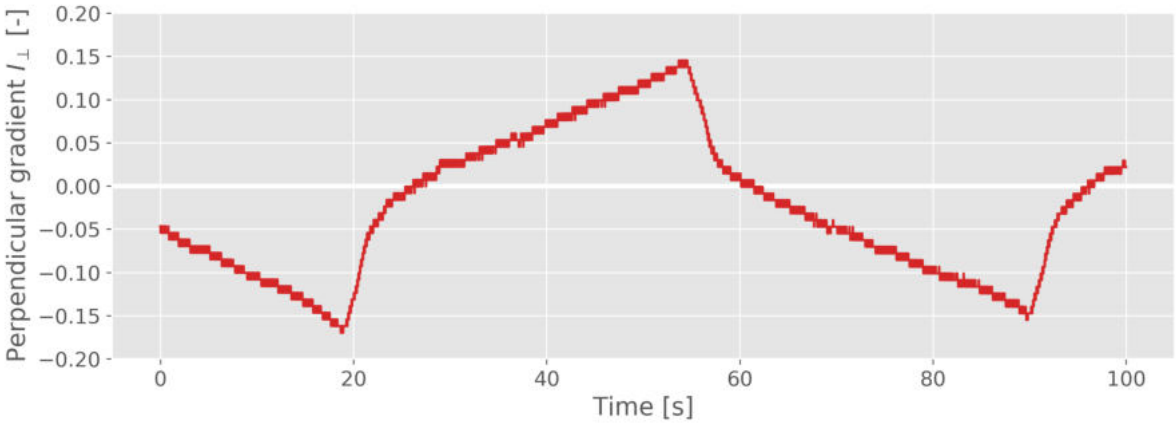

Figure D.30: Critical gradient for test: Perp_8.0

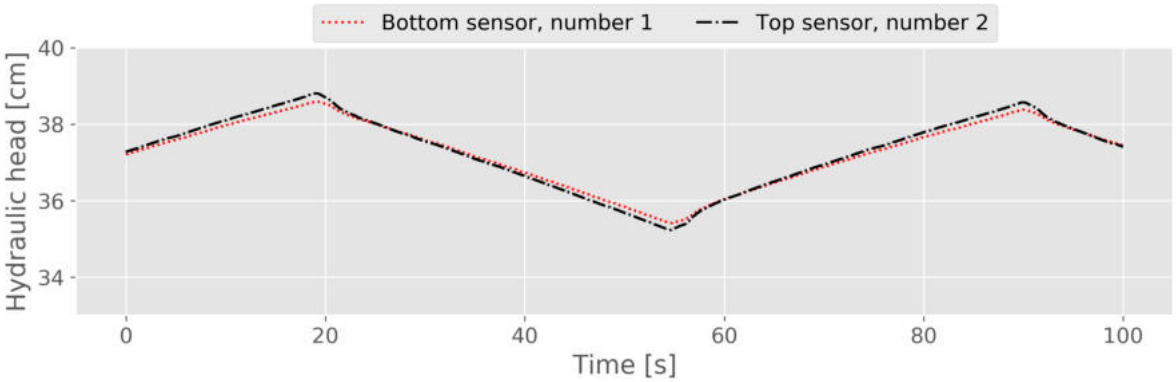

Figure D.31: Pressure sensor signal for the critical parallel gradient test: Perp_8.0

D.7.4. Perp_9.5

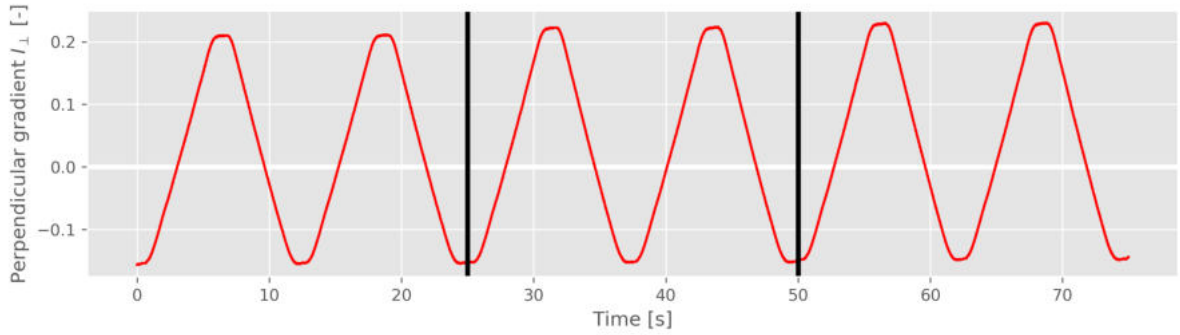

Figure D.32: Critical perpendicular gradient for test: Perp_9.5

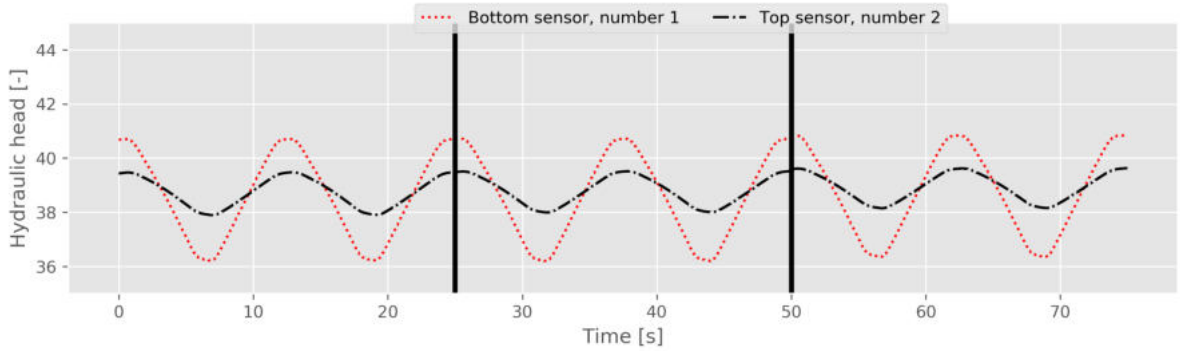

Figure D.33: Pressure sensor signal for the critical perpendicular gradient test: Perp_9.5

D.7.5. Perp_16.5

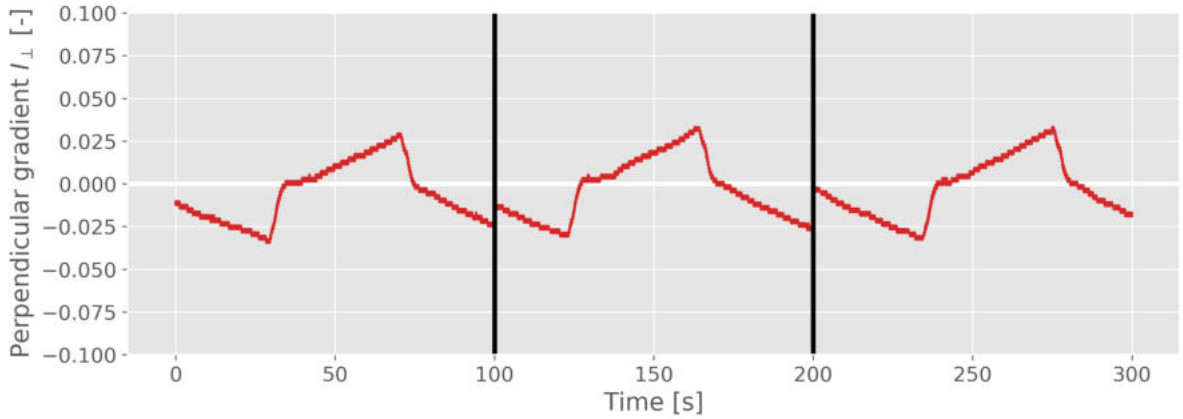

Figure D.34: Critical gradient for test: Perp_16.5

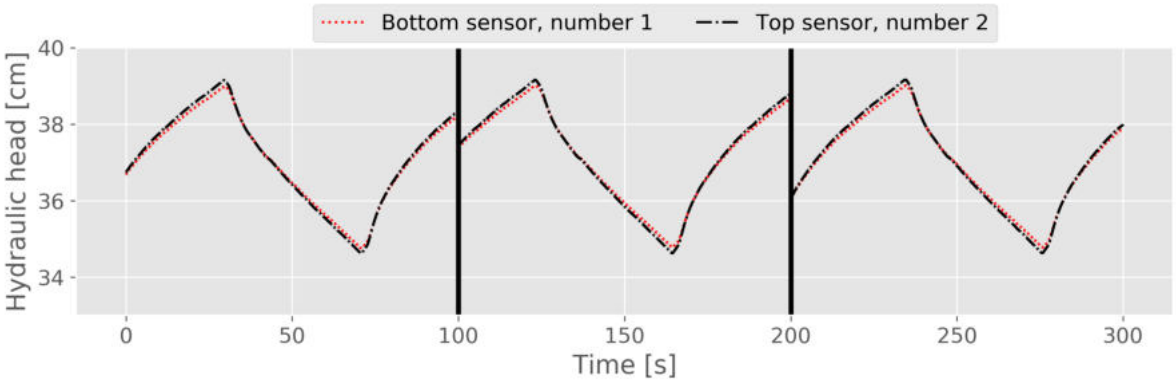

Figure D.35: Pressure sensor signal for the critical parallel gradient test: Perp_16.5

Index

Acceleration, 51
Arching, 13

Block signal, 56

Critical gradient, 14, 49

DAQ module, 37
Darcy, 7
DASYlab, 37
Direction of flow, 30

Empirical model, 21
Erosion, 12

Filtering, 40
Forchheimer, 8
Forcing, 35

Geometrically closed filter, 2, 14
Geometrically open filter, 2, 14
Geotextile, 2, 19
Gradient, 21
Grain size, 36, 65
Granular filter, 2

Hydraulic gradient, 35, 49

Land reclamations, 1

Numerical model, 12, 22

OpenFOAM model, 12, 22

Parallel flow, 16
Parallel gradient, 26
Perpendicular flow, 15
Perpendicular gradient, 28
Phase, 54
Piping, 42
Plunger, 43
Porous flow, 7
Pressure gradient, 15

Reference tests, 46
Rubble mound breakwater, 1

Sand trap, 41
Spreading of granular filter layer, 60
Stability ratio, 14, 64
Superimposed load, 18, 65

Velocity, 51
Vibrations, 40, 43

Waiting time, 51
Wall effects, 42
Wave attenuation, 9